

RADIATIVE TRANSFER IN PULVERIZED COAL SUSPENSIONS

by

HUSSEIN KHALIL

B.S., Kansas State University, 1978

A MASTER'S THESIS

submitted in partial fulfillment of the
requirements for the degree

MASTER OF SCIENCE

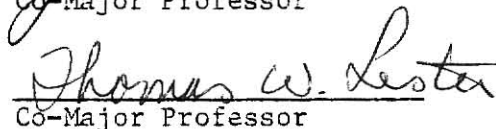
Department of Nuclear Engineering

KANSAS STATE UNIVERSITY
Manhattan, Kansas

1980

Approved by:


Co-Major Professor


Co-Major Professor

Spec. Coll.
LD
2668
.T4
1980
K52
C.2

TABLE OF CONTENTS

	<u>Page</u>
LIST OF FIGURES.	iii
LIST OF TABLES	vi
1.0 MODELING OF PULVERIZED COAL SUSPENSIONS	1
1.1 Introduction	1
1.2 General Conservation Equations	3
1.2.1 Gas-Phase Continuity.	5
1.2.2 Solid-Phase Continuity.	6
1.2.3 Gas-Phase Momentum.	6
1.2.4 Solid-Phase Momentum.	7
1.2.5 Gas-Phase Energy.	8
1.2.6 Solid-Phase Energy.	10
1.3 Simplified Forms of the Conservation Laws.	11
1.3.1 Common Simplifications.	12
1.3.2 Auxiliary Equations	13
1.3.3 Additional Simplifications.	14
1.4 Summary of Existing Solutions for Coal Suspensions.	16
2.0 THERMAL RADIATION TRANSPORT	19
2.1 Thermal Radiation.	19
2.2 The Equation of Radiative Transfer	20
2.2.1 The Extinction Coefficient.	23
2.2.2 The Source Function	23
2.3 Simplifications of the Equation of Transfer.	25
2.3.1 Steady State.	26
2.3.2 Local Thermodynamic Equilibrium	26
2.3.3 Plane-Symmetric Geometry.	27
2.3.4 Multi-Frequency Range Approximation	30
2.3.5 The Gray Case	33
2.3.6 No-Scattering Case.	34
2.3.7 No-Emission Case.	34
2.4 The Integrated Intensity and Net Flux Distributions.	35
2.5 Radiative Equilibrium.	36
2.6 Radiation Transport in Pulverized Coal Suspensions.	37
2.7 Summary.	40
3.0 RADIATIVE PROPERTIES OF MATERIALS IN PULVERIZED COAL COMBUSTION	42
3.1 Classes of Materials	42
3.2 Particulates	43
3.2.1 Absorption and Scattering Efficiencies.	43
3.2.2 Coal, Char, and Ash Particles	45
3.2.3 Soot Particles.	53
3.3 Combustion Gases	54
3.4 Combustor Walls.	57

TABLE OF CONTENTS - continued

	<u>Page</u>
4.0 SOLUTION OF THE EQUATION OF TRANSFER	60
4.1 The Equation of Transfer and Boundary Conditions. .	61
4.2 The Discrete Ordinates Method	64
4.2.1 Chandrasekhar's Method	64
4.2.2 A Numerical Discrete Ordinates Method. . . .	69
4.2.3 Evaluation of the Scattering Matrix.	74
4.3 Flux Methods.	75
4.4 The Diffusion Approximation	79
4.5 Solution of the Equation of Transfer when the Temperature is Unknown.	86
4.5.1 Energy Balance Relations	87
4.5.2 Summary of Solution Procedure for Coupled Temperature - Intensity Equations.	91
5.0 NUMERICAL EXAMPLES	93
5.1 Statement of the Problem.	93
5.2 The Energy Balance.	95
5.2.1 The Chemical Heat Generation Term.	97
5.2.2 The Inter-Species Conduction Term.	101
5.3 Dimensionless Form of the Energy Balance.	101
5.4 Calculation of the Equilibrium Temperature at a Fixed Point	104
5.5 Simultaneous Solution of the Energy Balance with the Equation of Transfer.	108
5.6 Simultaneous Solution with the Diffusion Equation.	113
5.7 Numerical Results	117
5.7.1 Testing the Computer Codes	117
5.7.2 Comparison of the Discrete Ordinates and Diffusion Results.	121
5.7.3 Effect of Scattering	125
5.7.4 Effect of Boundary Conditions.	128
5.7.5 Effect of Particle Size.	130
5.7.6 Effect of Conduction to Gas Phase.	132
5.7.7 Effect of Optical Thickness.	135
6.0 SUMMARY, CONCLUSIONS, AND RECOMMENDATIONS.	149
6.1 Summary and Conclusions	149
6.2 Recommendations for Further Study	152
7.0 REFERENCES	155
8.0 ACKNOWLEDGEMENTS	160
9.0 APPENDICES	161
9.1 RATREQ Computer Code.	161
9.2 DIFFEQ Computer Code.	161

LIST OF FIGURES

<u>Figure</u>		<u>Page</u>
2.1	The electromagnetic spectrum.	21
2.2	Coordinates in plane geometry	28
2.3	Discretization of the frequency range $(0, \infty)$ into N discrete intervals.	31
3.1	The scattering phase function for a large, diffusely reflecting, opaque sphere	47
3.2	Variation of the radiation efficiency factors for high carbon coal particles with the particle diameter.	49
4.1	Indexing of the discrete ordinates of an even quadrature set.	67
4.2	Discretization of the optical thickness ξ_t of a plane-symmetric medium into N-1 intervals ^t	70
5.1	Infinitely long combustion chamber model used in numerical examples	94
5.2	The rate of heat generation by chemical reaction as a function of the particle temperature	100
5.3	Determination of the equilibrium particle tempera- ture from the intersection of the displaced gene- ration function $H+\Psi$ and the emission function E . . .	105
5.4	Convergence of the iterative calculation of the equilibrium particle temperature.	107
5.5	Comparison of the temperature distribution calcu- lated by the discrete ordinates method and the diffusion approximation to result obtained by the solution of Usiskin and Sparrow ⁶⁴	119
5.6	Comparison of temperature distributions computed by the discrete ordinates method and by the diffusion approximation to a two-flux solution ¹⁶ . .	120
5.7	Comparison of the particle temperature and in- tegrated intensity distributions computed by RATREQ and DIFFEQ for a one-meter thick system	122

LIST OF FIGURES - continued

<u>Figure</u>		<u>Page</u>
5.8	Comparison of the particle temperature and integrated intensity distributions computed by RATREQ and DIFFEQ for a two-meter thick system	124
5.9	Effect of scattering on the particle temperature distributions	126
5.10	The effect of the backward-peaked phase function on the angular dependence of the radiation intensity. .	127
5.11	Effect of the wall temperature and reflectivity on the particle temperature distribution	129
5.12	Comparison of temperature distributions calculated for suspensions of different sized particles. .	131
5.13	Effect of the assumed gas temperature distribution and the heat generation rate on the computed particle temperature distribution	133
5.14	Particle temperature distributions for two different suspension optical thicknesses.	136
5.15	Variation of the maximum particle temperature with optical thickness in a suspension surrounded by cold, non-reflecting walls for two heat generation rates and two different gas temperatures	138
5.16	Effect of the activation energy on the variation of the maximum particle temperature with the system optical thickness	140
5.17	Variation of the maximum particle temperature with the optical thickness of the medium for different temperatures of the bounding walls.	142
5.18	The critical optical thickness as a function of wall temperature for different values of wall reflectivity.	143
5.19	Variation of the maximum particle temperature with the optical thickness of the medium for different values of the wall reflectivity	145

LIST OF FIGURES - continued

<u>Figure</u>		<u>Page</u>
5.20	The critical optical thickness as a function of wall reflectivity for several values of the wall temperature.	146
5.21	Maximum particle temperature as a function of system optical thickness computed by the discrete ordinates (RATREQ) and the diffusion equation (DIFFEQ) solutions	147

LIST OF TABLES

<u>Table</u>		<u>Page</u>
3.1	The extinction and scattering efficiencies and the single scatter albedo for different sized coal particles,	51
3.2	The extinction and scattering efficiencies and the single scatter albedo as a function of the assumed particle refractive index, $m=\eta(1-i\kappa)$	52

1.0 MODELING OF PULVERIZED COAL SUSPENSIONS

1.1 Introduction

At the elevated temperatures normally encountered in combustion chambers, thermal radiation is the dominant mode of energy transfer.^{1,2} Therefore, a successful prediction of combustor performance, which requires knowledge of the temperature and heat flux distributions, must be based on a realistic model of radiant energy transfer in the system. The radiation transport in systems fired with pulverized coal has recently received considerable attention³⁻⁵ because of the expected increase in the importance of coal to meet world energy needs.

A pulverized coal flame is a non-uniform, multi-component, gas-particle cloud which generates heat by chemical reaction. The presence of coal and char particles (whose sizes are greater than or comparable to the wavelengths of thermal radiation) causes the reacting suspension to scatter, as well as absorb and emit radiant energy.⁶ Unfortunately, the majority of flame radiation studies have been restricted to non-scattering gaseous flames⁷⁻⁹, or to flames containing very small carbon particles (soot) for which scattering is negligible relative to emission and absorption.^{10,11} Simple computational methods which are used to determine the radiant energy transfer in non-scattering media (e.g., Bouguer's law,¹² Hottel's zone method¹³) are generally not applicable to media in which scattering is significant.

A number of additional factors contribute to the difficulty of the radiative transfer problem in pulverized coal combustion.

These factors include the complexity of coal composition and its associated reactions,¹⁴ the non-uniformity of the reacting system,¹⁵ and the serious lack of knowledge of many system properties¹⁶ (e.g., optical properties of coal particles at combustion temperatures and thermal radiation wavelengths). Furthermore, the equations which describe the radiative interchange are coupled with equations governing the conservation of energy, mass, and momentum for each component in the gas-particle mixture. Consequently, a large number of unknowns is required to describe completely the system. This description of a coal suspension yields a formidable set of coupled differential equations whose solution has never been attempted for the most general case.⁴

A number of simpler computational models have been developed to determine the composition, velocity, temperature, and radiant flux distributions in propagating coal dust flames.^{5,15,17,18} These models are based on a wide range of simplifications of the general conservation laws, with the overall treatment ranging from very simple to very complex. The treatment of radiative heat transfer is highly approximate and often unrealistic. The scattering of radiation is commonly neglected despite its significance in media which contain dispersed particles of sizes greater than, or comparable to, the wavelengths of the radiation.¹² Models which do allow for scattering generally are based on approximate forms of the radiative transfer equation (e.g., flux methods and the diffusion approximation). For these approximate

radiative transfer models, the emission of thermal energy is often neglected for added simplicity, even though it is of major importance at combustion temperatures. Finally, most existing radiation models for which solutions have been obtained neglect radiative heat losses at the combustor walls by assuming that radiant energy is transferred only along the propagation direction of the coal dust cloud, and therefore, transverse radiation leakage from the system is neglected.

In this work, a more sophisticated treatment of radiant heat exchange in chemically reacting coal suspensions is presented. The radiative transfer equation is solved for the detailed variation of the radiation field in an absorbing, emitting, and multiply-scattering medium. The effects of scattering, anisotropic scattering, and conditions at the combustor boundaries on computed temperature and heat flux distributions are examined. A detailed description of the radiative transfer equation and its solution in pulverized coal systems is presented in the following chapters. The remainder of this chapter is devoted to the presentation of the general form and common simplifications of the conservation laws appropriate to pulverized coal media. In addition, a number of solution models and their treatment of the radiant energy exchange are reviewed.

1.2 General Conservation Equations

Generalized mass, momentum, and energy conservation equations for gas-particle mixtures are given in references 4, 19-22. Specific forms applicable to coal dust clouds undergoing chemical reactions are

presented here. The equations are written separately for the gas phase (which is a mixture of various gaseous species) and for the solid phase (which is composed of particles with a distribution of sizes). The mass, momentum, and energy conservation equations for the two-phase mixture can be obtained by addition of the corresponding equations for the two separate phases.

The basic conservation laws for any medium property can be derived with the aid of the Reynolds Transport Theorem, which relates the Lagrangian and Eulerian descriptions of the motion of a fluid. For an arbitrary control volume cv surrounded by the control surface cs , the Reynolds Transport Theorem may be expressed as^{4,23}

$$\frac{d}{dt} (m\beta) = \frac{\partial}{\partial t} \int_{cv} \rho\beta dV + \int_{cs} \rho\beta \vec{v} \cdot d\vec{A}. \quad (1.1)$$

In this equation, β is an intensive property (property per unit mass) of the fluid element that occupies the control volume at time t , $d\vec{A}$ is the differential area vector in the direction of the outward normal to the control surface, and m , ρ , and \vec{v} are, respectively, the mass, the mass density, and the velocity of the fluid element. The theorem states that the instantaneous rate of change of any extensive property of the fluid element, $m\beta$, is equal to its rate of change within the control volume plus its net efflux across the control surface at the instant the fluid element occupies the control volume. It should be noted that the derivative appearing in the left side of equation (1.1) is a substantial derivative, since both local and convective changes contribute to the time rate of change of the extensive property $m\beta$ of the fluid element.

1.2.1 Gas-Phase Continuity

The Reynolds Transport Theorem is applied with $\beta=1$ and with $\rho=\rho_g$, where ρ_g is the mass of gas per unit volume of the gas-particle mixture (i.e., the bulk density). The resulting equation is

$$\frac{dm}{dt} = \frac{\partial}{\partial t} \int_{cv} \rho_g dV + \int_{cs} \rho_g \vec{v}_g \cdot d\vec{A}. \quad (1.2)$$

The rate of increase of gaseous mass $\frac{dm}{dt}$ can be related to the volumetric rate of solid particle consumption r_p by

$$\frac{dm}{dt} = \int_{cv} r_p dV. \quad (1.3)$$

Substitution of Eq. (1.3) into Eq. (1.2) and use of the divergence theorem²⁴ to convert the surface integral to a volume integral yields

$$\frac{\partial \rho_g}{\partial t} + \nabla \cdot (\rho_g \vec{v}_g) = r_p, \quad (1.4)$$

where the volume integrals have been dropped because the volume of integration is arbitrary.

If the gas phase is composed of a mixture of gaseous species, the gas velocity \vec{v}_g and bulk density ρ_g are expressed in terms of the individual gas velocities and densities by⁴

$$\vec{v}_g = \frac{1}{\rho_g} \sum_i \rho_{gi} \vec{v}_{gi} \quad (1.5)$$

$$\rho_g = \sum_i \rho_{gi}, \quad (1.6)$$

where ρ_{gi} and \vec{v}_{gi} are the bulk density and the velocity of gas i , respectively.

1.2.2 Solid-Phase Continuity

Application of Eq. (1.1) to the conservation of mass of the particulate phase in the pulverized coal cloud yields^{19,20}

$$\frac{\partial \rho_p}{\partial t} + \nabla \cdot (\rho_p \vec{v}_p) = -r_p, \quad (1.7)$$

where ρ_p , \vec{v}_p , and r_p are the particle bulk density, the particle velocity, and the rate of consumption of the coal particles per unit volume of the mixture, respectively. For a cloud with a distribution of particle sizes, these quantities are related to those of particles in each size class k by the relations⁴

$$\vec{v}_p = \frac{1}{\rho_p} \sum_k \rho_{pk} \vec{v}_{pk} \quad (1.8)$$

$$\rho_p = \sum_k \rho_{pk} \quad (1.9)$$

$$r_p = \sum_k r_{pk}. \quad (1.10)$$

1.2.3 Gas-Phase Momentum

Setting the quantity β in Eq. (1.1) equal to the gas momentum per unit mass (i.e., the gas velocity \vec{v}_g) yields

$$\frac{d}{dt} (m \vec{v}_g) = \frac{\partial}{\partial t} \int_{cv} \rho_g \vec{v}_g dV + \int_{cs} \rho_g \vec{v}_g \vec{v}_g \cdot d\vec{A}, \quad (1.11)$$

in which the left side is simply the rate of change of momentum of the gaseous species in the fluid element. This rate of change is given by Newton's second law as the sum of the forces acting on the gas (i.e., pressure forces, viscous forces, gravitational forces, etc.). Substitution for these forces in the left side of Eq. (1.11), and

use of the divergence theorem yields the gas-phase momentum equation. This equation may be written^{4,19}

$$\begin{aligned} \frac{\partial}{\partial t} (\rho_g \vec{v}_g) + \nabla \cdot (\rho_g \vec{v}_g \vec{v}_g) = -\nabla p + \nabla \cdot (1-\theta) \underline{\tau}_s + \nabla \cdot \theta \underline{\tau} - \vec{f}_p \\ + \rho_g \vec{g} + \sum_k r_{pk} \vec{v}_{pk}, \end{aligned} \quad (1.12)$$

where P is the pressure, $\underline{\tau}_s$ is the shear stress at the gas-particle interface, $\underline{\tau}$ is the shear stress tensor attributed to the gas viscosity (and includes the stress due to gaseous species interdiffusion), \vec{f}_p is the aerodynamic force on the particles per unit volume of the gas-particle mixture, and \vec{g} is the gravitational acceleration. The quantity θ is the void fraction defined as the volume occupied by the gas per unit volume of the mixture.

The left side of Eq. (1.12) represents the total rate of gain of momentum by the gas phase per unit volume. The first three terms on the right side are, respectively, the pressure force per unit volume, the rate of momentum gain per unit volume by viscous transfer at the gas-particle interface, and the rate of momentum increase by viscous transfer (in the gas phase) per unit volume. The last two terms of Eq. (1.12) are the gravitational force per unit volume, and the volumetric rate of momentum addition to the gas phase due to particle combustion.

1.2.4 Solid-Phase Momentum

As with the gas-phase momentum equation, the momentum equation of a cloud of particles is obtained by application of Eq. (1.1) in conjunction with Newton's second law and the divergence theorem. Neglecting inter-particle collisions, the particle momentum equation may be written^{4,19,20}

$$\begin{aligned} \frac{\partial}{\partial t} (\rho_p \vec{v}_p) + \nabla \cdot (\rho_p \vec{v}_p \vec{v}_p) + \sum_k \nabla \cdot (\rho_{pk} \delta \vec{v}_{pk} \delta \vec{v}_{pk}) = \\ - \sum_k r_{pk} \vec{v}_{pk} + \vec{f}_p + \rho_p \vec{g}. \end{aligned} \quad (1.13)$$

The quantity $\delta \vec{v}_{pk}$ is the diffusion velocity of particles in the k^{th} size class and is defined by

$$\delta \vec{v}_{pk} = \vec{v}_{pk} - \vec{v}_p. \quad (1.14)$$

The last term on the left side of Eq. (1.13) represents the rate of momentum addition per unit volume associated with the motion of the particles about their mass-averaged velocity \vec{v}_p . This term is analogous to the stress due to species interdiffusion that is encountered in the gas-phase momentum equation. The first term on the right side is the rate of momentum gain per unit volume due to particle combustion, and the last two terms are the aerodynamic and gravitational forces on the particles per unit volume.

1.2.5 Gas-Phase Energy

The Reynolds Transport Theorem [Eq. (1.1)] is written with β equal to the total energy of the gas per unit mass, i.e.,

$$\beta = e_g + v_g^2/2, \quad (1.15)$$

where e_g is the internal energy of the gas per unit mass, and v_g is the gas speed. The potential energy contribution to the total energy of the gas is neglected. Combination of Eq. (1.1) with the first law of thermodynamics and substitution for the work and heat

transfer terms yields the gas-phase energy equation:^{4,19,20}

$$\begin{aligned}
 \frac{\partial}{\partial t} [\rho_g (e_g + v_g^2/2)] + \nabla \cdot [\rho_g (h_g + v_g^2/2) \vec{v}_g] = \\
 -\nabla \cdot \theta \vec{q} + Q_{cp} - Q_{rg} + \sum_k r_{pk} \left(h_{gs} + \frac{v'_{gs}{}^2}{2} + \frac{v_p^2}{2} \right)_k \\
 -\nabla \cdot [(1-\theta) P \vec{v}_p] + \nabla \cdot [\theta \underline{\tau} \cdot \vec{v}_g + (1-\theta) \underline{\tau}_s \cdot \vec{v}_p] \\
 - \sum_k \vec{v}_{pk} \cdot \vec{f}_{pk} + \rho_g \vec{g} \cdot \vec{v}_g + P_s \dot{V}.
 \end{aligned} \tag{1.16}$$

In this equation, \vec{q} is the net heat transferred by conduction and species interdiffusion, and Q_{rg} and Q_{cp} are the volumetric rates of energy loss by radiation and energy gain by convection (from the particulate phase), respectively. The quantities h_g and h_{gs} are the gas enthalpy and the average gas enthalpy at the particle surface, respectively. The speed v'_{gs} is given by

$$v'_{gs} = |\vec{v}_{gs} + \vec{r}|, \tag{1.17}$$

where \vec{v}_{gs} is the gas velocity at the particle surface relative to the particle's center of mass, and \vec{r} is the surface regression velocity of the particle. Finally, P_s is the average pressure over the particle surface, and \dot{V} is the rate of change of total particle volume per unit volume of the mixture.

The first term on the right side of Eq. (1.16) is the rate of energy transfer per unit volume by gas phase conduction and species interdiffusion. The second and third terms represent the energy gains per unit volume by convection from the dispersed particles

and by radiation, respectively. The next three terms are the volumetric rate of energy addition to the gas phase due to particle consumption, the rate of work done on the gas per unit volume due to the pressure forces at the surface of the particles, and the rate of work done on the gas per unit volume by viscous forces. The seventh and eighth terms are the rates of work done on the gas per unit volume by aerodynamic forces and gravitational forces, respectively. Finally, the last term is the rate of work done on the gas per unit volume due to the swelling or shrinking of the dispersed particles.

For a mixture of gaseous species, overall properties are defined in terms of the properties of the i^{th} species by⁴

$$e_g = \frac{1}{\rho_g} \sum_i \rho_{gi} e_{gi} \quad (1.18)$$

$$h_g = \frac{1}{\rho_g} \sum_i \rho_{gi} h_{gi} \quad (1.19)$$

$$v_g^2 = \frac{1}{\rho_g} \sum_i \rho_{gi} v_{gi}^2 \quad (1.20)$$

$$\tau \cdot v_g = \frac{1}{\rho_g} \sum_i \tau_i \cdot \vec{v}_{gi} \quad (1.21)$$

1.2.6 Solid-Phase Energy

Combining the Reynolds Transport Theorem (with β equal to the solid phase energy per unit mass) and the first law of thermodynamics yields the solid phase energy equation^{4,19}

$$\begin{aligned}
& \frac{\partial}{\partial t} [\rho_p (e_p + v_p^2/2)] + \nabla \cdot [\rho_p \vec{v}_p (e_p + v_p^2/2)] + \\
& \nabla \cdot [\sum_k \rho_{pk} \delta \vec{v}_{pk} (e_{pk} + \frac{v_{pk}^2}{2})] = - \sum_k r_{pk} \left(h_{gs} + \frac{v_p^2}{2} + \frac{v_{gs}^2}{2} \right)_k \\
& + \sum_k \vec{v}_{pk} \cdot \vec{f}_{pk} + \vec{g} \cdot \sum_k \rho_{pk} \vec{v}_{pk} - Q_{cp} - Q_{rp} - P_s \dot{V}, \quad (1.22)
\end{aligned}$$

where

$$e_p = \frac{1}{\rho_p} \sum_k \rho_{pk} e_{pk}, \quad (1.23)$$

and

$$v_p^2 = \frac{1}{\rho_p} \sum_k \rho_{pk} v_{pk}^2. \quad (1.24)$$

The quantities e_{pk} and v_{pk} are the internal energy (including surface energy) and the speed of particles in the k^{th} size class, respectively, and Q_{rp} is the volumetric rate of energy loss by radiation.

The last term on the left side of Eq. (1.22) is the rate of energy transfer per unit volume associated with the motion of the particles about their mass-averaged velocity. The first term on the right side is the volumetric rate of energy gain due to particle consumption, while the second and third terms are the rates of work done per unit volume by aerodynamic forces and gravitational forces, respectively. The last three terms represent the volumetric rates of heat transfer by convection from the gas phase, of energy gain by radiation, and of work done on the particles by pressure forces due to particle swelling or shrinking.

1.3 Simplified Forms of the Conservation Laws

The general equations presented in the preceding section are

extremely complex and contain a large number of independent and dependent variables. No solution of these general three-dimensional, time-dependent equations has been attempted to date. Several simplifying assumptions are invariably introduced to reduce the dimensionality of the equations and eliminate a number of the unknowns. Furthermore, a number of auxiliary equations are needed to obtain a closed system of equations.

1.3.1 Common Simplifications

The continuity, momentum, and energy equations can be simplified somewhat by setting the void fraction of coal dust cloud, θ , equal to unity. This approximation is well justified because the volume occupied by the particulate matter in the two-phase mixture is typically less than 0.01% of the total volume.⁴ In addition, the complexity of the equations is reduced greatly if it is assumed that the particles in all size classes move at the same local velocity (i.e., $\vec{v}_{pk} = \vec{v}_p$, and $\delta\vec{v}_{pk} = 0$). With these simplifications, the conservation equations become

$$\frac{\partial \rho_g}{\partial t} + \nabla \cdot (\rho_g \vec{v}_g) = r_p \quad (\text{gas continuity}) \quad (1.25)$$

$$\frac{\partial \rho_p}{\partial t} + \nabla \cdot (\rho_p \vec{v}_p) = -r_p \quad (\text{particle continuity}) \quad (1.26)$$

$$\begin{aligned} \rho_g \frac{\partial \vec{v}_g}{\partial t} + \rho_g \vec{v}_g \cdot \nabla \vec{v}_g &= -\nabla P + \nabla \cdot \underline{\underline{\tau}} - \vec{f}_p \\ &+ \rho_g \vec{g} + (\vec{v}_p - \vec{v}_g) r_p \quad (\text{gas momentum}) \end{aligned} \quad (1.27)$$

$$\rho_p \frac{\partial \vec{v}_p}{\partial t} + \rho_p \vec{v}_p \cdot \nabla \vec{v}_p = \vec{f}_p + \rho_p \vec{g} \quad (\text{solid momentum}) \quad (1.28)$$

$$\begin{aligned}
\rho_g \frac{\partial}{\partial t} \left(h_g + \frac{v_g^2}{2} \right) + \rho_g \vec{v}_g \cdot \nabla \left(h_g + \frac{v_g^2}{2} \right) = & - \frac{\partial P}{\partial t} - \nabla \cdot \vec{q} + Q_{cp} - Q_{rg} \\
+ \sum_k r_{pk} \left[\left(h_{gs} + \frac{v_{gs}^2}{2} + \frac{v_p^2}{2} \right)_k - \left(h_g + \frac{v_g^2}{2} \right) \right] - \nabla \cdot (\underline{\tau} \cdot \vec{v}_g) \\
- \vec{v}_p \cdot \vec{f}_p + \rho_g \vec{g} \cdot \vec{v}_g + P_s \dot{V} \quad (\text{gas energy})
\end{aligned} \tag{1.29}$$

$$\begin{aligned}
\rho_p \frac{\partial}{\partial t} \left(e_p + \frac{v_p^2}{2} \right) + \rho_p \vec{v}_p \cdot \nabla \left(e_p + \frac{v_p^2}{2} \right) = & \sum_k r_{pk} \left[e_p - \left(h_{gs} + \frac{v_{gs}^2}{2} \right)_k \right] \\
+ \vec{v}_p \cdot \vec{f}_p + \rho_p \vec{g} \cdot \vec{v}_p - Q_{cp} - Q_{rp} - P_s \dot{V} \quad (\text{particle energy}).
\end{aligned} \tag{1.30}$$

The momentum and energy equations [Eqs. (1.25)-(1.28)] have been written with the aid of the relations:

$$\frac{\partial}{\partial t} (\beta_g \rho_g) = \rho_g \frac{\partial \beta_g}{\partial t} + \rho_g \vec{v}_g \cdot \nabla \beta_g - \nabla \cdot \rho_g \beta_g \vec{v}_g + \beta_g r_p \tag{1.31}$$

and

$$\frac{\partial}{\partial t} (\beta_p \rho_p) = \rho_p \frac{\partial \beta_p}{\partial t} + \rho_p \vec{v}_p \cdot \nabla \beta_p - \nabla \cdot \rho_p \beta_p \vec{v}_p - \beta_p r_p, \tag{1.32}$$

in which β_g and β_p are arbitrary intensive properties of the gas and solid phases, respectively. Equations (1.31) and (1.32) are easily verified using the continuity equation for each phase.

1.3.2 Auxiliary Equations

Equations (1.27)-(1.30) are a set of 10 equations in $31 + 8$ NS unknowns, where NS is the total number of particle size classes.

Auxiliary equations relating the unknowns to each other or to known system properties are therefore needed. The auxiliary equations give the gas physical properties and transport coefficients, the solid-phase physical properties, the chemical reaction rates, and

the heat transfer rates. The calculation of the radiation heat loss terms (Q_{rg} and Q_{rp}) is discussed in detail in Chapter 2, and the remaining auxiliary equations are listed and discussed in References 4 and 16. In these equations, the overall gas properties are computed from those of the individual gaseous species and related to conditions of temperature, pressure, etc. The solid phase is assumed to contain char, ash, volatiles, and moisture, and overall solid phase properties are computed from those of the individual components for each particle size class. Finally, the equations account for a complete sequence physio-chemical processes including devolatilization, gas phase hydrocarbon oxidation, moisture vaporization, and char oxidation.

Complete specification of the problem also requires a number of boundary conditions and initial conditions. The boundary conditions generally specify a linear combination of each unknown and its gradient at the system boundaries.¹⁹ Initial conditions specify the system properties at time $t=0$.

1.3.3 Additional Simplifications

Most investigators have modeled propagating pulverized coal flames by assuming that the properties of the two-phase mixture vary in a one-dimensional manner along the direction of propagation.^{5,15,17,18} This one-dimensional treatment is valid if the flame can be considered infinite in extent normal to the direction of propagation (i.e., a plane flame), or if sufficient mixing occurs that the flame is homogeneous over any cross section perpendicular to the flow. Furthermore, the momentum equations are eliminated based on the following assumptions:

- a) Body forces are negligible
- b) Viscous dissipation is negligible
- c) Pressure is uniform in the gas phase
- d) Relative motion between the coal particles and the gaseous species is negligible, and hydrodynamic forces (primarily drag) can therefore be neglected.

The conservation laws are further simplified by assuming that the inlet particle suspension is monodisperse, that the flow is low-speed, that the heat capacity of each phase is constant, and that system properties are time independent. Equations (1.25)-(1.30) become

$$\frac{d}{dz} (\rho_g v) = r_p \quad (\text{gas continuity}) \quad (1.33)$$

$$\frac{d}{dz} (\rho_p v) = - r_p \quad (\text{particle continuity}) \quad (1.34)$$

$$\rho_g v c_g \frac{dT_g}{dz} = - \frac{dq}{dz} + Q_{cp} - Q_{rg} + H_g \quad (\text{gas energy}) \quad (1.35)$$

$$\rho_p v c_p \frac{dT_p}{dz} = - Q_{cp} - Q_{rp} + H_p \quad (\text{particle energy}), \quad (1.36)$$

where the flow is along the z-axis, v is the flow speed, and c_g and c_p are the heat capacities (at constant pressure) of the gas and solid phases, respectively. The terms H_g and H_p are the volumetric rates of heat release to the gas and particle phases, respectively, due to the surface burning of the coal particles. These quantities are defined by [cf. Eqs. (1.29) and (1.30)].

$$H_g = (h_{gs} - h_g) r_p \quad (1.37)$$

$$H_p = (e_p - h_{gs}) r_p. \quad (1.38)$$

The evaluation of the particle burning rate r_p is simplified enormously if the particles are assumed to contain negligible amounts of volatiles and moisture. In this case, only the heterogeneous reaction of carbon with oxygen needs to be considered.¹⁶ Generally, only the reactions $C + 1/2 O_2 \rightarrow CO$ and $C + O_2 \rightarrow CO_2$ are considered.^{5,16,18}

1.4 Summary of Existing Solutions for Coal Suspensions

Essenhig and Csaba¹⁷ considered a plane flame which is at uniform temperature (the ignition temperature) and is decoupled from the pre-ignition zone. The coal particles in the pre-ignition zone are heated by radiant energy transfer from the flame, and part of this energy is transferred to the gas by convection. The gas phase conduction term $\frac{dq}{dz}$ is neglected. Analytical expressions are obtained for the spatial variation of the gas and particle temperatures, with the ignition temperature and the length of the pre-ignition zone as parameters. Special forms of these expressions are given for the cases $T_p = T_g$ (i.e., infinite heat transfer rate between the two species) and $T_g = \text{constant}$ (i.e., infinite gas heat capacity). The treatment of radiative heat transfer is very approximate, as both scattering and thermal emission are neglected in the pre-ignition zone. The thermal energy emitted by the flame is attenuated in the pre-ignition zone according to Bouguer's law.¹²

Bhaduri and Bandyopadhyay¹⁸ have determined the axial variation of composition and temperature for plane flame and jet flame models. They assumed that particles and the gas have the same

local temperature (i.e., $Q_{cp} = 0$), and that the particle diameter decreases linearly with position along the flame axis. Heat conduction by the gas phase is neglected (i.e., $\frac{dq}{dz} = 0$). The entire system is assumed adiabatic, and thermal radiation and chemical energy release are spent exclusively in heating the two-phase mixture. The treatment of radiation is similar to that of Essenhigh and Csaba, with both scattering and thermal energy emission neglected. Again, Bouguer's law is used to compute the attenuation of the radiant energy in the system.

In the model of Krazinski et al.⁵, the gas and solid phases are allowed to have differing temperatures, and the gas phase conduction term $\frac{dq}{dz}$ is retained. Part of the heat generated by chemical reaction is released into the particulate phase with the remainder released in the gaseous phase. The exact partition of heat release between the two phases is unknown, but it is estimated that roughly 30% of the total heat of reaction is delivered to the particles. The particle burning rate r_p is controlled by both chemical kinetics at the particle surface and diffusion of oxygen to the particle surface. Radiant energy transfer is computed using the diffusion approximation of the radiative transfer equation, which allows for scattering, absorption, and thermal energy emission. The basic limitation of this work is the neglect of radiant energy losses at the system boundaries.

Smoot et al.¹⁵ considered a more complex model of reacting coal dust suspensions. Effects of gaseous species diffusion, coal pyrolysis, gas phase volatiles reactions, and char oxidation on the propagation of pulverized coal-air mixtures are included. The variation of the

gas and particle temperatures, the mass fractions of the gaseous species, and the diameter of the coal particles with distance along the flame are computed. The gas heat capacity, density, and transport coefficients are not assumed constant and are computed as functions of the gas composition, which varies with position in the system. Although the model is more sophisticated in its description of the reacting mixture, it is of limited usefulness because radiative heat transfer is neglected entirely, and because the system is assumed to be adiabatic.

A number of investigators have considered simple one-dimensional models to compute the spatial variation of the temperature and radiation intensity distributions in the direction normal to the propagation direction. For example Field et al.¹⁶ considered a reacting pulverized coal suspension bounded by infinite, parallel, flat walls. The energy release rate (due to chemical reaction) and the non-radiative energy loss rates are assumed a priori, and therefore the conservation equations are reduced to a simple energy balance which must be solved simultaneously with the radiation equations. Models of this type can be used to study the effects of scattering, particle size, wall temperature, and the rates of heat generation on the temperature and intensity distributions, as well as on the energy loss rates at the system boundaries.

2.0 THERMAL RADIATION TRANSPORT

Calculation of the radiant heat loss terms by the gas and solid phases in a pulverized coal suspension requires evaluation of the thermal radiation intensity throughout the medium. The radiation intensity distribution in an absorbing, emitting, and scattering medium can be determined by solution of the radiative transfer equation. In this chapter, the general form and common simplifications of the equation of transfer are presented, and the evaluation of the radiant heat loss terms Q_{rg} and Q_{rp} in the gas and solid phase energy balances is discussed. The dual nature of radiant energy as electromagnetic waves and particles (photons) is recognized, and both the classical electromagnetic wave and the quantum mechanical particle viewpoints are used in the description of radiant energy emission and propagation in a medium.

2.1 Thermal Radiation

All substances constantly emit electromagnetic radiation as a result of atomic and molecular agitation associated with the internal energy of the material.²⁵ The mechanisms by which electromagnetic radiation is produced include conversion of matter to radiant energy, deceleration of energetic charged particles, electronic transitions, and changes in the vibrational-rotational energy states of molecules. Depending on the production mechanism, the emitted radiation can vary greatly in frequency ν from radiowaves ($\nu \leq 10^6 \text{ s}^{-1}$) to cosmic rays ($\nu \geq 10^{22} \text{ s}^{-1}$).

Thermal radiation constitutes a small part of the spectrum over which energy can be transmitted by electromagnetic waves and is confined to the frequency range of roughly 10^{11} s^{-1} to 10^{15} s^{-1} ,² as shown in Fig. 2.1. This radiation is emitted by matter by virtue of its temperature and is generally detectable as heat or light. Gaseous bodies emit thermal energy which is confined to a number of single frequencies (line spectra) or to bands of frequencies that result from the overlap of a number of lines (band spectra). This thermal emission from gases is caused either by electronic transitions in the visible region of the spectrum or by vibrational-rotational molecular transitions in the infrared. Solid bodies are characterized by much higher densities of atoms or molecules, and the large number of possible transitions causes the emission by solids to be continuous over a wide range of frequencies.²⁵ Thermal emission from solids is a result of lattice vibrations in the far infrared, and molecular vibrations and bound electron transitions in the near infrared.

2.2 The Equation of Radiative Transfer

Radiative transfer encompasses all phenomena that involve the propagation and interaction of electromagnetic radiation in a medium. The fundamental quantity which describes the radiation field is the specific radiation intensity (or simply the intensity), $I_{\nu}(\vec{r}, \vec{\Omega}, t)$, which may be defined as

$$I_{\nu}(\vec{r}, \vec{\Omega}, t) \equiv h\nu c n(\vec{r}, \vec{\Omega}, \nu, t). \quad (2.1)$$

**THIS BOOK
CONTAINS
NUMEROUS PAGES
WITH DIAGRAMS
THAT ARE CROOKED
COMPARED TO THE
REST OF THE
INFORMATION ON
THE PAGE.**

**THIS IS AS
RECEIVED FROM
CUSTOMER.**

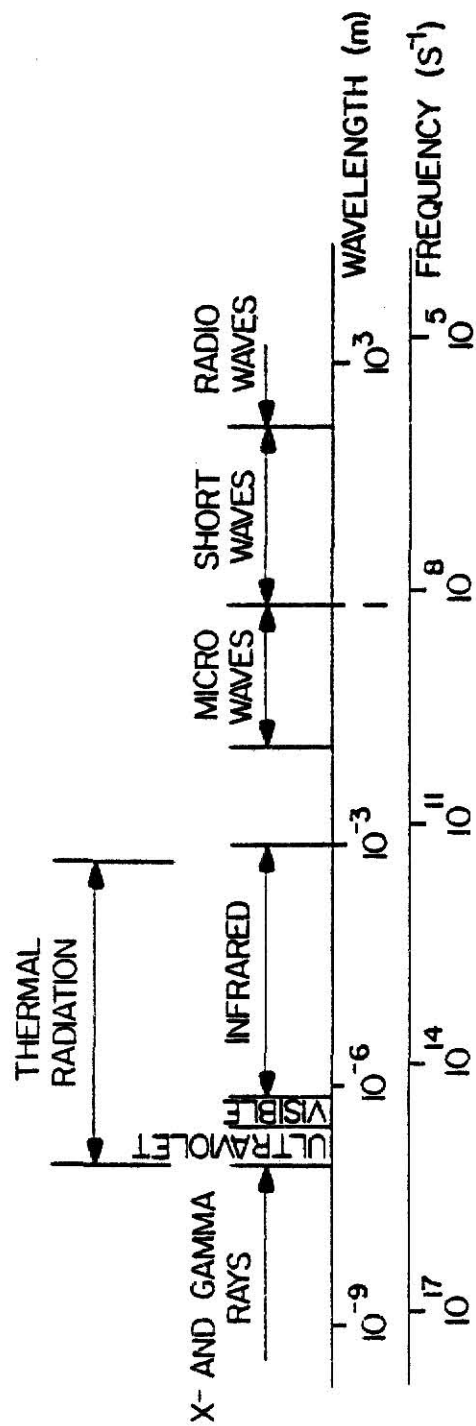


Fig. 2.1. The electromagnetic spectrum.

In this equation, h is Planck's constant, c is the photon speed (i.e., the speed of light in the medium), and $n(\vec{r}, \vec{\Omega}, \nu, t)$ is the photon angular density. This angular density is defined as the expected number of photons per unit volume about the point \vec{r} , per unit frequency about ν , traveling at time t in a unit solid angle about the direction $\vec{\Omega}$. From Eq. (2.1), it may be seen that the intensity is the product of the energy per photon ($h\nu$), the photon speed (c), and the photon angular density (n), and therefore the intensity can be interpreted as an energy angular flux, i.e., the energy crossing a unit area perpendicular to $\vec{\Omega}$ in a unit time at point \vec{r} .

The radiative transfer equation expresses the change of the radiation intensity with position and time in a medium that absorbs, scatters, and emits photons. This equation has been derived by Chandrasekhar,²⁶ Sobolev,²⁷ Kourganoff,²⁸ and others by equating the net gain of radiant energy by a beam of photons to the total rate of change in the beam's intensity. Upon neglecting effects of polarization and photon-photon collisions, the equation of transfer may be written

$$\left[\frac{1}{c} \frac{\partial}{\partial t} + \vec{\Omega} \cdot \nabla + \sigma_{ev}(\vec{r}, t) \right] I_{\nu}(\vec{r}, \vec{\Omega}, t) = \Gamma_{\nu}(\vec{r}, \vec{\Omega}, t), \quad (2.2)$$

where $\sigma_{ev}(\vec{r}, t)$ is the extinction coefficient, and $\Gamma_{\nu}(\vec{r}, \vec{\Omega}, t)$ is the source function. The extinction coefficient represents the probability per unit differential path length of the medium of all processes which remove radiant energy from a beam of photons. The source function is the radiant energy that is added to the beam per unit frequency about ν ,

per unit solid angle about $\vec{\Omega}$, per unit volume, and per unit time. Equation (2.2) therefore states that the total rate of change of the intensity is simply the difference between the energy added and the energy removed from a beam of radiation per units of volume, solid angle, frequency, and time.

2.2.1 The Extinction Coefficient

In general, both absorption and scattering of photons contribute to the attenuation of a beam of radiation.²⁹ The extinction coefficient σ_{ev} can therefore be related to the absorption coefficient σ_{av} and the scattering coefficient σ_{sv} by

$$\sigma_{ev}(\vec{r}, t) = \sigma_{av}(\vec{r}, t) + \sigma_{sv}(\vec{r}, t). \quad (2.3)$$

The absorption and scattering coefficient are the probabilities that a photon of frequency ν will be absorbed or scattered, respectively, per unit differential path length at point \vec{r} and at time t . If the photon frequency remains unchanged after a scattering event, the scattering is termed elastic. Photons may also undergo inelastic scattering, and the photon frequency changes by some $\Delta\nu$, where $h\Delta\nu$ is the energy lost or gained by the "target" particle.

2.2.2 The Source Function

Radiation inscattering and thermal energy emission are sources of energy to a beam of radiation, and hence the source function $\Gamma_\nu(\vec{r}, \vec{\Omega}, t)$ is composed of an elastic scattering contribution and an emission contribution. Inelastic scattering processes (e.g., Compton

scattering and Raman Scattering) are usually negligible in the transport of thermal radiation, and therefore no frequency changes occur as a result of scattering. With the assumption of elastic scattering as the sole scattering process, the source function may be written as

$$\Gamma_v(\vec{r}, t) = \frac{\sigma_{sv}(\vec{r}, t)}{4\pi} \int_{4\pi} I_v(\vec{r}, \vec{\Omega}', t) p_v(\vec{\Omega}' \rightarrow \vec{\Omega}, \vec{r}, t) d\Omega' + E_v(\vec{r}, \vec{\Omega}, t), \quad (2.4)$$

where $p_v(\vec{\Omega}' \rightarrow \vec{\Omega}, \vec{r}, t)$ is the scattering phase function defined as the probability at point \vec{r} and time t that a beam of radiation of frequency ν moving in the direction $\vec{\Omega}'$ will be scattered into unit solid angle about the direction $\vec{\Omega}$. The term $E_v(\vec{r}, \vec{\Omega}, t)$ in Eq. (2.4) is the emission coefficient and is the energy added to the beam per unit volume, frequency, solid angle, and time.

In general, the scattering phase function p_v depends on both the initial and final directions in a scattering event (i.e., the directions $\vec{\Omega}'$ and $\vec{\Omega}$, respectively). However, the phase function in most media is rotationally invariant and depends only on the angle θ between the initial and final directions ($\cos\theta = \vec{\Omega} \cdot \vec{\Omega}'$). With the assumption of rotational invariance, the phase function is denoted by $p_v(\vec{\Omega} \cdot \vec{\Omega}', \vec{r}, t)$.

It should be noted that in order to conserve radiant energy, the phase function must satisfy the constraint³⁰

$$\frac{1}{4\pi} \int_{4\pi} p_v(\vec{\Omega} \cdot \vec{\Omega}', \vec{r}, t) d\Omega = 1. \quad (2.5)$$

The phase function is thus equal to unity for the case of isotropic scattering, and hence p_v may be interpreted as the ratio of the scattered intensity in a given direction to the scattered intensity in the same direction if scattering were isotropic.

2.3 Simplifications of the Equation of Transfer

The general form of the radiative transfer equation may be written using Eqs. (2.3) and (2.4) as

$$\begin{aligned} & \left[\frac{1}{c} \frac{\partial}{\partial t} + \vec{\Omega} \cdot \nabla + \sigma_{av}(\vec{r}, t) + \sigma_{sv}(\vec{r}, t) \right] I_v(\vec{r}, \vec{\Omega}, t) \\ &= \frac{\sigma_{sv}(\vec{r}, t)}{4\pi} \int_{4\pi} I_v(\vec{r}, \vec{\Omega}', t) p_v(\vec{\Omega} \cdot \vec{\Omega}', \vec{r}, t) d\Omega' + E_v(\vec{r}, \vec{\Omega}, t). \end{aligned} \quad (2.6)$$

Solution of this first order, integro-differential equation, subject to prescribed boundary conditions and initial conditions, gives the intensity as a function of three position coordinates, three components of the directional variable, frequency, and time. If the radiation properties (i.e., σ_{av} , σ_{sv} , and p_v) and the emission coefficient (E_v) are known, this solution could, in principle, be found. However, a general analytical solution is not known, and a numerical solution of Eq. (2.6) would not be practical in view of the large number of independent variables. Furthermore, the general solution (if available) would be so excessively detailed as to be of little direct practical use in most cases. Therefore, a number of simplifications are invariably introduced before attempting the solution of the radiative transfer equation.

2.3.1 Steady-State

Since radiant energy propagates at the speed of light, the radiation field in a medium relaxes nearly instantaneously to a steady configuration determined by existing hydrodynamic conditions and material properties of the medium. This assumption of a quasi-steady radiation field simplifies Eq. (2.6) to

$$\vec{\Omega} \cdot \nabla I_v(\vec{r}, \vec{\Omega}) + \sigma_{ev}(\vec{r}) I_v(\vec{r}, \vec{\Omega}) = \frac{\sigma_{sv}(\vec{r})}{4\pi} \int_{4\pi} I_v(\vec{r}, \vec{\Omega}') p_v(\vec{\Omega} \cdot \vec{\Omega}', \vec{r}) d\Omega' + E_v(\vec{r}, \vec{\Omega}). \quad (2.7)$$

The time-dependent equation is considered only in the manner in which the radiation intensity approaches its quasi-steady state configuration is of interest.

2.3.2 Local Thermodynamic Equilibrium

The emission coefficient $E_v(\vec{r}, \vec{\Omega})$ is generally a complicated function of frequency which is determined from detailed quantum statistical calculations involving the population of energy states in the medium.¹³ However, the existence of local thermodynamic equilibrium (LTE) at every point in the medium simplifies greatly the calculation of the emission coefficient. The condition of LTE is based on the assumption that the emitted spectrum from each volume element in the medium depends solely on its temperature and absorption coefficient, and is unaffected by the spectrum of the incident radiation.²⁶ This assumption is generally valid for solids and particulates, since the absorbed energy is quickly redistributed into internal energy states with an equilibrium distribution characteristic of the tempera-

ture of the medium. For gases, this redistribution of absorbed energy occurs by molecular collisions, and the LTE assumption is valid only if the redistribution is rapid relative to the time required for re-emission.²⁵

With the assumption of LTE, the emission coefficient is given by the Kirchhoff-Planck law:²⁷

$$E_v(\vec{r}, \vec{\Omega}) = \sigma_{av}(\vec{r}) B_v[T(\vec{r})], \quad (2.8)$$

with

$$B_v[T(\vec{r})] = \frac{2 h \nu^3}{c^2} \left\{ \exp\left(\frac{h\nu}{kT(\vec{r})}\right) - 1 \right\}^{-1}, \quad (2.9)$$

and where k is Boltzmann's constant. The quantity $B_v[T(\vec{r})]$ is the Planck intensity function and gives the spectral variation of the radiant energy emitted by a black-body at temperature T in any direction, per unit area normal to that direction, and per units of frequency, solid angle, and time. With the LTE assumption, the quasi-steady radiative transfer equation becomes

$$\vec{\Omega} \cdot \nabla I_v(\vec{r}, \vec{\Omega}) + \sigma_{ev}(\vec{r}) I_v(\vec{r}, \vec{\Omega}) = \frac{\sigma_{sv}(\vec{r})}{4\pi} \int_{4\pi} I_v(\vec{r}, \vec{\Omega}') p_v(\vec{\Omega} \cdot \vec{\Omega}', \vec{r}) d\Omega' + \sigma_{av}(\vec{r}) B_v[T(\vec{r})]. \quad (2.10)$$

2.3.3 Plane-Symmetric Geometry

For plane-symmetric problems (i.e., the medium and boundary conditions do not depend on the y or z coordinates), the radiation intensity is a function of one spatial coordinate (x), and two angular variables (the polar angle θ and the azimuthal angle ϕ).³¹ This planar coordinate system is illustrated in Fig. 2.2. In this geometry,

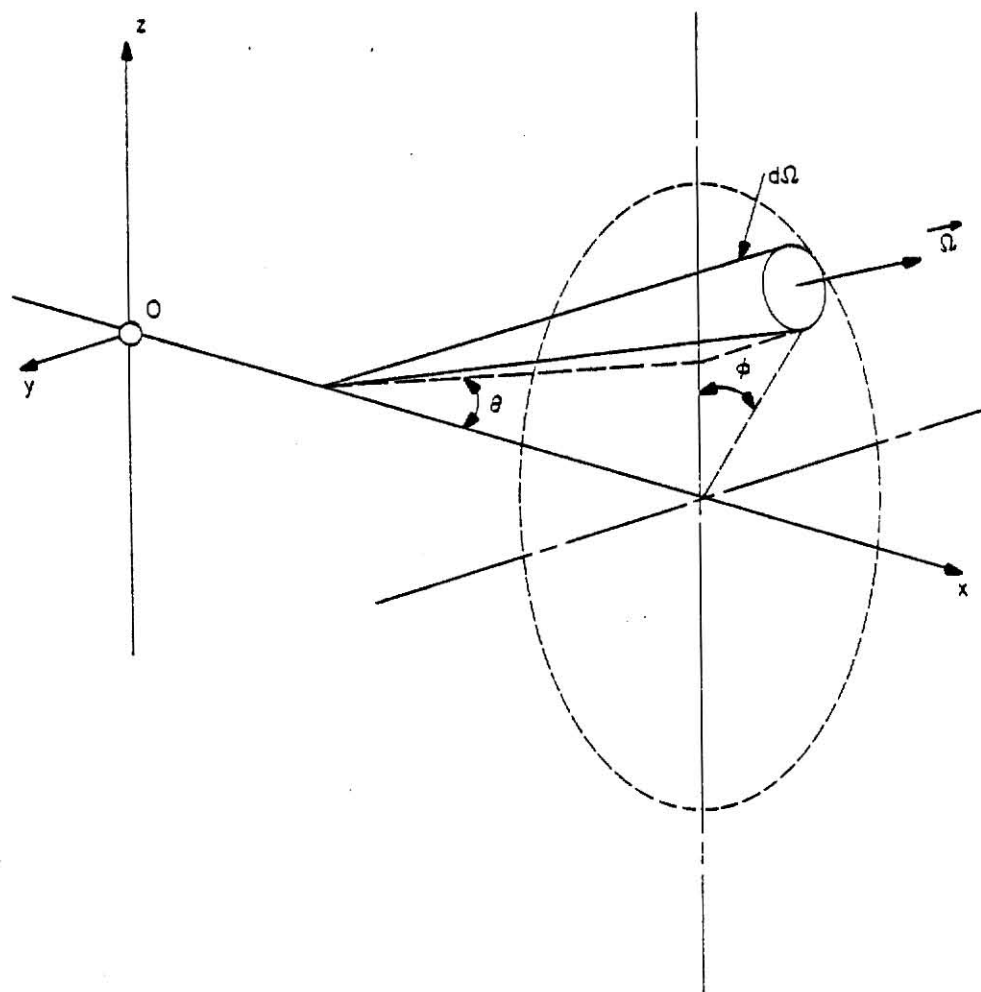


Fig. 2.2. Coordinates in plane geometry.

the quasi-steady, LTE, radiative transfer equation becomes

$$\begin{aligned} \cos\theta \frac{\partial I_v(x, \theta, \phi)}{\partial x} + \sigma_{ev}(x) I_v(x, \theta, \phi) = \\ \frac{\sigma_{sv}(x)}{4\pi} \int_0^{2\pi} d\phi' \int_0^\pi I_v(x, \theta', \phi') p_v(\theta', \phi' \rightarrow \theta, \phi; x) \sin\theta' d\theta' \\ + \sigma_{av}(x) B_v[T(x)] . \end{aligned} \quad (2.11)$$

To simplify further the radiative transfer equation, the azimuthal angle ϕ may be eliminated from Eq. (2.11) by averaging the equation over ϕ (i.e., by operating on each term with $\frac{1}{2\pi} \int_0^{2\pi} d\phi$).³² With the assumption of rotational invariance, the phase function $p_v(\theta', \phi' \rightarrow \theta, \phi; x)$ in Eq. (2.11) depends only on the cosine of the scattering angle Θ , which is related to the initial and final directions in a scattering event $[(\theta', \phi')$ and (θ, ϕ) , respectively] by³¹

$$\cos\Theta \equiv \vec{\Omega} \cdot \vec{\Omega}' = \mu\mu' + (1-\mu^2)^{1/2} (1-\mu'^2)^{1/2} \cos(\phi-\phi'), \quad (2.12)$$

where $\mu \equiv \cos\theta$ and $\mu' \equiv \cos\theta'$. Since $\cos\Theta$ depends on the difference between ϕ and ϕ' (and not on their individual values), the azimuthally averaged phase function,

$$p_v(\mu' \rightarrow \mu, x) = \frac{1}{2\pi} \int_0^{2\pi} p_v(\phi', \phi' \rightarrow \theta, \phi; x) d\phi, \quad (2.13)$$

is independent of ϕ' . Thus the averaging of Eq. (2.11) over ϕ yields

$$\begin{aligned} \mu \frac{\partial I_v(x, \mu)}{\partial x} + \sigma_{ev}(x) I_v(x, \mu) = \\ \frac{\sigma_{sv}(x)}{2} \int_{-1}^1 I_v(x, \mu') p_v(\mu' \rightarrow \mu, x) d\mu' + \sigma_{av}(x) B_v[T(x)], \end{aligned} \quad (2.14)$$

where the azimuthally averaged intensity $I_v(x, \mu)$ is defined as

$$I_v(x, \mu) = \frac{1}{2\pi} \int_0^{2\pi} I_v(x, \theta, \phi) d\phi. \quad (2.15)$$

2.3.4 Multi-Frequency Range Approximation

In the multi-frequency range approximation, the total frequency spectrum is divided into a number of contiguous frequency ranges Δv_n , $n=1, \dots, N$, as shown in Fig. 2.3. Integration of the steady-state, plane-symmetric, LTE form of the radiative transfer equation over each of the discrete frequency intervals yields³³

$$\begin{aligned} \mu \frac{\partial I_n(x, \mu)}{\partial x} + \sigma_{en}(x) I_n(x, \mu) = \\ \frac{\sigma_{sn}(x)}{2} \int_{-1}^1 I_n(x, \mu') p_n(\mu' \rightarrow \mu, x) d\mu' + \sigma_{an}(x) B_n[T(x)], \\ n = 1, \dots, N, \end{aligned} \quad (2.16)$$

where

$$I_n(x, v) = \int_{\Delta v_n} I_v(x, \mu) dv \quad (2.17)$$

$$\sigma_{in}(x) = \int_{\Delta v_n} \sigma_{iv}(x) I_v(x, \mu) dv / I_n(x, \mu) \quad (i=e, s, \text{ or } a) \quad (2.18)$$

$$\sigma_{sn}(x) p_n(\mu' \rightarrow \mu, x) = \int_{\Delta v_n} \sigma_{sv}(x) p_v(\mu' \rightarrow \mu, x) I_v(x, \mu') dv / I_n(x, \mu) \quad (2.19)$$

$$\sigma_{an}(x) B_n[T(x)] = \int_{\Delta v_n} \sigma_{av}(x) B_v[T(x)] dv. \quad (2.20)$$

Unfortunately, evaluation of the radiation properties σ_{en} , σ_{sn} , σ_{an} , and p_n is seen to require a knowledge of the unknown intensity

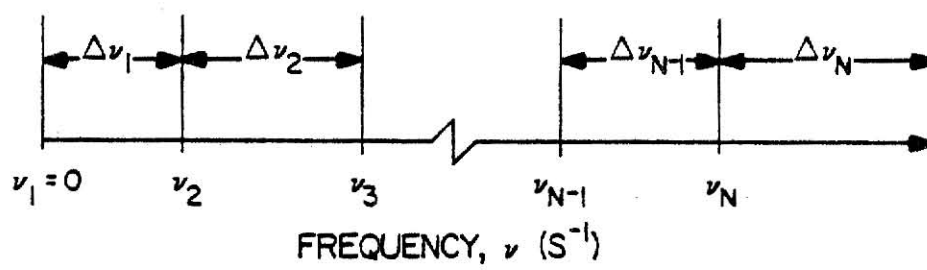


Fig. 2.3. Discretization of the frequency range $(0, \infty)$ into N discrete intervals.

distribution $I_v(x, \mu)$. However, if the Δv_n are made sufficiently small that the intensity I_v and Planck's function B_v can be assumed constant over each Δv_n , these radiation properties become simply the averages of the corresponding frequency-dependent properties over each frequency interval. Alternatively, the Δv_n can be chosen so that the radiation properties may be well approximated as constants over each interval, whereby σ_{en} , σ_{sn} , σ_{an} , and p_n are simply the radiation properties in Δv_n . With either of these assumptions (i.e., constant I_v and B_v or constant radiation properties over Δv_n), the quantity $B_n[T(x)]$ in Eq. (2.20) becomes

$$B_n[T(x)] = \int_{\Delta v_n} B_v[T(x)] dv = f_n(x) \int_0^\infty B_v[T(x)] dv. \quad (2.21)$$

In this equation, $f_n(x)$ is defined as

$$f_n(x) = \frac{\int_{\Delta v_n} B_v[T(x)] dv}{\int_0^\infty B_v[T(x)] dv}. \quad (2.22)$$

Equation (2.16) may thus be rewritten as

$$\begin{aligned} \mu \frac{\partial I_n(x, \mu)}{\partial x} + \sigma_{en}(x) I_n(x, \mu) = \\ \frac{\sigma_{sn}(x)}{2} \int_{-1}^1 I_n(x, \mu') p_n(\mu' \rightarrow \mu) d\mu' + \sigma_{an}(x) f_n(x) \hat{\sigma} T^4(x) / \pi, \end{aligned} \quad n = 1, \dots, N, \quad (2.23)$$

where the Planck function $B_v[T(x)]$ integrated over all frequencies gives the emissive power of a black body in any direction per unit area normal to that direction,²⁶ i.e.,

$$\int_0^{\infty} B_{\nu}[T(x)] d\nu = \hat{\sigma} T^4(x)/\pi. \quad (2.24)$$

The quantity $\hat{\sigma}$ is the Stefan-Boltzmann Constant, and $T(x)$ is the local temperature.

Equation (2.23) represents a set of N uncoupled equations for the intensities integrated over each of the frequency intervals. The solution of these equations yields the intensity as a function of position and direction in each frequency interval and thus approximates the spectral dependence of the intensity distribution.

2.3.5 The Gray Case

In a gray medium, the absorption and scattering coefficients and the scattering phase function are independent of frequency. The steady-state, one-dimensional, LTE radiative transfer equation becomes

$$\begin{aligned} \mu \frac{\partial I_{\nu}(x, \mu)}{\partial x} + \sigma_e(x) I_{\nu}(x, \mu) &= \frac{\sigma_s(x)}{2} \int_{-1}^1 I_{\nu}(x, \mu') p(\mu' \rightarrow \mu, x) d\mu' \\ &+ \sigma_a(x) B_{\nu}[T(x)]. \end{aligned} \quad (2.25)$$

The local emission term $\sigma_a(x) B_{\nu}[T(x)]$ is seen to have the same spectral variation as the emission from a black body. Equation (2.25) may be integrated over all frequencies to obtain

$$\begin{aligned} \mu \frac{\partial I(x, \mu)}{\partial x} + \sigma_e(x) I(x, \mu) &= \frac{\sigma_s(x)}{2} \int_{-1}^1 I(x, \mu') p(\mu' \rightarrow \mu, x) d\mu' \\ &+ \sigma_a(x) \hat{\sigma} T^4(x)/\pi, \end{aligned} \quad (2.26)$$

where

$$I(x, \mu) = \int_0^{\infty} I_{\nu}(x, \mu) d\nu. \quad (2.27)$$

2.3.6 No-Scattering Case

If scattering is neglected in Eq. (2.26) [i.e., $\sigma_s(x)=0$, and $\sigma_e(x)=\sigma_a(x)$], this equation becomes

$$\mu \frac{\partial I(x, \mu)}{\partial x} + \sigma_a(x) I(x, \mu) = \sigma_a(x) \hat{\sigma} T^4(x) / \pi. \quad (2.28)$$

This equation may be rewritten

$$\frac{\partial I(\xi, \mu)}{\partial \xi} + \frac{1}{\mu} I(\xi, \mu) = S(\xi, \mu), \quad (2.29)$$

where

$$d\xi = \sigma_a(x) dx, \quad (2.30)$$

and

$$S(\xi, \mu) = \frac{1}{\mu} \hat{\sigma} T^4(\xi) / \pi. \quad (2.31)$$

Equation (2.29) is a first order differential equation which is easily solved analytically by use of the integrating factor $\exp(\xi/\mu)$. The solution is

$$I(\xi, \mu) = I(0, \mu) \exp\left(-\frac{\xi}{\mu}\right) + \int_0^\xi S(\xi', \mu) \exp[(\xi' - \xi)/\mu] d\xi', \quad \mu > 0, \quad (2.32a)$$

and

$$I(\xi, \mu) = I(\xi_t, \mu) \exp\left[\frac{\xi_t - \xi}{\mu}\right] + \int_{\xi_t}^\xi S(\xi', \mu) \exp[(\xi' - \xi)/\mu] d\xi', \quad \mu < 0, \quad (2.32b)$$

where $I(0, \mu)$ is the intensity at $\xi=0$ (known for positive μ), and $I(\xi_t, \mu)$ is the intensity at $\xi=\xi_t$ (known for negative μ).

2.3.7 No-Emission Case

If the thermal energy emission term is additionally neglected, Eq. (2.28) becomes

$$\mu \frac{\partial I(x, \mu)}{\partial x} + \sigma_a(x) I(x, \mu) = 0. \quad (2.33)$$

The solution of this equation is given by Eqs. (2.32a) and (2.32b)

with $S(\xi, \mu) = 0$, i.e.,

$$I(\xi, \mu) = I(0, \mu) \exp\left(\frac{-\xi}{\mu}\right), \quad \mu > 0, \quad (2.34a)$$

and

$$I(\xi, \mu) = I(\xi_t, \mu) \exp\left(\frac{\xi_t - \xi}{\mu}\right), \quad \mu < 0. \quad (2.34b)$$

For constant σ_a ($\xi = \sigma_a x$), Eqs. (2.34a) and (2.34b) reduces to Bouguer's law:

$$I(x, \mu) = I(0, \mu) \exp(-\sigma_a x / \mu), \quad \mu > 0, \quad (2.35a)$$

and

$$I(x, \mu) = I(x_t, \mu) \exp[\sigma_a (x_t - x) / \mu], \quad \mu < 0. \quad (2.35b)$$

2.4 The Integrated Intensity and Net Flux Distributions

The integrated intensity $\Phi_v(\vec{r})$ and the net flux vector $\vec{J}_v(\vec{r})$ are defined by

$$\Phi_v(\vec{r}) \equiv \int_{4\pi} I_v(\vec{r}, \vec{\Omega}) d\Omega, \quad (2.36)$$

and

$$\vec{J}_v(\vec{r}) \equiv \int_{4\pi} \vec{\Omega} I_v(\vec{r}, \vec{\Omega}) d\Omega. \quad (2.37)$$

The net flux vector gives the net flow rate of radiant energy at point \vec{r} , per unit frequency about ν , across a unit area perpendicular to the direction of \vec{J} . The net energy flow rate across an arbitrarily oriented surface dA whose outward normal is \vec{n} is found from

$\vec{J}_v(\vec{r}) \cdot \vec{n} dA$. The integrated intensity $\Phi_v(\vec{r})$ cannot be related to an

energy flow but may be regarded simply as 4π times the average intensity $\bar{I}_v(\vec{r})$ [$= \frac{1}{4\pi} \int_{4\pi} I_v(\vec{r}, \vec{\Omega}) d\Omega$]. Alternatively, $\Phi_v(\vec{r})$ may be interpreted as the product of the photon energy $h\nu$ and the total path length travelled by photons in unit frequency about ν , in a unit volume at point \vec{r} , and in a unit time.

By division of the total solid angle about every point \vec{r} into a number of smaller solid angles, $\Delta\Omega_j$, $j = 1, \dots, M$, it is possible to define the partial flux vector over each of the intervals $\Delta\Omega_j$ by

$$\vec{J}_{vj}(\vec{r}) = \int_{\Delta\Omega_j} \vec{\Omega} I_v(\vec{r}, \vec{\Omega}) d\Omega, \quad j=1, \dots, M, \quad (2.38)$$

where

$$\sum_{j=1}^M \Delta\Omega_j = 4\pi.$$

Clearly, the net flux is the resultant vector obtained from addition of all the partial flux vectors, i.e.,

$$\vec{J}_v(\vec{r}) = \sum_{j=1}^M \vec{J}_{vj}(\vec{r}). \quad (2.39)$$

The partial fluxes characterize the total flow of radiant energy per unit frequency and per unit area perpendicular to their respective directions. Although it is also possible to define similarly the partial integrated intensities $\Phi_{vj}(\vec{r})$, these quantities are seldom used in radiative transfer calculations.

2.5 Radiative Equilibrium

The radiative equilibrium condition is a statement of the steady-state energy balance in a medium in which heat sources are absent,

and heat transfer by conduction and convection is negligible. This condition may be written as²⁷

$$\int_0^{\infty} dv \int_{4\pi} E_v(\vec{r}, \vec{\Omega}) d\Omega = \int_0^{\infty} \sigma_{av}(\vec{r}) dv \int_{4\pi} I_v(\vec{r}, \vec{\Omega}) d\Omega, \quad (2.40)$$

i.e., the volumetric rates of radiant energy emission and radiant energy absorption are equal at every point in the medium. Clearly, this condition must be satisfied to maintain steady-state conditions in a purely radiating medium.

If radiation is not the only mode of heat transfer, the radiative equilibrium condition is not applicable, and the steady-state energy balance is of the form

$$\int_0^{\infty} dv \int_{4\pi} E_v(\vec{r}, \vec{\Omega}) d\Omega = \int_0^{\infty} \sigma_{av}(\vec{r}) dv \int_{4\pi} I_v(\vec{r}, \vec{\Omega}) d\Omega + G(\vec{r}). \quad (2.41)$$

In this equation, $G(\vec{r})$ represents the net rate of energy addition per unit volume at point \vec{r} by all non-radiative energy transfer processes. Equation (2.41) states that the volumetric rate of radiant energy emission must equal the sum of the volumetric rates of radiant energy absorption and non-radiative energy addition at every point in the medium.

2.6 Radiation Transport in Pulverized Coal Suspensions

The absorption, scattering, and emission coefficients characterizing a pulverized coal suspension are computed from

$$\sigma_{av} = \sigma_{avg} + \sigma_{avp} \quad (2.42)$$

$$\sigma_{sv} = \sigma_{svg} + \sigma_{svp} \quad (2.43)$$

$$E_v = E_{vg} + E_{vp}. \quad (2.44)$$

where the subscripts p and g imply the various coefficients are evaluated separately for the particulate and gaseous phases, respectively. If the pulverized coal cloud is in local thermodynamic equilibrium, the emission coefficient becomes

$$E_v \stackrel{\text{LTE}}{=} \sigma_{avg} B_v(T_g) + \sigma_{avp} B_v(T_p). \quad (2.45)$$

Thus with the LTE assumption, only the absorption coefficient and the temperature of each phase are needed to compute E_v .

The evaluation of the radiation properties (the absorption and scattering coefficients, and the scattering phase function) for the particulate and gaseous components in pulverized coal combustors is discussed in Chapter 3. If it is assumed that these properties are known (as functions of position and frequency), the quasi-steady LTE equation of transfer contains three unknown functions: $I_v(\vec{r}, \vec{\Omega})$, $T_p(\vec{r})$, and $T_g(\vec{r})$. Two additional equations involving the unknown particle and gas temperature distributions are the particle and gas phase energy balances, Eqs. (1.29) and (1.30). These equations are rewritten symbolically as

$$Q_{rp}(\vec{r}) = G_p[T_p(\vec{r}), T_g(\vec{r}), \rho_p(\vec{r}), \rho_g(\vec{r}), \dots], \quad (2.46)$$

and

$$Q_{rg}(\vec{r}) = G_g[T_p(\vec{r}), T_g(\vec{r}), \rho_p(\vec{r}), \rho_g(\vec{r}), \dots], \quad (2.47)$$

where all the nonradiative energy transfer terms have been lumped as G_p for the solid phase and G_g for the gas phase. The non-radiative energy inputs include the work done by surface and body forces, the energy released by chemical reaction, the heat transferred by conduction, and the sensible energy change for each phase.¹⁶ The terms $Q_{rp}(\vec{r})$ and $Q_{rg}(\vec{r})$ represent the net loss of radiant energy (i.e., emission minus absorption) from each phase per unit volume of the mixture and per unit time. With the assumption of LTE, these terms can be expressed as

$$Q_{rp}(\vec{r}) = 4\pi \int_0^\infty \sigma_{avp}(\vec{r}) B_v[T_p(\vec{r})] dv - \int_0^\infty \sigma_{avp}(\vec{r}) dv \int_{4\pi} I_v(\vec{r}, \vec{\Omega}) d\Omega \quad (2.48)$$

$$Q_{rg}(\vec{r}) = 4\pi \int_0^\infty \sigma_{avg}(\vec{r}) B_v[T_g(\vec{r})] dv - \int_0^\infty \sigma_{avg}(\vec{r}) dv \int_{4\pi} I_v(\vec{r}, \vec{\Omega}) d\Omega. \quad (2.49)$$

Substitution for $Q_{rp}(\vec{r})$ and $Q_{rg}(\vec{r})$ from Eqs. (2.48) and (2.49) into Eqs. (2.46) and (2.47), respectively, yields

$$4\pi \int_0^\infty \sigma_{avp} B_v(T_p) dv - \int_0^\infty \sigma_{avp} dv \int_{4\pi} I_v d\Omega = G_p \quad (2.50)$$

$$4\pi \int_0^\infty \sigma_{avg} B_v(T_g) dv - \int_0^\infty \sigma_{avg} dv \int_{4\pi} I_v d\Omega = G_g. \quad (2.51)$$

Equations (2.50) and (2.51) are the additional equations relating the intensity $I_v(\vec{r}, \vec{\Omega})$ to the temperature distributions of the two phases, $T_p(\vec{r})$ and $T_g(\vec{r})$. In general, the terms G_p and G_g are also

functions of the velocity, composition, and physical properties of each phase. The additional unknowns introduced by these terms necessitates consideration of the continuity and momentum equations for each phase, as well as additional (auxiliary) equations and simplifying assumptions as discussed in Chapter 1.

2.7 Summary

In this chapter, the radiative transfer equation, which must be solved to compute the radiant energy propagation and the radiation heat transfer in an absorbing, emitting, and scattering medium has been presented. The complexity and excessive detail of a general solution of the equation of transfer create a need for simplifications of the general equation. Simplifications of the time dependence, the emission coefficient (for LTE conditions), the frequency dependence, and the medium geometry have been outlined. An analytical solution was given for the no scattering case, and the equation of transfer was shown to reduce to Bouguer's law when both scattering and thermal energy emission were neglected. Finally, definitions were given for the integrated intensity and net flux distributions, which are required to formulate the diffusion approximation of the radiative transfer equation (see Chapter 4).

The solution of the equation of transfer (subject to boundary conditions for the intensity) is needed to compute the radiant heat losses in pulverized coal media. However, it has been shown that the temperature dependence of the emission coefficient in the equation of transfer causes the equation to be coupled with the conservation laws

that were presented in Chapter 1. A number of techniques for solving the equation of transfer are discussed in Chapter 4.

3.0 RADIATIVE PROPERTIES OF MATERIALS IN PULVERIZED COAL COMBUSTION

3.1 Classes of Materials

Solution of the radiative transfer equation in pulverized coal flames requires numerical values of the radiative properties for the various materials present in the system. These materials are divided into the broad categories of particulates and gaseous radiators. The accurate evaluation of the radiation properties of these materials is difficult because of their strong dependence on temperature and composition, and because of the uncertainty in the complex mechanism by which coal ignites and burns out. Gaseous radiators are non-gray, and data for their absorption coefficient as a function of frequency are mostly unavailable. Only recently have attempts been made to evaluate theoretically the radiation properties of gases. The optical properties of particles are continuous functions of frequency, but they have been measured only over limited ranges of temperature and frequency. Although the particles in coal flames are irregular in shape, these particles are usually assumed to be spherical, since the theory of the interaction of electromagnetic radiation with spheres is well developed. Furthermore, effects of surface asperities, particle agglomeration, and coherent scattering in particle suspensions are commonly neglected.

Clearly, the great uncertainty (or unavailability) of radiation properties is the major problem in the accurate evaluation of the radiation heat transfer in pulverized coal media. Sensitivity

studies are needed to determine which data are important, and additional theoretical and experimental investigations are needed to determine the important parameters more accurately.

The radiation properties of particulates and gaseous radiators are discussed in this chapter to the extent that they are known. The particulates are subdivided into two classes: 1) coal, char, and ash particles, whose size parameter α ($= \pi d_p / \lambda$, where d_p is the particle diameter, and λ is the radiation wavelength) is greater than or roughly equal to unity and 2) soot particles which are characterized by values of α much smaller than unity. The radiation properties of the various categories are discussed separately because of the fundamental differences in their interaction with thermal radiation. Finally, the radiation properties of combustor walls are also discussed in this chapter, since these properties are required to formulate the boundary conditions for the radiation intensity and to calculate the radiant energy leakage through the medium boundaries.

3.2 Particulates

3.2.1 Absorption and Scattering Efficiencies

The absorption and scattering coefficients of a particle suspension are related to the effective cross sectional areas for absorption, C_{avk} , and for scattering, C_{svk} , of particles in the k^{th} size class for radiation of frequency ν by

$$\sigma_{av} = \sum_k C_{avk} N_k \quad (3.1)$$

and

$$\sigma_{sv} = \sum_k C_{svk} N_k \quad (3.2)$$

where N_k is the number density of particles in the k^{th} size class. The absorption or scattering efficiency of a spherical particle of diameter d_{pk} is the ratio of the cross sectional area for the given interaction to the geometric cross sectional area of the particle, $\pi d_{pk}^2/4$. Denoting the absorption and scattering efficiencies of particles in the k^{th} size class (for radiation of frequency ν) by F_{avk} and F_{svk} , respectively, the absorption and scattering coefficients may be written as

$$\sigma_{av} = \frac{1}{4} \sum_k F_{avk} S_{vk}, \quad (3.3)$$

and

$$\sigma_{sv} = \frac{1}{4} \sum_k F_{svk} S_{vk}, \quad (3.4)$$

where

$$S_{vk} = \pi d_{pk}^2 N_k. \quad (3.5)$$

The quantity S_{vk} represents the total surface area of particles in the k^{th} size class per unit volume. The extinction efficiency F_{evk} is the sum of the absorption and scattering efficiencies, and thus the extinction coefficient σ_{ev} ($\equiv \sigma_{av} + \sigma_{sv}$) can be computed from

$$\sigma_{ev} = \sum_k F_{evk} S_{vk}. \quad (3.6)$$

Therefore, the absorption, scattering, and extinction coefficients of a particle suspension can be computed given the corresponding efficiencies and the number density of particles for each size class

present in the suspension.

3.2.2 Coal, Char, and Ash Particles

The absorption or scattering efficiency of a single coal, char, or ash particle depends on the complex refractive index of the particle, $m = \eta (1 - i\kappa)$, and on the particle size relative to the radiation wavelength, $\alpha = \pi d_p / \lambda$.^{4,5} The refractive index is generally a function of radiation wavelength, particle temperature, and particle composition.^{16,34} Most data giving the refractive index of carbonaceous solids (ash is neglected for the moment) were measured at room temperature and over the visible portion of the electromagnetic spectrum. However, these data and simple theoretical calculations of the real and imaginary parts of the refractive index (η and κ) indicate only a weak dependence on temperature and wavelength.^{2,34} Accurate values of the optical properties are thus not known at flame temperatures, but it is generally thought that $1.5 \leq \eta \leq 3$ and $0.1 \leq \kappa \leq 1.0$, with both values increasing as the hydrogen to carbon (H/C) ratio of the coal decreases.¹⁶ Additional uncertainty is introduced by the rapid change of this H/C ratio during the preheating and combustion of the coal particles in a boiler flame.

Coal and char particles can be divided into two size groups, large particles ($\alpha \gg 1$) and intermediate sized particles ($\alpha \approx 1$).¹³ The principal radiative properties of each group are reviewed below.

a) Large Particles: Scattering of thermal radiation by large particles ($\alpha \gg 1$) is significant and generally quite anisotropic in nature.¹² The absorption and scattering efficiencies and the

scattering phase function are determined from simple laws of geometric optics which describe scattering in terms of reflection, diffraction, and refraction.²⁵ For opaque coal and char particles, the scattered radiation is separable into reflected and diffracted components. The diffracted component is concentrated within a small solid angle about the incident direction and is difficult to distinguish from the unscattered radiation.^{6,12,16} The energy diffracted by a spherical particle is the same as that diffracted by a hole of the same diameter,²⁵ and consequently the cross section for diffraction equals $\pi d_p^2/4$. In radiative transfer calculations, this diffracted radiation is usually treated as if it were unscattered and totally transmitted. When the diffracted radiation is thus neglected, its contribution must be subtracted from the total scattering and extinction efficiencies.

In the large particle limit, the extinction efficiency approaches unity, while the scattering efficiency approaches the reflectivity of the material composing the particle. The scattering phase function is backward peaked (see Fig. 3.1) and may be expressed as^{4,12,25}

$$p(\theta) = \frac{8}{3\pi} (\sin\theta - \theta\cos\theta), \quad (3.7)$$

where θ is the scattering angle. This phase function is derived by first computing the intensity of radiation that is diffusely reflected through an observation angle θ by an elemental area on the surface of an opaque sphere. Integration of this intensity over the portion of the sphere surface that is visible to the observer yields the total in-

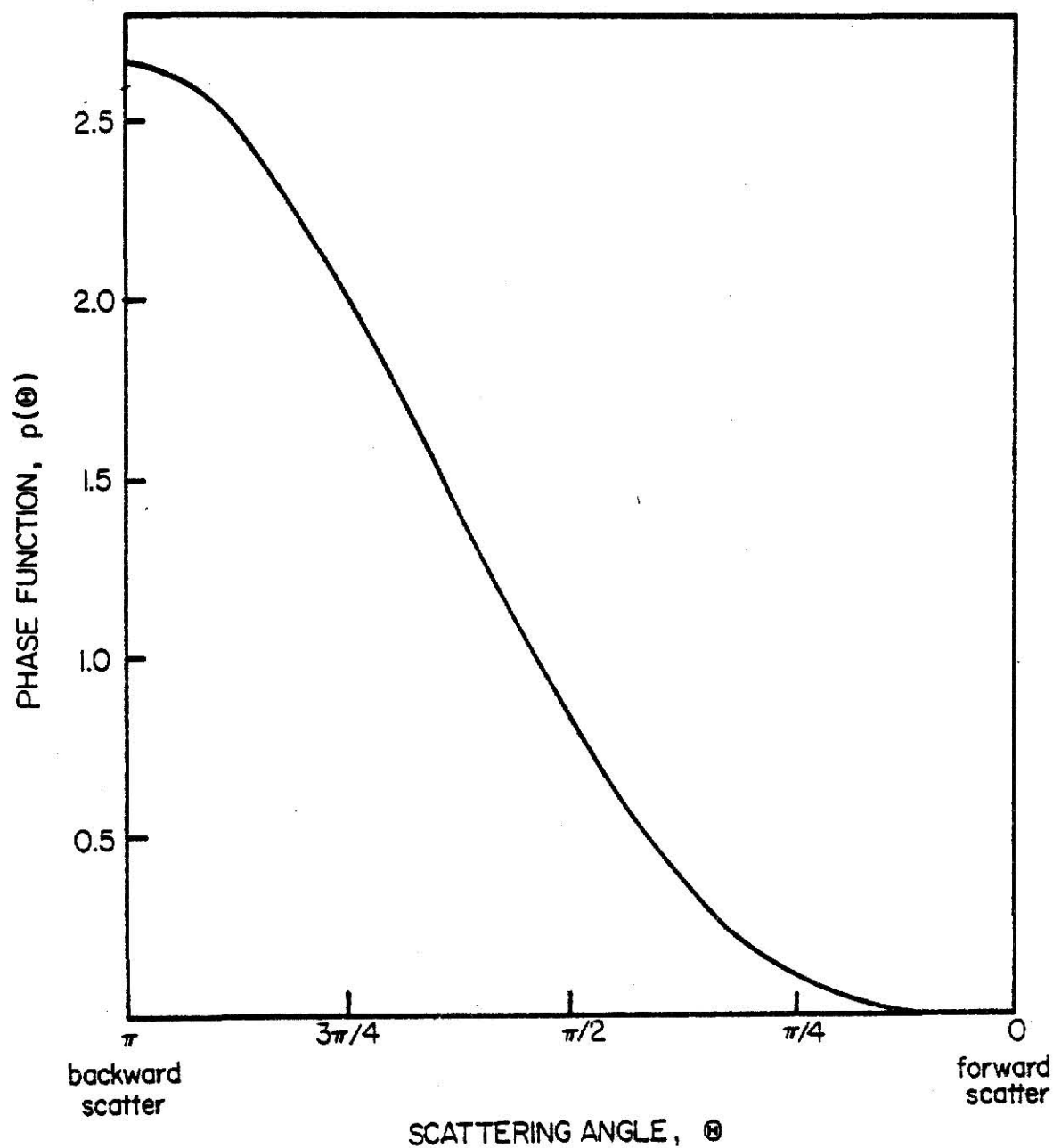


Fig. 3.1. The scattering phase function for a large, diffusely reflecting, opaque sphere - $P(\theta) = 8(\sin\theta - \theta\cos\theta)/(3\pi)$.

tensity scattered at an angle θ . Division of this intensity by the intensity which would be scattered if scattering were isotropic yields the phase function of Eq. (3.7).

b) Intermediate Sized Particles: Geometric optics cannot be used to describe scattering by intermediate sized particles ($\alpha \approx 1$) since the diffracted radiation is not distinguishable from scattering which occurs within the bulk of the particle.^{12,13} Scattering is significant, and Mie's scattering theory is used to compute extinction and scattering efficiencies, as well as the scattering phase function.^{4,16}

Blokh³⁵ has computed the extinction and scattering efficiencies (using Mie theory) for a high carbon coal at a radiation wavelength of 2 μm for a wide range of particle sizes using a representative value of the refractive index of $m = 1.93 (1-i0.53)$.¹⁶ These results are shown in Fig. 3.2 and indicate a weak dependence of the efficiencies on particle size for particles larger than roughly 5 μm in diameter.

The coal and char particles in a pulverized coal flame are of widely varying sizes, and a number of distribution functions describing the fraction of particles exceeding a given size have been postulated (e.g., the Rosin-Rammler distribution¹⁶). The sizes of pulverized coal and char particles given by these distributions are typically between 10 and 100 μm . The radiation wavelengths of importance at combustion temperatures ($\sim 1500 \text{ K} - 3000 \text{ K}$) are in the range 0.5 μm to 10 μm ,^{2,4,16} with the maximum radiation intensity at roughly 2 μm .^{2,16} Therefore, the particle size parameter α in pulverized coal combustion is typically between 15 and 150. Consequently, the extinction and

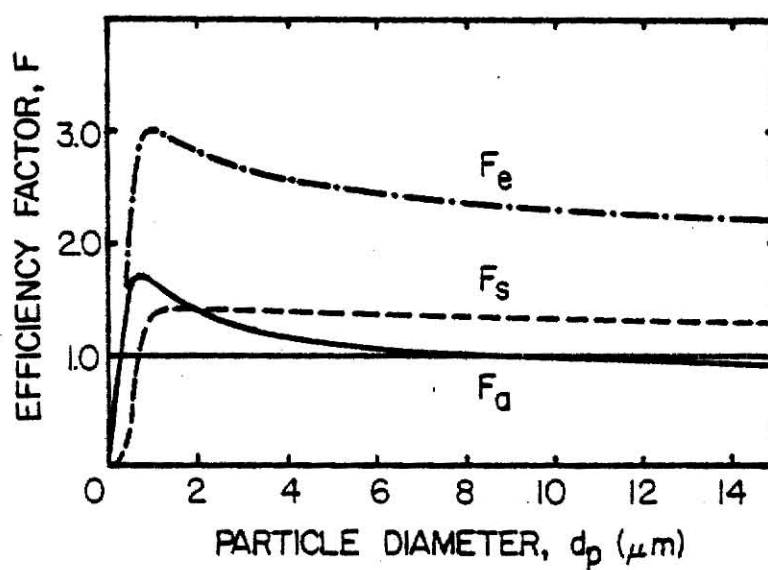


Fig. 3.2. Variation of the radiation efficiency factors for high carbon coal particles with the particle diameter. The radiation wavelength, $\lambda = 2 \mu\text{m}$, and the assumed refractive index, $m = 1.93(1-i0.53)$.

scattering efficiencies for these particles can be expected to approach their limiting values which apply for a $\gg 1$. Efficiencies have been computed in this study using the subroutine DBMIE³⁶ (which solves the Mie equations) for a range of particle size parameters with an assumed refractive index of $m = 1.93 (1-i0.53)$. These results are shown in Table 3.1. A contribution of unity has been subtracted from the computed efficiencies to exclude diffracted radiation. These results indicate a weak dependence of the extinction and scattering efficiencies on the particle size for the range of size parameters considered. Furthermore, the relative importance of scattering (the single scatter albedo $\omega = F_s/F_e$) is nearly unaffected by a ten-fold increase in the particle size.

The effect of the assumed refractive index of coal and char particles on the computed extinction and scattering efficiencies was also examined in this study. These efficiencies were calculated for values of the real part of the refractive index of 1.5 and 3 and values of the imaginary part ranging from 0.1 to 1. The particle size and radiation wavelength were taken as 50 μm and 2 μm , respectively, both typical for pulverized coal combustion. The efficiencies were again calculated by the subroutine DBMIE and are compared in Table 3.2. It may be seen from this table that the relative importance of scattering increases with an increase in either the real or imaginary parts of the refractive index. For the upper limits of both η and κ ($\eta=3$, $\kappa=1$), the contribution of scattering to the total extinction of radiation is greater than 50%.

Table 3.1. The extinction and scattering efficiencies and the single scatter albedo as a function of particle size. Values computed by DBMIE³⁶ for $m=1.93$ (1-10.53), and $\lambda=2\mu\text{m}$.

Particle Diameter, d_p (μm)	Particle Size Parameter, $\alpha = \pi d_p / \lambda$	Extinction Efficiency, F_e	Scattering Efficiency, F_s	Single Scatter Albedo, $\omega = F_s / F_e$
10	15.71	1.326036	0.352368	0.2657
50	78.54	1.117158	0.300529	0.2690
100	157.08	1.073761	0.284531	0.2650

Table 3.2. The extinction and scattering efficiencies and the single scatter albedo as a function of the refractive index, $m = \eta(1 - i\kappa)$. Values computed by DBMIE³⁶ for 50 μm particles at a radiation wavelength of 2 μm ($\alpha = \pi d_p / \lambda = 78.54$).

η	κ	Extinction Efficiency F_e	Scattering Efficiency F_s	Scattering Albedo $\omega = F_s / F_e$
1.5	0.1	1.104177	0.138063	0.1250
	0.5	1.108103	0.233199	0.2105
	1.0	1.129336	0.408763	0.3619
3.0	0.1	1.104387	0.327257	0.2963
	0.5	1.121173	0.414433	0.3696
	1.0	1.144074	0.588127	0.5141

Ash particles are non-carbonaceous, and the main constituents of ash are the oxides of magnesium, aluminum, and calcium, although a large number of other metallic oxides are also present.⁴ Ash is non-absorbing over the visible portion of the electromagnetic spectrum, but little is known of its radiative properties in the infrared.¹⁶ It is widely believed that the radiant emission and scattering by ash particles may be quite important in the post-burn regions of pulverized coal flames, where most of the carbon content of the coal particles has been consumed by chemical reaction. However, since there are no reported data on its optical properties, further discussion of ash particles is omitted.

3.2.3 Soot Particles

Soot particles consist primarily of carbon and hydrogen and are formed when the hydrocarbons and tarry constituents of coal volatiles are heated in an oxygen-deficient atmosphere. There is little data on soot concentrations in pulverized-coal flames, but if combustion conditions are poor and allow for its formation, soot can be a significant contributor to the absorption and emission of thermal radiation.¹⁶

Soot particles are very small ($\alpha \ll 1$), although they may agglomerate to form larger bodies. If this agglomeration is neglected, it can be assumed that the electric field which is established within each particle by the incident radiation is uniform throughout the particle and equal to that of the incident radiation.^{6,12} This assumption simplifies greatly the calculation of the radiation properties, and the associated scattering is known as Rayleigh scattering.^{6,25}

The efficiencies for scattering and absorption are given by:^{2,12}

$$F_a = 24 \alpha \frac{n^2 \kappa}{[\eta^2(1-\kappa^2)+2]^2 + 4 \eta^4 \kappa^2} \quad (3.8)$$

$$F_s = \frac{8}{3} \alpha^4 \frac{\{[\eta^2(1-\kappa^2)-1][\eta^2(1-\kappa^2)+2] + 4\eta^4 \kappa^2\}^2 + 36\eta^4 \kappa^2}{\{[\eta^2(1-\kappa^2) + 2]^2 + 4\eta^4 \kappa^2\}^2}, \quad (3.9)$$

where η and κ are the real and imaginary parts of the refractive index, and α is the particle size parameter. As is the case for coal and char particles, values of η and κ are weak functions of particle temperature and radiation wavelength and are expected to fall in the ranges 1.5 to 3 and 0.1 to 1, respectively. Evaluation of the absorption and scattering efficiencies indicates that scattering is negligible, and that the absorption coefficient varies as λ^{-1} . Therefore, a soot suspension is non-gray, and the radiation calculations must be based on either spectral values or suitable frequency averages of the absorption coefficient.

3.3 Combustion Gases

Radiant emission and absorption by gases at combustion temperatures are primarily due to asymmetric gas molecules.^{2,12,13} Carbon dioxide and water vapor are of major importance, while carbon monoxide is a weaker emitter. Other minor constituents such as hydroxyl radicals and nitrogen oxides are typically ignored. Atomic species (H, O, N), and homonuclear diatomic molecules (H_2 , O_2 , N_2) are non-emitting.¹² The emission and absorption of thermal radiation

by gases is restricted to a number of discrete wavelength intervals (bands), and scattering is negligible. The overall behavior of gaseous radiators is very non-gray, although the simultaneous presence of many gases tends to increase the grayness of the mixture.¹⁶

The non-grayness of gaseous radiators introduces a number of difficulties. The monochromatic emissivity of a gaseous volume is given by $1 - \exp(-\sigma_{\text{avg}} L)$, where σ_{avg} and L are the absorption coefficient and the mean beam length¹² of the volume, respectively. However, the majority of gas radiation data gives experimentally determined values of the total emissivity ϵ_g , which is defined as¹²

$$\epsilon_g = \frac{\int_0^\infty \epsilon_{\nu g} B_\nu(T_g) d\nu}{\int_0^\infty B_\nu(T_g) d\nu} = \frac{\pi}{\hat{\sigma} T_g^4} \int_0^\infty [1 - \exp(-\sigma_{\text{avg}} L)] B_\nu(T_g) d\nu. \quad (3.10)$$

Clearly, data for ϵ_g cannot be converted to data for the absorption coefficient needed for solution of the radiative transfer equation. Moreover, even if the absorption coefficient is known as a function of frequency, the non-grayness of the gas volume complicates the calculation of the radiation intensity distribution, which must be determined by solving the equation of transfer integrated over a number of frequency intervals using the multi-frequency range model discussed in Section 2.3.4. Finally, the absorption coefficients of gases are strong functions of gas temperature and pressure,^{2,13} which further complicates the solution of the radiative transfer equation if these quantities are not known a priori.

Although total emissivity data are of limited usefulness in radiative transfer theory, the data are required for zone calculations,^{4,16} where the total gas emissivity is used to compute the radiant energy emitted by each zone. Hottel and Sarofim¹² treat the subject of gas emissivity in detail and present charts which give:

- i) The emissivity of carbon dioxide at 1 atm total pressure as a function of temperature for several values of $p_c L$, where p_c is the partial pressure of CO_2 . (A correction factor for total pressures different from 1 atm is also given.)
- ii) The emissivity of water vapor at 1 atm pressure as a function of temperature for several values of $p_w L$ in the limit $p_w \rightarrow 0$, where p_w is the partial pressure of the water vapor. (Correction factors for total pressures other than 1 atm, and $p_w \neq 0$ are also given.)
- iii) The correction factor $\Delta\epsilon$ needed to compute the emissivity of a mixture of CO_2 and H_2O from

$$\epsilon_{\text{mixture}} = \epsilon_{CO_2} + \epsilon_{H_2O} - \Delta\epsilon.$$

The term $\Delta\epsilon$ accounts for the partial overlap of the absorption bands of the two gases and is a function of temperature and the quantities $p_w L$ and $p_c L$.

A number of theoretical models have also been developed for calculation of the emissivity of gaseous mixtures. These models give the gas emissivity integrated over either narrow frequency bands³⁷ (corresponding to rotational transitions within a vibrational-rotational band) or wide frequency bands associated with the princi-

pal vibrational transitions of the gaseous molecules.³⁸ With the narrow band model, the thermal radiation spectrum is divided into numerous small intervals for each radiating species. Within each of these intervals, the spectral lines are assumed to be randomly located, while the line intensities are assumed to follow an exponential probability distribution. This model suffers from the massive amounts of input data and large computer time requirements needed to compute the parameters of the model.³⁹ In the wide band model, the detailed positions and intensities of the spectral lines within each band are assumed unimportant and are approximated by a simple exponential function.³⁸ Although these wide band models are simple enough for hand calculations, they are applicable only to homogeneous gaseous mixtures and are accurate only over limited ranges of temperature.³⁹

In summary, data required to solve the radiative transfer equations in gaseous media are largely unavailable. Fortunately, the radiant energy emission by gases is small compared to emission by particulates in pulverized coal flames. Gaseous radiation exceeds that by particles only once a large fraction of the solid fuel has been consumed.¹⁶ The radiation by gases is therefore often neglected in pulverized coal combustors.^{5,15,17}

3.4 Combustor Walls

The walls of conventional combustion chambers are either lined with refractory materials or are metals cooled by water or steam.¹⁶ Refractory walls are poor conductors which either reflect or absorb and subsequently re-emit all incident radiant energy. Water cooled

walls can be considered cold (i.e., non-radiating), and incident radiant energy is either reflected or absorbed by the wall and subsequently removed by the coolant. Both types of walls are diffuse reflectors, and their reflectivity and emissivity values may vary with radiation wavelength λ and wall temperature T_w . If the wavelength dependence is weak (i.e., the walls are gray), the reflectivity ρ_w and the emissivity ϵ_w must sum to unity. Typical emissivity values are 0.5 to 0.9, with refractory walls characterized by the lower emissivities.

The general case of walls which are part refractory and part heat sink can be treated by assuming the walls to reflect a fraction of the incident radiant energy, and to absorb the remaining fraction. Part of the absorbed energy is reradiated back to the combustor (at a rate determined by the wall temperature), while the remainder is removed by the coolant. Therefore, if the partial radiant flux incident from a medium on a gray, diffusely reflecting wall is denoted by J^- , then the flux J^+ from the wall to the medium (i.e., the radiosity of the wall) is given by

$$J^+ = \rho_w J^- + \epsilon_w \hat{\sigma} T_w^4, \quad (3.11)$$

where T_w , ρ_w , and ϵ_w are, respectively, the wall temperature, reflectivity, and emissivity. The radiant energy which is lost by the system is simply the net radiant flux J in the outward direction to the medium, i.e.,

$$J = J^- - J^+ = (1 - \rho_w) J^- - \epsilon_w \hat{\sigma} T_w^4. \quad (3.12)$$

Since for a gray wall, the reflectivity and emissivity sum to unity, the net outward flux simplifies to

$$J = \epsilon_w (J^- - \hat{\sigma} T_w^4). \quad (3.13)$$

The uncertainty in the mechanism of coal combustion and the unavailability of detailed data for the radiation properties of the various components of coal flames have proven to be major obstacles in the accurate evaluation of the radiation transport in these media. This unavailability or uncertainty in radiation properties has effectively crippled most computer codes that attempt to model radiative transfer in coal suspensions. Fortunately, it is likely that the presence of large particles (relative to the radiation wavelength) causes these suspensions to be essentially gray,^{13,16} which simplifies greatly the solution of the equation of transfer. Radiant emission by gases has little effect on the spectral dependence of emitted radiation until most of the large coal and char particles have been consumed. Even after this consumption, it is possible that radiant emission by ash particles dominates that by gases, leading to a continuous (and possibly gray) emission spectrum. In conclusion, a real need exists for further investigation of the radiative properties of gases and ash particles, of the formation mechanism and expected concentrations of soot particles in coal flames, and of the effects of particle shape irregularity, composition, and agglomeration on the radiation properties of particle suspensions.

4.0 SOLUTION OF THE EQUATION OF TRANSFER

In this chapter, it is assumed that the radiation properties are known throughout a medium, and methods for obtaining the solution of the radiative transfer equation are discussed. Analytical solutions are known only for very specialized situations such as non-scattering media and non-emitting, infinite or semi-infinite media.⁴⁰ No exact solution is known for the general form of the equation of transfer, and, consequently, a number of approximate and numerical methods have been developed to compute the radiant interchange in scattering and emitting media. These methods include the discrete ordinates method,²⁶ flux methods,^{41,42} spherical harmonics (a special case of which is the diffusion approximation)^{1,5} and Monte Carlo methods.^{43,44} The most commonly used techniques are Chandrasekhar's discrete ordinates method^{26,45,46} and the flux methods. In this chapter, various solution methods are reviewed, with particular emphasis on the solution of the equation of transfer by a numerical discrete ordinates method and by the diffusion approximation. These two methods, which were originally developed for solution of the neutron transport equation, are used extensively and will be applied later in this work to compute the radiation field in a coal suspension model (see Chapter 5).

For illustrative purposes, the various numerical methods are presented for the case of quasi-steady radiative transfer in a plane-symmetric medium which is in local thermodynamic equilibrium and in

which the temperature distribution is specified. (The solution of the equation of transfer in a medium with an unknown temperature distribution is discussed in the final section of this chapter.) Discussion of the Monte Carlo method, which is used primarily for multi-dimensional or complicated geometries is omitted altogether, and the interested reader should consult references 43 and 44.

4.1 The Equation of Transfer and Boundary Conditions

The quasi-steady, plane-symmetric, azimuthally averaged equation of transfer in plane geometry can be written as [see Eq. (2.14)]

$$\mu \frac{\partial I_v(x, \mu)}{\partial \mu} + \sigma_{ev}(x) I_v(x, \mu) = \frac{\sigma_{sv}(x)}{2} \int_{-1}^1 I_v(x, \mu') p_v(\mu' \rightarrow \mu, x) d\mu' + E_v(x). \quad (4.1)$$

For a particle-gas mixture, the extinction and absorption coefficients are computed from the sum of the coefficients evaluated separately for each phase, and the emission term $E_v(x)$ depends on the temperature of each phase as

$$E_v(x) = \sigma_{avp} B_v[T_p(x)] + \sigma_{avg} B_v[T_g(x)].$$

Equation (4.1) may thus be used to compute the intensity in a medium of arbitrary composition if the radiation properties and the emission term are evaluated properly from those of the individual components.

The single scatter albedo ω_v and the differential optical thickness $d\xi_v$ are defined by

$$\omega_v = \sigma_{sv}/\sigma_{ev}, \quad (4.2)$$

and

$$d\xi_v = \sigma_{ev} dx \quad \text{or} \quad \xi_v = \int_0^x \sigma_{ev}(x) dx \quad (4.3)$$

Division of each term in Eq. (4.1) by σ_{ev} and use of Eqs. (4.2) and (4.3) yields

$$\begin{aligned} \mu \frac{\partial I_v(\xi_v, \mu)}{\partial \xi_v} + I_v(\xi_v, \mu) &= \frac{\omega_v(\xi_v)}{2} \int_{-1}^1 I_v(\xi_v, \mu') p_v(\mu' \rightarrow \mu, \xi_v) d\mu' \\ &+ E_v(\xi_v) / \sigma_{ev}(\xi_v) \end{aligned} \quad (4.4)$$

The emission term E_v is a known function of position if the temperature of each phase is specified a priori throughout the medium.

For ease of notation, the monochromatic subscript is omitted in the subsequent discussion; however it should be remembered that the quantities I_v , ξ_v , a_v , ρ_v , and E_v are all frequency-dependent. Equation (4.4) can thus be written as

$$\mu \frac{\partial I(\xi, \mu)}{\partial \xi} + I(\xi, \mu) = \frac{\omega(\xi)}{2} \int_{-1}^1 I(\xi, \mu') p(\mu' \rightarrow \mu, \xi) d\mu' + \frac{E(\xi)}{\sigma_e(\xi)}. \quad (4.5)$$

It is important to note that Eq. (4.5) also applies to the multi-frequency range and gray cases if the emission source term $E(\xi)$ is redefined as

$$E(\xi) \equiv E_n(\xi) = \int_{\Delta\nu_n} E_v(\xi) d\nu, \quad n = 1, N, \quad (4.6a)$$

(multi-frequency case)

or

$$E(\xi) \equiv \sigma_a(\xi) \hat{\sigma} T^4(\xi) / \pi, \quad (\text{gray case}) \quad (4.6b)$$

where, for the multi-frequency case, the intensity [in Eq. (4.5)]

is understood to be integrated over the various frequency intervals, while for the gray case, the intensity is integrated over all frequencies.

The radiative transfer equation is a first order integro-differential equation and its solution requires a boundary condition for the intensity $I(\xi, \mu)$. The simplest boundary condition specifies the incident intensity on the medium at its boundaries (assumed for the present plane geometry example to be at $x=0$ and $x=x_t$). If the boundaries are non-reflecting, the boundary conditions may thus be expressed as

$$I(0, \mu) = f(\mu) \quad \text{for } \mu > 0 \quad (4.7a)$$

$$I(\xi_t, \mu) = g(\mu) \quad \text{for } \mu < 0, \quad (4.7b)$$

where ξ_t is the optical thickness of the medium ($= \int_0^{x_t} \sigma_e(x) dx$, x_t = actual thickness of medium), and $f(\mu)$ and $g(\mu)$ are functions expressing the directional dependence of the incident intensity.

If, in addition to a specified incident intensity at the boundaries, it is assumed that a fraction of the outwardly moving intensity is diffusely reflected back into the system, the boundary conditions become

$$I(0, \mu) = f(\mu) + 2\rho_{w1} \int_0^{-1} \mu' I(0, \mu') d\mu' \quad \mu > 0 \quad (4.8a)$$

$$I(\xi_t, \mu) = g(\mu) + 2\rho_{w2} \int_0^1 \mu' I(0, \mu') d\mu' \quad \mu < 0, \quad (4.8b)$$

where ρ_{w1} and ρ_{w2} are the reflectivities of the boundaries at $\xi=0$ and $\xi=\xi_t$, respectively. A physical example of these boundary conditions is provided by combustor walls, which are typically diffuse

reflectors and which emit radiant energy at a rate proportional to the fourth power of their temperature. This wall emission gives rise to the function $f(\mu)$ and $g(\mu)$ that appear in Eqs. (4.8a) and (4.8b), respectively.

4.2 The Discrete Ordinates Method

In the discrete ordinates method, the solution of the equation of transfer, $I(\xi, \mu)$, is sought for discrete values of μ which are usually the ordinates of a numerical quadrature set. The scattering integral of Eq. (4.5) is thus replaced by an appropriate numerical integration formula, and the radiative transfer equation is transformed into a set of coupled, ordinary, differential equations. The results can be written as

$$\mu_i \frac{dI(\xi, \mu_i)}{d\xi} + I(\xi, \mu_i) = \frac{\omega(\xi)}{2} \sum_{j=1}^M w_j I(\xi, \mu_j) p(\mu_j \rightarrow \mu_i, \xi) + E(\xi) / \sigma_e(\xi),$$

$$i = 1, M, \quad (4.9)$$

where M is the number of discrete directions considered, and μ_j and w_j are the ordinates and weights, respectively, of an M^{th} order quadrature set.

4.2.1 Chandrasekhar's Method

In the discrete ordinates method of Chandrasekhar, the solution of Eqs. (4.9) is determined analytically as a continuous function of the spatial variable ξ for each discrete direction μ_i . Equation (4.9) can be rewritten in the form

$$\frac{d\underline{I}(\xi)}{d\xi} + \underline{F}(\xi) \underline{I}(\xi) = \underline{S}(\xi), \quad (4.10)$$

where the elements of \underline{I} , \underline{F} , and \underline{S} are

$$I_i = I(\xi, \mu_i) \quad (4.11a)$$

$$F_{ij} = \frac{1}{\mu_i} \delta_{ij} - \frac{\omega(\xi)}{2} \frac{w_j}{\mu_i} p(\mu_j \rightarrow \mu_i, \xi) \quad (4.11b)$$

$$S_i = \frac{E(\xi)}{\mu_i \sigma_e(\xi)} \quad (4.11c)$$

and where δ_{ij} is the Kronecker delta. Equation (4.10) represents a set of coupled first order differential equations which may be solved by standard methods (see References 47 and 48). The analytical solution of these equations, while expressible in closed form, is complex and leads to unwieldy expressions for the intensity $I(\xi, \mu_i)$ which are not readily amenable to numerical evaluation.

A number of features of Chandrasekhar's method can be illustrated by considering the simple case of isotropic scattering in a homogeneous, non-emitting medium. In this case, the single scatter albedo is independent of position, the emission term vanishes, and the phase function $p(\mu' \rightarrow \mu)$ becomes unity. The quasi-steady, plane symmetric discrete ordinates equations [Eqs. (4.9)] thus become

$$\mu_i \frac{dI(\xi, \mu_i)}{d\xi} + I(\xi, \mu_i) = \frac{\omega}{2} \sum_{j=1}^M w_j I(\xi, \mu_j), \quad i=1, M. \quad (4.12)$$

The solution of this homogeneous equation can be written^{26,49}

$$I(\xi, \mu_i) = \sum_{s=1}^M \frac{A_s}{1 + \mu_i k_s} \exp(k_s \xi), \quad (4.13)$$

where the A_s are constants to be determined from the boundary conditions, and the k_s are computed from the so-called characteristic equation²⁶

$$1 = \frac{\omega}{2} \sum_{j=1}^M \frac{w_j}{1+\mu_j k}. \quad (4.14)$$

This equation arises because substitution of Eq. (4.13) into Eq. (4.12) yields a homogeneous equation for $A_s/(1+\mu_j k)$. The right side of this equation can thus be arbitrarily normalized to unity to obtain Eq. (4.14).

Since the μ_j of most quadrature sets are symmetrically placed about the origin ($\mu=0$), the values of k_s computed from Eq. (4.14) are also paired as $\pm k_s$. To compute these values of k_s the characteristic equation is rewritten in the form

$$\prod_{j=1}^M (1+k\mu_j) - \frac{\omega}{2} \sum_{j=1}^M w_j \prod_{\substack{i=1 \\ i \neq j}}^M (1+k\mu_i) = 0, \quad (4.15)$$

which is a polynomial equation of degree M in k . Hence, there are M roots (k_s , $s=1, \dots, M$) which are found to be symmetrically placed about the origin and which fall between successive values of $1/\mu_j$.⁴⁹

The constants A_s in Eq. (4.13) are determined from the boundary conditions. If it is assumed (for simplicity) that the boundaries are non-reflecting, the A_s are given by

$$I(0, \mu_i) = \sum_{s=1}^M \frac{A_s}{1+\mu_i k_s} = f(\mu_i), \quad i=1, \dots, \frac{M}{2} \quad (4.16a)$$

$$I(\xi_t, \mu_i) = \sum_{s=1}^M \frac{A_s \exp(\xi_t k_s)}{1+\mu_i k_s} = g(\mu_i), \quad i = \frac{M}{2}+1, \dots, M, \quad (4.16b)$$

where $\mu_1, \dots, \mu_{M/2}$ are the positive discrete values of μ , and $\mu_{1+M/2}, \dots, \mu_M$ are the negative values (see Fig. 4.1).

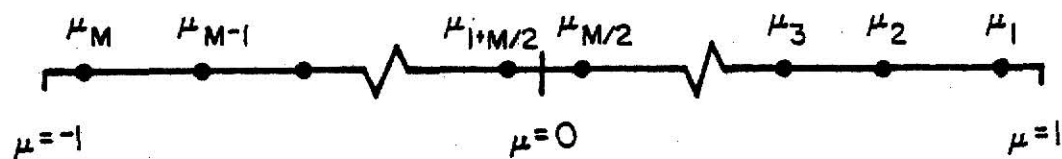


Fig. 4.1. Indexing of the discrete ordinates of an even quadrature set.

Equations (4.16a) and (4.16b) can be written in matrix form as

$$\underline{Z} \underline{Y} = \underline{B} \quad (4.17)$$

where the elements of \underline{Z} , \underline{Y} , and \underline{B} are

$$Z_{ij} = \begin{cases} \frac{1}{1+\mu_i k_j} & i = 1, \dots, \frac{M}{2} \\ \frac{\exp(k_j \xi_t)}{1+\mu_i k_j} & i = \frac{M}{2}+1, \dots, M \end{cases} \quad (4.18a)$$

$$Y_i = A_i \quad i = 1, \dots, M \quad (4.18b)$$

$$B_i = \begin{cases} I(0, \mu_i) & i = 1, \dots, M/2 \\ I(\xi_t, \mu_i) & i = \frac{M}{2}+1, \dots, M. \end{cases} \quad (4.18c)$$

The constants A_s , $s=1, \dots, M$ must be determined by solution of this matrix equation. For high orders of angular approximation (i.e., small $\mu_{\min} = \mu_{M/2}$, and therefore, large $k_{\max} = k_{M/2}$), the matrix elements in Eq. (4.17) related to $\exp(k_{\max} \xi_t)$ and $\exp(-k_{\max} \xi_t)$ become very large and very small, respectively. Thus the matrix \underline{Z} becomes ill-conditioned, and the numerical solution of Eq. (4.17) is inherently unstable.^{41,50} This numerical instability with large quadrature orders is the fundamental problem with the use of Chandrasekhar's discrete ordinates method.

Chandrasekhar's method suffers from a number of additional disadvantages. The roots of the characteristic equation must be calculated by an iterative numerical procedure, since explicit expressions for the roots cannot be written. Therefore, even

though the discrete ordinates equations [Eq. (4.12)] are solved analytically as continuous functions of position, an error is introduced by the numerical calculation of the roots. Furthermore, the calculation of the roots k_s and the constants A_s requires considerable computational effort if a large number of discrete ordinates are required. Finally, the inclusion of thermal emission or the consideration of non-homogeneous or multi-dimensional media increases greatly the difficulty of solving the discrete ordinates equations and performing the associated numerical computations.

4.2.2 A Numerical Discrete Ordinates Method

The modern discrete ordinates method, which is superior in many respects to Chandrasekhar's original method, is based on a numerical solution of the discrete ordinates equations. This method is used extensively for solving gamma photon and neutron transport problems, and its versatility has caused Chandrasekhar's method to be primarily of historical interest. In this numerical method, the intensity in each discrete direction is sought at a number of spatial mesh points which are used to discretize the spatial variable. No attempt is made to determine the intensity analytically as a continuous function of position.

The total optical thickness of a medium, ξ_t , is divided into $N-1$ intervals (nodes) of thickness $\Delta [= \xi_t / (N-1)]$ using N mesh points, as illustrated in Fig. 4.2. The discrete ordinates equations [Eq. (4.9)] are evaluated at the center of each node, and the spatial derivatives

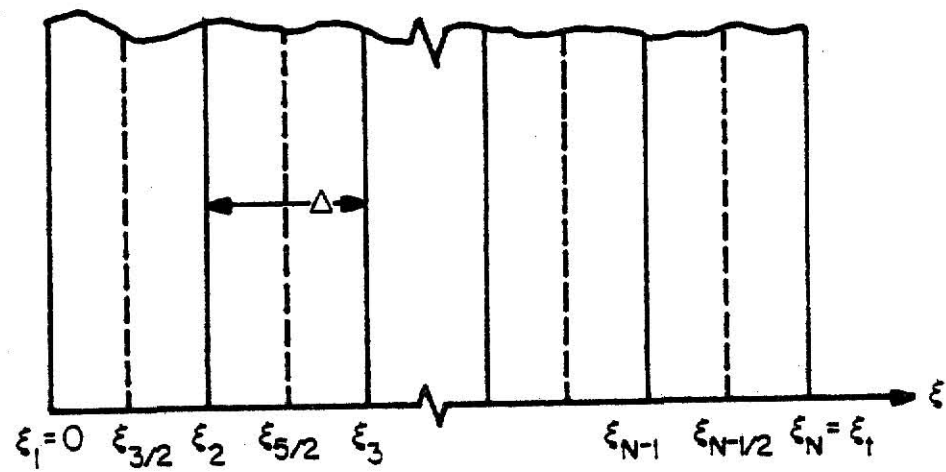


Fig. 4.2. Discretization of the optical thickness ξ_t of a plane-symmetric medium into $N-1$ intervals (each of thickness Δ) using N mesh points.

in these equations are then approximated in terms of intensities at the node boundaries. The simplest approximation is to use a central difference scheme to obtain

$$\mu_i \frac{I_i(\xi_{k+1}) - I_i(\xi_k)}{\Delta} + I_i(\xi_{k+1/2}) = Q_i(\xi_{k+1/2}), \quad k=1, \dots, N-1 \quad (4.19)$$

$$i=1, \dots, M,$$

where

$$I_i(\xi_k) \equiv I(\xi_k, \mu_i) \quad (4.20)$$

$$Q_i(\xi_{k+1/2}) \equiv \frac{\omega(\xi_{k+1/2})}{2} \sum_{j=1}^M w_j I_j(\xi_{k+1/2}) P(\mu_j \rightarrow \mu_i, \xi_{k+1/2}) + \frac{E(\xi_{k+1/2})}{\sigma_e(\xi_{k+1/2})} \quad (4.21)$$

The quantity $Q_i(\xi_{k+1/2})$ is called the source term and is seen to be composed of a scattering component and a thermal emission component. The node center intensity $I_i(\xi_{k+1/2})$ is assumed to be the average of the node boundary values, i.e.,

$$I_i(\xi_{k+1/2}) = \frac{1}{2} [I_i(\xi_{k+1}) + I_i(\xi_k)], \quad k=1, N-1. \quad (4.22)$$

Substitution for the node-center intensity from Eq. (4.22) into Eq. (4.19) and solving for the node boundary intensities yields

$$I_i(\xi_{k+1}) = \frac{1-\Delta/2\mu_i}{1+\Delta/2\mu_i} I_i(\xi_k) + \frac{\Delta/\mu_i}{1+\Delta/2\mu_i} Q_i(\xi_{k+1/2}), \quad (4.23)$$

or

$$I_i(\xi_k) = \frac{1+\Delta/2\mu_i}{1-\Delta/2\mu_i} I_i(\xi_{k+1}) - \frac{\Delta/\mu_i}{1-\Delta/2\mu_i} Q_i(\xi_{k+1/2}). \quad (4.24)$$

Equations (4.23) and (4.24) can be used to compute the radiation intensity successively at each mesh point ξ_k and for each direction μ_i given the source term Q_i at the node centers. Numerical round-

off error is minimized if Eq. (4.23) is used to compute the intensity for positive values of μ [i.e., photons moving toward increasing ξ (forward)], and Eq. (4.24) is used to compute the intensity for negative μ [i.e., photons moving toward decreasing ξ (backward)].³¹ These equations can be viewed as forward and backward sweeps, respectively, since the intensity is computed at successive points along the forward or backward directions of the photon travel.

To initiate the forward and backward sweeps, the boundary values of the radiation intensity are required. These boundary intensities are given by Eqs. (4.8a) and (4.8b) and are rewritten for discretized values of the spatial and angular variables as

$$I_i(\xi_1) = f_i + 2\rho_{w1} \sum_{j=M/2+1}^M w_j |\mu_j| I_j(\xi_1), \quad i=1, \dots, M/2 \quad (4.25a)$$

$$I_i(\xi_N) = g_i + 2\rho_{w2} \sum_{j=1}^{M/2} w_j \mu_j I_j(\xi_N), \quad i=\frac{M}{2}+1, \dots, M, \quad (4.25b)$$

where $f_i = f(\mu_i)$ and $g_i = g(\mu_i)$. Equation (4.25a) is used to initiate the forward sweep of Eq. (4.23) (for positive μ_i), while Eq. (4.25b) initiates the backward sweep of Eq. (4.24) (for negative μ_i).

Since the source distribution $Q_i(\xi_{k+1/2})$ and the reflected component of the boundary intensities depend on the unknown intensity distribution, an iterative solution procedure is used to converge to the solution. This iteration procedure is outlined below:

- a) guess an initial source distribution $Q_i(\xi_{k+1/2})$, $k=1, N-1$;
 $i=1, M$.

- b) guess the incident intensity distribution $I_i(\xi_1)$ for positive μ_i .
- c) compute the radiation intensity at all mesh points and for all directions using the forward and backward sweeps from Eqs. (4.23) and (4.24).
- d) compute the node-center intensity in each node for all directions using Eq. (4.22).
- e) recompute the source distribution using Eq. (4.21).
- f) return to step c to recompute the radiation intensities based on updated values of the source distribution and the incident intensity.
- g) repeat steps c to f until convergence to a specified accuracy is achieved for the intensity at all mesh points and discrete angles.

This numerical discrete ordinates method is a powerful technique that is readily applied to the calculation of the intensity in non-homogeneous, multi-dimensional media which emit and scatter radiant energy. The primary disadvantage of this method is the need for a sufficiently fine spatial grid so that the spatial derivative in the equation of transfer is well approximated by its finite difference representation. As a result, large arrays are often needed to store the intensity at all the discrete grid points and directions, particularly in the solution of multi-dimensional problems. New methods (e.g., nodal methods⁵¹ and coarse-mesh techniques⁵²) are presently being developed to solve the discrete ordinates equations very accurately using coarse spatial grids, thereby reducing computer storage requirements and computational effort. Another possible

disadvantage of the numerical technique is the slow rate of convergence of the intensity (i.e., the need for many iterations) in media characterized by large values of the source term.⁵³ However, the convergence rate may be accelerated by extrapolation of source distributions computed in previous iterations prior to recalculation of the intensity distribution.

4.2.3 Evaluation of the Scattering Matrix

The scattering matrix element $p(\mu_j \rightarrow \mu_i, x)$ is obtained directly by evaluation of the azimuthally averaged phase function $p(\mu' \rightarrow \mu, x)$ at the discrete directions μ_j and μ_i . If the phase function is rotationally invariant, $p(\mu' \rightarrow \mu, x)$ is given by [cf. Eq. (2.13)]

$$p(\mu' \rightarrow \mu) = \frac{1}{2\pi} \int_0^{2\pi} p(\mu' \rightarrow \mu, \phi) d\phi, \quad (4.26)$$

where the explicit dependence of p on position is omitted for simplicity. The most common method of obtaining $p(\mu' \rightarrow \mu)$ is to expand $p(\mu' \rightarrow \mu, \phi)$ [$= p(\cos\theta)$, where $\cos\theta = \mu\mu' + (1-\mu^2)^{1/2}(1-\mu'^2)^{1/2}\cos\phi$] in terms of Legendre polynomials, i.e.,

$$p(\cos\theta) = \sum_{\ell=0}^L \gamma_{\ell} P_{\ell}(\cos\theta), \quad (4.27)$$

where the series has been truncated after $L+1$ terms. The expansion coefficients γ_{ℓ} may be computed by utilizing the orthogonality of Legendre polynomials to obtain^{26,31}

$$\gamma_{\ell} = \frac{2\ell+1}{2} \int_{-1}^1 p(\cos\theta) P_{\ell}(\cos\theta) d\cos\theta. \quad (4.28)$$

Substitution of $p(\cos\theta)$ [$\equiv p(\mu' \rightarrow \mu, \phi)$] from Eq. (4.27) into Eq. (4.26) and use of the addition theorem of spherical harmonics⁵⁴ gives the azimuthally averaged phase function

$$p(\mu' \rightarrow \mu) = \sum_{\ell=0}^L \gamma_{\ell} P_{\ell}(\mu) P_{\ell}(\mu'). \quad (4.29)$$

The premature truncation of the Legendre polynomial expansion of Eq. (4.27) may lead to oscillatory behavior or negative values in the evaluation of the scattering source for the discrete ordinates equations.³² To avoid these truncation errors, the azimuthally averaged phase function can be computed directly from Eq. (4.26) by numerical evaluation of the azimuthal integral.

4.3 Flux Methods

A number of so-called flux methods have been developed to compute the transport of radiation in scattering media.⁴¹ The flux methods are based on the approximation of the continuous angular variation of the intensity by a finite number of partial radiant fluxes over a set of discrete solid angle ranges. The most widely used flux techniques are the two-flux method due to Schuster,²⁶ and the six-flux method of Chu and Churchill.⁵⁵ The two-flux method describes the radiation field at every point by two oppositely directed radiant fluxes, while in the six-flux method, the radiation field at any point is decomposed into six orthogonal components. The flux equations are derived by assuming the intensity of radiation to be uniform within each of the contiguous solid angles into which the total solid angle about a given point is subdivided. The sub-

sequent integration of the radiative transfer equation over each of these solid angle ranges reduces the integro-differential equation of transfer to a set of approximate, coupled, ordinary differential equations.

Here, a general M-flux method is derived for use in plane-symmetric, quasi-steady radiative transfer problems. The radiative transfer equation is written as

$$\mu \frac{\partial I(\xi, \mu)}{\partial \xi} + I(\xi, \mu) = \frac{\omega(\xi)}{2} \int_{-1}^1 I(\xi, \mu') p(\mu' \rightarrow \mu) d\mu' + \frac{E(\xi)}{\sigma_e(\xi)}. \quad (4.30)$$

The total solid angle at any ξ is divided into M contiguous ranges $\Delta\Omega_i$, $i=1, M$, with the various ranges defined by

$$\Delta\Omega_i : \mu_i \leq \mu \leq \mu_{i-1}, \quad 0 \leq \phi \leq 2\pi, \quad i=1, M, \quad (4.31)$$

where $\mu_0 = 1$ and $\mu_M = -1$. Integration of Eq. (4.30) over the i^{th} solid angle range yields

$$\begin{aligned} 2\pi \int_{\mu_i}^{\mu_{i-1}} \mu \frac{\partial I(\xi, \mu)}{\partial \xi} d\mu + 2\pi \int_{\mu_i}^{\mu_{i-1}} I(\xi, \mu) d\mu = \\ 2\pi \int_{\mu_i}^{\mu_{i-1}} \frac{\omega(\xi)}{2} d\mu \int_{-1}^1 I(\xi, \mu') p(\mu' \rightarrow \mu) d\mu' + 2\pi \int_{\mu_i}^{\mu_{i-1}} \frac{E(\xi)}{\sigma_e(\xi)} d\mu, \end{aligned} \quad (4.32)$$

$i=1, M.$

The partial radiant flux for the i -th solid angle, $J_i(\xi)$ [cf. Eq. (2.38)], may be written for the assumed one-dimensional geometry as

$$J_i(\xi) = 2\pi \int_{\mu_i}^{\mu_{i-1}} \mu I(\xi, \mu) d\mu. \quad (4.33)$$

If the intensity is assumed constant over the i^{th} solid angle range $[\equiv I_i(\xi)]$, the partial flux $J_i(\xi)$ becomes

$$J_i(\xi) = \pi(\mu_{i-1}^2 - \mu_i^2) I_i(\xi). \quad (4.34)$$

With this assumption of constant intensity in each solid angle, Eq. (4.32) yields the flux equations:

$$\begin{aligned} \frac{dJ_i(\xi)}{d\xi} + \frac{2}{\mu_{i-1} + \mu_i} J_i(\xi) &= \omega(\xi) \sum_{j=1}^M \frac{p_{ji}}{2(\mu_{j-1} - \mu_j)} J_j(\xi) \\ &+ 2\pi(\mu_{i-1} - \mu_i) \frac{E(\xi)}{\sigma_e(\xi)}, \quad i=1, M, \end{aligned} \quad (4.35)$$

where

$$p_{ji} = \int_{\mu_j}^{\mu_{j-1}} d\mu' \int_{\mu_i}^{\mu_{i-1}} p(\mu' \rightarrow \mu) d\mu. \quad (4.36)$$

For the two flux case ($M=2$), $J_1(\xi)$ is the partial flux over the forward hemisphere ($0 \leq \mu \leq 1$, $0 \leq \phi \leq 2\pi$), while $J_2(\xi)$ is defined over the backward hemisphere ($-1 \leq \mu \leq 0$, $0 \leq \phi \leq 2\pi$).

Equation (4.35) becomes:

$$\frac{dJ_1(\xi)}{d\xi} + 2 J_1(\xi) = \omega(\xi) [p_{11} J_1(\xi) + p_{21} J_2(\xi)] + 2\pi \frac{E(\xi)}{\sigma_e(\xi)}, \quad (4.37)$$

and

$$\frac{dJ_2(\xi)}{d\xi} - 2 J_2(\xi) = \omega(\xi) [p_{12} J_1(\xi) - p_{22} J_2(\xi)] + 2\pi \frac{E(\xi)}{\sigma_e(\xi)}. \quad (4.38)$$

If backward scattering is neglected (i.e., $p_{12} = p_{21} = 0$), these equations reduce to the two-flux equations derived by Schuster.¹⁶

For the general M -flux case, Eq. (4.35) may be rewritten in matrix form as

$$\frac{d\mathbf{J}(\xi)}{d\xi} + \mathbf{F}(\xi) \mathbf{J}(\xi) = \mathbf{S}(\xi), \quad (4.39)$$

where the elements of \underline{J} , \underline{F} , and \underline{S} are

$$J_i = J_i(\xi) \quad (4.40a)$$

$$F_{ij} = \frac{2 \delta_{ij}}{\mu_{i-1} + \mu_i} - \frac{\omega(\xi)}{\mu_{j-1}^2 - \mu_j^2} p_{ji} \quad (4.40b)$$

$$S_i = 2\pi(\mu_{i-1} - \mu_i) E(\xi) / \sigma_e(\xi). \quad (4.40c)$$

These equations are similar in form to the discrete ordinates equations and can be solved by the same analytical or numerical techniques used in the discrete ordinates method.

Solution of the flux equations requires boundary conditions on the partial radiant fluxes. These conditions are obtained by angular integration of the boundary conditions for the radiation intensity, Eqs. (4.8a) and (4.8b). The resulting conditions are

$$J_i(0) = \pi(\mu_{i-1}^2 - \mu_i^2) f_i + \rho_{w1}(\mu_{i-1}^2 - \mu_i^2) \sum_{j=\frac{M}{2}+1}^M J_j(0), \quad i=1, M/2, \quad (4.41a)$$

and

$$J_i(\xi_t) = \pi(\mu_{i-1}^2 - \mu_i^2) g_i + \rho_{w2}(\mu_{i-1}^2 - \mu_i^2) \sum_{j=1}^{M/2} J_j(\xi_t), \quad i=\frac{M}{2}+1, M, \quad (4.41b)$$

where f_i and g_i are the incident functions $f(\mu)$ and $g(\mu)$, which have been assumed constant over the i^{th} range of μ .

The flux methods are generally less accurate than the discrete ordinates method (based on the same number of discrete directions as the number of partial fluxes) because of the key assumption made

in the derivation of the flux equations that the intensity is constant within each solid angle range. The accuracy of the flux methods can be improved, however, if better approximations of the directional dependence of the intensity within each range are used. The assumption of linear⁵⁶ or higher order polynomial variations⁵⁷ have been shown to yield excellent results in neutron transport problems.

4.4 The Diffusion Approximation

In many cases, details of the directional dependence of the radiation intensity are not required, and only the integrated intensity is of interest. An approximate equation for the integrated intensity Φ may be derived by integration of the equation of transfer and its first angular moment over all directions. The intensity distribution in the latter equation is then expanded in a series of spherical harmonics (Legendre polynomials in one-dimensional geometry). Truncation of this series after the linear terms yields two equations in two unknowns, the integrated intensity and the net flux. This truncation is termed the P_1 approximation and is equivalent to assuming the intensity to be only linearly anisotropic. Elimination of the net flux from the two equations then yields⁵⁸

$$-\nabla \cdot [D_v(\vec{r}) \nabla \phi_v(\vec{r})] + \sigma_{av}(\vec{r}) \phi_v(\vec{r}) = 4\pi E_v(\vec{r}), \quad (4.42)$$

where

$$\phi_v(\vec{r}) = \int_{4\pi} I_v(\vec{r}, \vec{\Omega}) d\Omega \quad (4.43)$$

$$D_v(\vec{r}) = \frac{1}{3} [\sigma_{ev}(\vec{r}) - \bar{\mu}_v^* \sigma_{sv}(\vec{r})]^{-1}, \quad (4.44)$$

and

$$\bar{\mu}_v^* = \frac{1}{(4\pi)^2} \int_{4\pi} d\Omega \int_{4\pi} \vec{\Omega} \cdot \vec{\Omega}' p_v(\vec{\Omega}' \cdot \vec{\Omega}) d\Omega', \quad (4.45)$$

and where the scattering phase function p_v is assumed to be rotationally invariant. The quantities D_v and $\bar{\mu}_v^*$ are the diffusion coefficient and the average cosine of the scattering angle θ , respectively.

If the quantity $\vec{\Omega} \cdot \vec{\Omega}' (= \cos\theta)$ is denoted by μ^* , Eq. (4.45) simplifies to

$$\bar{\mu}_v^* = \frac{1}{2} \int_{-1}^1 \mu^* P_v(\mu^*) d\mu^*. \quad (4.46)$$

The numerical solution of the diffusion equation will be illustrated for one-dimensional plane geometry. In this geometry, the diffusion equation, Eq. (4.42), becomes

$$-\frac{d}{dx} [D(x) \frac{d\phi(x)}{dx}] + \sigma_a(x) \phi(x) = S(x), \quad (4.47)$$

where

$$\phi(x) = 2\pi \int_{-1}^1 I(x, \mu) d\mu, \quad (4.48)$$

and

$$S(x) = 4\pi E(x), \quad (4.49)$$

and where the monochromatic subscript v has been suppressed.

Equation (4.47) describes equally well the multi-frequency range case or the gray case if the directionally integrated intensity $\phi(x)$ is understood to be integrated over various frequency ranges or over all frequencies, respectively, and if the emission

source term $S(x)$ is given by either

$$S(x) = 4\pi E_n(x), \quad n=1, N \text{ (multi-frequency case)}, \quad (4.50a)$$

or

$$S(x) = 4 \sigma_a(x) \hat{\sigma} T^4(x) \quad (\text{gray case}). \quad (4.50b)$$

The diffusion equation, Eq. (4.47) is an inhomogeneous, second order differential equation with non-constant coefficients. If the emission source term $S(x)$ and the absorption and diffusion coefficients are known functions of position, the solution of the diffusion equation can in some cases be determined analytically. In general, however, the solution must be obtained numerically.

The diffusion equation can be written in terms of the optical coordinate ξ by division of each term in Eq. (4.47) by σ_e and multiplication of D in the first term by σ_e/σ_e , namely

$$-\frac{d}{d\xi} D'(\xi) \frac{d\phi(\xi)}{d\xi} + \sigma_a'(\xi) \phi(\xi) = S'(\xi), \quad (4.51)$$

where

$$D'(\xi) = D(\xi) \sigma_e(\xi) \quad (4.52a)$$

$$\sigma_a'(\xi) = \sigma_a(\xi)/\sigma_e(\xi) \quad (4.52b)$$

$$S'(\xi) = S(\xi)/\sigma_e(\xi), \quad (4.53)$$

and where the substitution $d\xi = \sigma_e(x)dx$ has been made.

Since the diffusion equation is a second order differential equation, its solution requires two boundary conditions involving the integrated intensity, $\phi(x)$. These conditions can be obtained by

multiplication of the boundary conditions on the intensity, Eqs. (4.8a) and (4.8b) by μ and integrating Eq. (4.8a) over positive values of μ and Eq. (4.8b) over negative values. These equations become

$$\int_0^1 \mu I(0, \mu) d\mu = \int_0^1 \mu f(\mu) d\mu + 2\rho_{w1} \int_0^1 \mu d\mu \int_0^{-1} \mu' I(\xi_t, \mu') d\mu' \quad (4.54)$$

$$\int_0^{-1} \mu I(\xi_t, \mu) d\mu = \int_0^{-1} \mu g(\mu) d\mu + 2\rho_{w2} \int_0^{-1} \mu d\mu \int_0^1 \mu' I(0, \mu') d\mu'. \quad (4.55)$$

The partial fluxes $J^+(\xi)$ and $J^-(\xi)$ are defined by

$$J^+(\xi) = 2\pi \int_0^1 \mu I(\xi, \mu) d\mu, \quad (4.56)$$

and

$$J^-(\xi) = 2\pi \int_0^{-1} \mu I(\xi, \mu) d\mu. \quad (4.57)$$

These quantities may be used to rewrite Eqs. (4.54) and (4.55) as

$$J^+(0) = F + \rho_{w1} J^-(0) \quad (4.58)$$

$$J^-(\xi_t) = G + \rho_{w2} J^+(\xi_t), \quad (4.59)$$

where

$$F = 2\pi \int_0^1 \mu f(\mu) d\mu, \quad (4.60)$$

and

$$G = 2\pi \int_0^{-1} \mu g(\mu) d\mu. \quad (4.61)$$

The partial fluxes $J^+(\xi)$ and $J^-(\xi)$ are related to the integrated intensity $\phi(\xi)$ by⁵⁹

$$J^+(\xi) = \frac{\phi(\xi)}{4} - \frac{D'(\xi)}{2} \frac{d\phi(\xi)}{d\xi} \quad (4.62)$$

$$J^-(\xi) = \frac{\Phi(\xi)}{4} + \frac{D'(\xi)}{2} \frac{d\Phi(\xi)}{d\xi} . \quad (4.63)$$

Substitution of these expressions into Eqs. (4.58) and (4.59) gives the boundary conditions in terms of the integrated intensity $\Phi(\xi)$ as

$$D'(0) \frac{d\Phi(0)}{d\xi} = a_1 \Phi(0) - b_1 \quad (4.64)$$

$$D'(\xi_t) \frac{d\Phi(\xi_t)}{d\xi} = -a_2 \Phi(\xi_t) + b_2, \quad (4.65)$$

where

$$a_1 = \frac{1}{2} \frac{1-\rho_{w1}}{1+\rho_{w1}} \quad (4.66a)$$

$$a_2 = \frac{1}{2} \frac{1-\rho_{w2}}{1+\rho_{w2}} \quad (4.66b)$$

$$b_1 = 2 \frac{F}{1+\rho_{w1}} \quad (4.66c)$$

$$b_2 = 2 \frac{G}{1+\rho_{w2}} . \quad (4.66d)$$

To obtain a numerical solution of the diffusion equation, the total optical thickness of the medium is divided into $N-1$ nodes using N mesh points (see Fig. 4.2). Integration of the diffusion equation over the thickness of one node about each interior (non-boundary) mesh point and approximation of spatial derivatives by finite differences yields

$$-D'_{k-1/2} \Phi_{k-1} + [D'_{k-1/2} + D'_{k+1/2} + \frac{\Delta^2}{2} (\sigma'_{a,k+1/2} + \sigma'_{a,k-1/2})] \Phi_k$$

$$-D'_{k+1/2} \Phi_{k+1} = S'_k \Delta^2, \quad k=2, \dots, N-1, \quad (4.67)$$

where

$$\phi_k = \frac{1}{\Delta} \int_{\xi_{k-1/2}}^{\xi_{k+1/2}} \phi(\xi) d\xi \quad (4.68)$$

$$S'_k = \frac{1}{\Delta} \int_{\xi_{k-1/2}}^{\xi_{k+1/2}} S'(\xi) d\xi \approx S'(\xi_k), \quad (4.69)$$

and where the subscripts $k-1/2$ and $k+1/2$ imply that the values of σ'_a and D' are evaluated in the nodes to the left and right of the point ξ_k , respectively.

Equation (4.67) represents a set of $N-2$ equations for the N unknown values of the integrated intensity at each mesh point. Two additional equations are needed and are obtained by integration of the diffusion equation over the first and last half-nodes, respectively. These integrations yield

$$(D'_{3/2} + \sigma'_{a,3/2} \frac{\Delta^2}{2} + a_1 \Delta) \phi_1 - D'_{3/2} \phi_2 = S'_1 \frac{\Delta^2}{2} + b_1 \Delta \quad (4.70)$$

and

$$-D'_{N-1/2} \phi_{N-1} + (D'_{N-1/2} + \sigma'_{a,N-1/2} \frac{\Delta^2}{2} + a_2 \Delta) \phi_N = S'_N \frac{\Delta^2}{2} + b_2 \Delta, \quad (4.71)$$

where the boundary conditions, Eqs. (4.67) and (4.68), have been used, and where

$$\phi_1 = \frac{1}{\Delta/2} \int_{\xi_1}^{\xi_{3/2}} \phi(\xi) d\xi \quad (4.72a)$$

$$S'_1 = \frac{1}{\Delta/2} \int_{\xi_1}^{\xi_{3/2}} S'(\xi) d\xi \approx S'(\xi_1) \quad (4.72b)$$

$$\phi_N = \frac{1}{\Delta/2} \int_{\xi_{N-1/2}}^{\xi_N} \phi(\xi) d\xi \quad (4.72c)$$

and

$$S'_N = \frac{1}{\Delta/2} \int_{\xi_{N-1/2}}^{\xi_N} S'(\xi) d\xi \approx S'(\xi_N). \quad (4.72d)$$

Equations (4.67), (4.70), and (4.71) represent a system of N equations in N unknowns. These equations can be written in matrix form as

$$\underline{A} \underline{\Phi} = \underline{S}, \quad (4.73)$$

where the coefficient matrix \underline{A} is tridiagonal, diagonally dominant, and symmetric. This matrix is therefore non-singular,⁶⁰ and the solution vector Φ (i.e., the integrated intensities at all mesh points) can be found by either a simple elimination or an iterative procedure given the source vector \underline{S} (i.e., the temperature is known at every point).

The numerical solution of the diffusion equation requires less computer storage and computing time than the numerical solution of the discrete ordinates equations or the flux equations. Only one quantity, the integrated intensity, is computed at every spatial mesh point (as opposed to a set of intensities or fluxes). Furthermore, if the temperature is known, the solution of the diffusion equation can be accomplished by a straight-forward elimination procedure, and iterative techniques are not required. The main limitation of diffusion theory is that the diffusion equation is based on the assumption that the intensity is only weakly dependent on angle. This assumption is poor near boundaries, in media where material properties vary dramatically from point to point within distances of the order of a mean free path (i.e., $\xi = 1$), and near localized sources of radiant energy. In

general, a strong angular dependence of the intensity occurs in regions where the spatial variation of the intensity is also rapid.⁵⁸ In optically thick media (which are characterized by slow spatial variations of the intensity), and at large distances from boundaries and sources, the diffusion approximation has been shown to give accurate results.⁵⁹

4.5 Solution of the Equation of Transfer When the Temperature is Unknown

The various techniques used to solve the equation of transfer have been presented with the assumption that the temperature distributions of all phases present in the system are known. Since in this case the emission term $E_v(x)$ is specified, the equation of transfer contains only one unknown function, the radiation intensity. In general, however, the temperature of each phase is not known a priori and must be computed from a total energy balance on the phase in question. Since the energy balance involves the net volumetric rate of radiant energy emission (which is computed from the radiation intensity), the temperature distribution depends intimately on the radiation intensity distribution. In other words, the temperature of each phase is needed to solve the radiative transfer equation, and the solution of the radiative transfer equation is needed to compute the temperature. In principle, it is possible to solve the energy balance of each phase for the temperature as an explicit function of the intensity, and to substitute the result into the equation of transfer to obtain an equation in terms of the intensity alone. However, this simple elimination is not possible because the energy balance involves derivatives and non-

linear functions of temperature. In this section, it is assumed that the velocity and composition of each phase are known and, consequently, the energy balance relates the temperature of the phase to the radiation intensity without introduction of additional unknowns.

The methods for solution of the radiative transfer equation which have been discussed in this chapter are still applicable when the temperature of each phase is unknown if the solutions are used as part of an iteration scheme in which the temperature distributions are initially assumed. With the assumed temperatures, the various solution techniques are readily applied to obtain a first estimate of the radiation intensity distribution. The computed intensity is then substituted into an energy balance relation for each phase, and updated (and more accurate) temperature profiles are obtained. This procedure is repeated until convergence of the radiation intensity and the temperature distribution of each phase is achieved.

4.5.1 Energy Balance Relations

For a gas-particle mixture, the energy balance relations for the two phases are given by Eqs. (2.46) and (2.47) and are rewritten for one-dimensional geometry in compact form as

$$Q_{rp}(x) = G_p[T_p(x), T_g(x), \rho_p(x), \dots] \quad (4.74)$$

$$Q_{rg}(x) = G_g[T_g(x), T_p(x), \rho_g(x), \dots] \quad (4.75)$$

The net volumetric rate of radiant energy emission by the particulate phase is given by

$$Q_{rp}(x) = 4\pi \int_0^\infty \sigma_{avp}(x) B_v[T_p(x)] dv - 2\pi \int_0^\infty \sigma_{avp}(x) dv \int_{-1}^1 I_v(x, \mu) d\mu. \quad (4.76)$$

This expression can be used to compute $Q_{rp}(x)$ only if the intensity is known as a continuous function of frequency. For the multi-frequency range case, the net emission rate becomes

$$Q_{rp}(x) = 4 \sum_{n=1}^N \sigma_{anp}(x) f_{np}(x) \hat{\sigma} T_p^4(x) - 2\pi \sum_{n=1}^N \sigma_{anp}(x) \int_{-1}^1 I_n(x, \mu) d\mu. \quad (4.77)$$

For the gray case, $Q_{rp}(x)$ becomes

$$Q_{rp}(x) = 4 \sigma_{ap}(x) \hat{\sigma} T_p^4(x) - 2\pi \sigma_{ap}(x) \int_{-1}^1 I(x, \mu) d\mu. \quad (4.78)$$

The same expressions give the volumetric rate of radiation emission by the gas phase if the subscripts p are replaced by g in Eqs. (4.76)-(4.78).

The non-radiative energy inputs to each phase, G_p and G_g , are written as [cf. Eqs. (1.35) and (1.36)]

$$G_p = -\rho_p(x) v(x) c_p \frac{dT_p(x)}{dx} - Q_{cp}(x) + H_p[T_p(x), T_g(x)], \quad (4.79)$$

and

$$G_g = -\rho_g(x) v(x) c_g \frac{dT_g(x)}{dx} + Q_{cp}(x) - \frac{dq(x)}{dx} + H_g[T_p(x), T_g(x)]. \quad (4.80)$$

These equations are based on several simplifications of the general energy conservation laws that have been discussed in Chapter 1. The

inter-species convection term $Q_{cp}(x)$ is proportional to the temperature difference between the two phases, i.e.,

$$Q_{cp}(x) = h [T_p(x) - T_g(x)], \quad (4.81)$$

where the proportionality constant h is assumed to be independent of temperature. If heat transfer by gaseous species inter-diffusion is neglected, the heat flux $q(x)$ is given by Fourier's law:

$$q(x) = -\lambda \frac{dT_g(x)}{dx}, \quad (4.82)$$

where the gas thermal conductivity λ is assumed constant. Finally, the energy release rates due to chemical reaction, $H_p[T_p(x), T_g(x)]$ and $H_g[T_p(x), T_g(x)]$, which are not written explicitly, are generally nonlinear functions of the gas and particle temperatures.

Substitution of Eqs. (4.79)-(4.82) into the energy balance relations of Eqs. (4.74) and (4.75) yields

$$\frac{dT_p(x)}{dx} + c_1(x) T_p(x) + S_p[T_p(x), T_g(x), Q_{rp}(x)] = 0 \quad (4.83)$$

$$\frac{d^2 T_g(x)}{dx^2} + c_2(x) \frac{dT_g(x)}{dx} + c_3 T_g(x) + S_g[T_p(x), T_g(x), Q_{rg}(x)] = 0, \quad (4.84)$$

where

$$c_1(x) = h [c_p \rho_p(x) v(x)]^{-1} \quad (4.85a)$$

$$c_2(x) = -c_g \rho_g(x) v(x) / \lambda \quad (4.85b)$$

$$c_3 = -h / \lambda \quad (4.85c)$$

$$S_p = [c_p \rho_p(x) v(x)]^{-1} \{-h T_g(x) + Q_{rp}(x) - H_p[T_p(x), T_g(x)]\} \quad (4.85d)$$

$$S_g = \frac{1}{\lambda} \{h T_p(x) - Q_{rg}(x) + H_g[T_p(x), T_g(x)]\}. \quad (4.85e)$$

The gas phase energy balance, Eq. (4.84) is a second order differential equation, which may be transformed into the following pair of first order differential equations:

$$\frac{dT_g(x)}{dx} - \hat{T}_g(x) = 0, \quad (4.86)$$

and

$$\frac{d\hat{T}_g(x)}{dx} + c_2(x) \hat{T}_g(x) + c_3 T_g(x) + S_g[T_p(x), T_g(x), Q_{rg}(x)] = 0. \quad (4.87)$$

To reduce further the notation for these energy balance equations, Eqs. (4.83), (4.86), and (4.87) are written in vector form as

$$\frac{d}{dx} \underline{T}(x) + \underline{S}[T_p(x), \hat{T}_g(x), T_g(x), x] = 0, \quad (4.88)$$

where

$$\underline{T} = \begin{pmatrix} T_p(x) \\ T_g(x) \\ \hat{T}_g(x) \end{pmatrix}, \quad (4.89)$$

and

$$\underline{S} = \begin{pmatrix} c_1(x) T_p(x) + S_p[T_p(x), T_g(x), Q_{rp}(x)] \\ -\hat{T}_g(x) \\ c_2(x) \hat{T}_g(x) + c_3 T_g(x) + S_g[T_p(x), T_g(x), Q_{rg}(x)] \end{pmatrix}. \quad (4.90)$$

Equation (4.88) can be solved by standard numerical methods [if the constants $c_1(x)$, $c_2(x)$, and c_3 are known] for given values of $Q_{rp}(x)$ and $Q_{rg}(x)$. For such a solution, two boundary conditions must be

specified for the gas temperature, since the gas energy balance is a second order differential equation. These conditions can be transformed into two conditions involving the functions $T_g(x)$ and $\hat{T}_g(x)$ [$= dT_g(x)/dx$], which are needed for the solution of Eq. (4.88). On the other hand, only one boundary condition is required for the particle temperature, as the solid phase energy balance is a first order differential equation.

4.5.2 Summary of Solution Procedure for Coupled Temperature-Intensity Equations

The overall iterative procedure for the simultaneous solution of the equation of transfer and the energy balances on each phase in a chemically reacting, multi-phase medium is summarized below. It should be noted that this procedure is applicable only when the velocity and composition of each phase are known throughout the medium.

- a) guess an initial temperature distribution for each phase.
- b) solve the radiative transfer equation by one of the methods discussed in this chapter based on these assumed temperature distributions.
- c) compute the radiant emission terms Q_{rp} and Q_{rg} using Eq. (4.76), (4.77), or (4.78).
- d) based on the computed emission terms, recompute the temperature of each phase by solution of Eq. (4.88).
- e) return to step b.
- f) repeat steps b to e until convergence is obtained.

If the velocity and composition of each phase in the system are also unknown, the continuity equation for each phase [Eqs. (1.33) and (1.34)] must be considered in addition to the energy balance

and radiation equations. These continuity equations can be incorporated into the solution methodology at the expense of a more complex iteration procedure and, consequently, increased computational effort.

In conclusion, a number of techniques which may be used to solve the equation of radiative transfer in a scattering and emitting medium have been discussed in this chapter. Two of these methods, the numerical discrete ordinates method and the diffusion approximation, will be used to compute the radiant energy transport in a pulverized coal suspension model in Chapter 5. An original M-flux method for solution of plane-symmetric radiative transfer problems has also been developed in this chapter. However, since flux methods are expected to be less accurate than discrete ordinates solutions using an equal number of discrete directions, the flux methods are not used in the numerical examples of Chapter 5.

5.0 NUMERICAL EXAMPLES

5.1 Statement of the Problem

In this chapter, the numerical solution of the radiative transfer equation is obtained in a chemically reacting pulverized coal suspension. The primary purposes of the many numerical examples presented are to demonstrate that the transport of radiant energy in a scattering-emitting medium can be accurately modelled, to show how the temperature dependence of the heat generation rate by chemical reaction can be incorporated, to compare results obtained with the discrete ordinates approximation and with the diffusion approximation of the equation of transfer, and to assess the effects of various parameters (e.g., optical properties, particle size, boundary conditions) on computed temperature and radiation intensity distributions. The numerical examples are not concerned with solution of the general forms of the conservation and hydrodynamic equations.

An example problem is considered in which the temperature and radiation intensity distributions are calculated for a homogeneous, infinitely long, pulverized coal suspension surrounded by parallel flat walls as shown in Fig. 5.1. The thickness of the medium is x_t , the bounding walls are at temperatures T_{w1} and T_{w2} , and the system properties vary in a one-dimensional manner between the walls. The solid phase is assumed to be composed of low-volatile coal and char particles, which generate heat by means of heterogeneous chemical reaction with the oxidizing gases in which they are dispersed. The

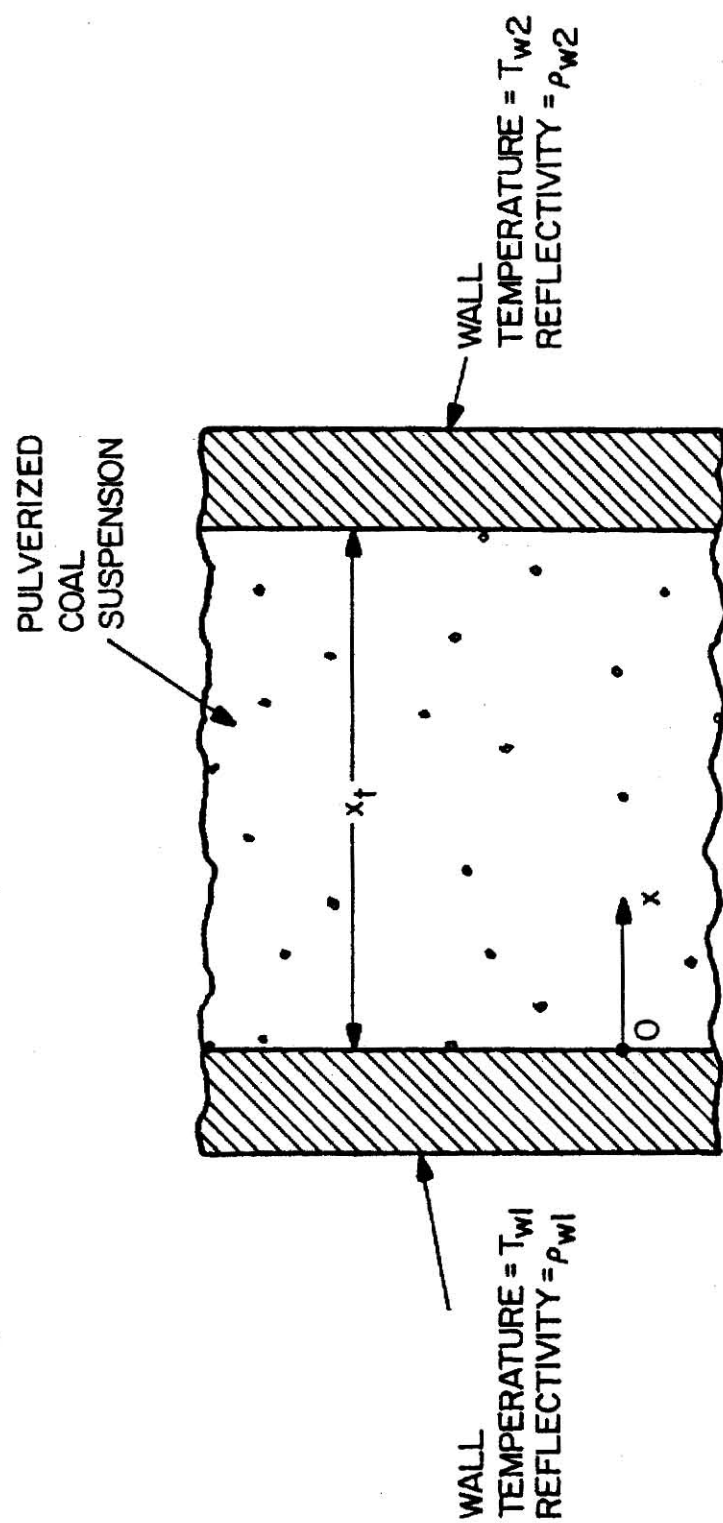


Fig. 5.1. Infinitely long combustion chamber model used in Numerical Examples.

composition of the system is assumed to be known, and effects of fuel consumption are neglected. The system is assumed to be at steady-state, and no net transfer of energy occurs in directions normal to the x-axis. These assumptions of steady state conditions and one-dimensional energy transfer are quite reasonable in the char burnout region of a pulverized coal flame.^{5,16}

5.2 The Energy Balance

The gas and solid phase energy balances are given by Eqs. (4.74) and (4.75) as

$$Q_{rp}(x) = G_p[T_p(x), T_g(x), \dots], \quad (5.1)$$

and

$$Q_{rg}(x) = G_g[T_g(x), T_p(x), \dots]. \quad (5.2)$$

The gaseous species are assumed transparent to radiation, and the gas energy balance becomes

$$0 = G_g[T_g(x), T_p(x), \dots], \quad (5.3)$$

i.e., the sum of the nonradiative energy inputs to the gas phase must also vanish. For a given net radiant emission by the solid phase [i.e., $Q_{rp}(x)$ is known], the gas and solid phase temperature distributions can be computed by the procedure explained in Section 4.5.

For simplicity, the gas phase temperature will be either assumed a priori or taken equal to the particle temperature, and thus only the solid phase energy balance is considered. Calculations by

Krazinski et al.⁵ and Smoot et al.¹⁵ (who considered the energy balance on both phases) predicted that the maximum difference in temperature between the two phases over a wide range of conditions is 100 K (roughly 5%). However, a number of recent experimental results⁶¹ indicate that under some conditions, the difference in temperature between the two phases can be significantly greater than 100 K.

The steady-state particle energy balance is written more explicitly using Eq. (4.79) as

$$Q_{rp}(x) = -c_p \rho_p(x) v(x) \frac{dT_p(x)}{dx} - Q_{cp}(x) + H_p[T_p(x), T_g(x)], \quad (5.4)$$

where allowance is made that the assumed gas temperature differs from the particle temperature by retaining the inter-species conduction term $Q_{cp}(x)$ in the energy balance. Since the velocity of the suspension, $v(x)$, is zero, the sensible energy term vanishes, and the particle energy balance becomes

$$Q_{rp}(x) = -Q_{cp}(x) + H_p[T_p(x), T_g(x)]. \quad (5.5)$$

The net emission term $Q_{rp}(x)$ is given by Eq. (4.78) as

$$Q_{rp}(x) = 4\sigma_a(x) \hat{\sigma} T_p^4(x) - 2\pi \sigma_a(x) \int_{-1}^1 I(x, \mu) d\mu, \quad (5.6)$$

where the gray-case form of $Q_{rp}(x)$ is used because the formation of (non-gray) soot particles is negligible in combustion of low volatile coal, and because the absorption coefficient of coal and char particles is largely independent of frequency. Expressions for the remaining

terms in the particle energy balance (i.e., H_p and Q_{cp}) are derived in the following two sections.

5.2.1 The Chemical Heat Generation Term

The volumetric rate of energy input to the particulate phase due to chemical reaction (i.e., the heat generation rate) is written as

$$H_p = r_p \Delta h, \quad (5.11)$$

where r_p is the mass burning rate of particles per unit volume, and Δh is the energy release to the solid phase per unit mass of fuel consumed. With the assumption that the burning particles contain negligible volatile matter and moisture, the mass burning rate r_p is determined solely by the rate of the heterogeneous reaction of the carbon particles with the oxidizing gases (assumed to be primarily oxygen, O_2). The burning rate may be expressed as¹⁶

$$r_p = P_{O_2} \sum_{k=1}^{NS} \frac{S_{vk}}{K_{dk}^{-1} + K_s^{-1}}, \quad (5.12)$$

where P_{O_2} is the partial pressure of oxygen, S_{vk} is the surface area per unit volume of particles in the k^{th} size class, and NS is the number of particle size classes. The parameters K_{dk} and K_s are reaction rate coefficients which account for the diffusion of oxygen to the particle surface and the reaction rate at the particle surface, respectively. Clearly, the smaller of the two coefficients controls the overall rate of fuel consumption, and the limits of $K_{dk} \ll K_s$ and $K_s \ll K_{dk}$ are termed diffusional control and surface reaction control, respectively.

The rate coefficients K_{dk} and K_s may be expressed^{5,16,62}

$$K_{dk} = \frac{24 J D_o (T_p + T_g)^{0.75}}{2^{0.75} T_o^{1.75} R d_{pk}}, \quad (5.13)$$

and

$$K_s = Z \exp(-E/RT_p), \quad (5.14)$$

where D_o is the binary diffusion coefficient of oxygen in air at the temperature T_o , J is an integer which equals unity if carbon dioxide is the reaction product and equals two if carbon monoxide is the product, E is the activation energy of the heterogeneous reaction of carbon with oxygen, Z is the pre-exponential factor (assumed independent of temperature), and R is the universal gas constant. From Eq. (5.13), the diffusional rate coefficient is seen to be a weak function of particle temperature and inversely proportional to particle diameter; whereas the surface reaction coefficient varies with temperature in the well-known Arrhenius manner and is assumed to be independent of particle size.

Substitution of Eqs. (5.12), (5.13), and (5.14) into Eq. (5.11) gives the heat generation rate as a function of the particle and gas temperatures, namely

$$H_p = P_{O_2} \Delta h \sum_{k=1}^{NS} \frac{S_{vk}}{\left(\frac{24 J D_o (T_p + T_g)^{0.75}}{2^{0.75} T_o^{1.75} R d_{pk}} \right)^{-1} + \left[Z \exp(-E/RT_p) \right]^{-1}}. \quad (5.15)$$

The volumetric surface area of particles in the k^{th} size class, S_{vk} , is given by

$$S_{vk} = \pi d_{pk}^2 N_k, \quad (5.16)$$

where N_k is the number density of particles in the k^{th} size class. This number density can be computed from the particle bulk density ρ_{pk} and the density of coal char ρ_c by

$$N_k = \frac{\rho_{pk}}{(\pi/6) d_{pk}^3 \rho_c}, \quad (5.17)$$

from which the quantity S_{vk} becomes

$$S_{vk} = \frac{6 \rho_{pk}}{d_{pk} \rho_c}. \quad (5.18)$$

The heat generation rate H_p is plotted as a function of the particle temperature T_p in Fig. 5.2. Representative values of the activation energy (35 kcal/mole), the pre-exponential factor ($6 \text{ kg cm}^{-2} \text{ s}^{-1} \text{ atm}^{-1}$), and the binary diffusion coefficient of oxygen ($3.49 \text{ cm}^2/\text{s}$ at 1600 K) were obtained from Field et al.¹⁶ and used to compute H_p . The mechanism factor J for the example was taken to be 2 (i.e., CO is the reaction product). The remaining parameters were chosen so that a monodisperse suspension of 50 μm particles with a particle density ρ_c of 1.5 g cm^{-3} and a particle concentration ρ_p of $10^{-4} \text{ g cm}^{-3}$ generates heat at a rate of 1 W cm^{-3} ($239 \text{ kcal m}^{-3} \text{ s}^{-1}$) at a temperature of 1750 K. This rate of heat generation is consistent with rates which occur in pulverized coal combustors.¹⁶

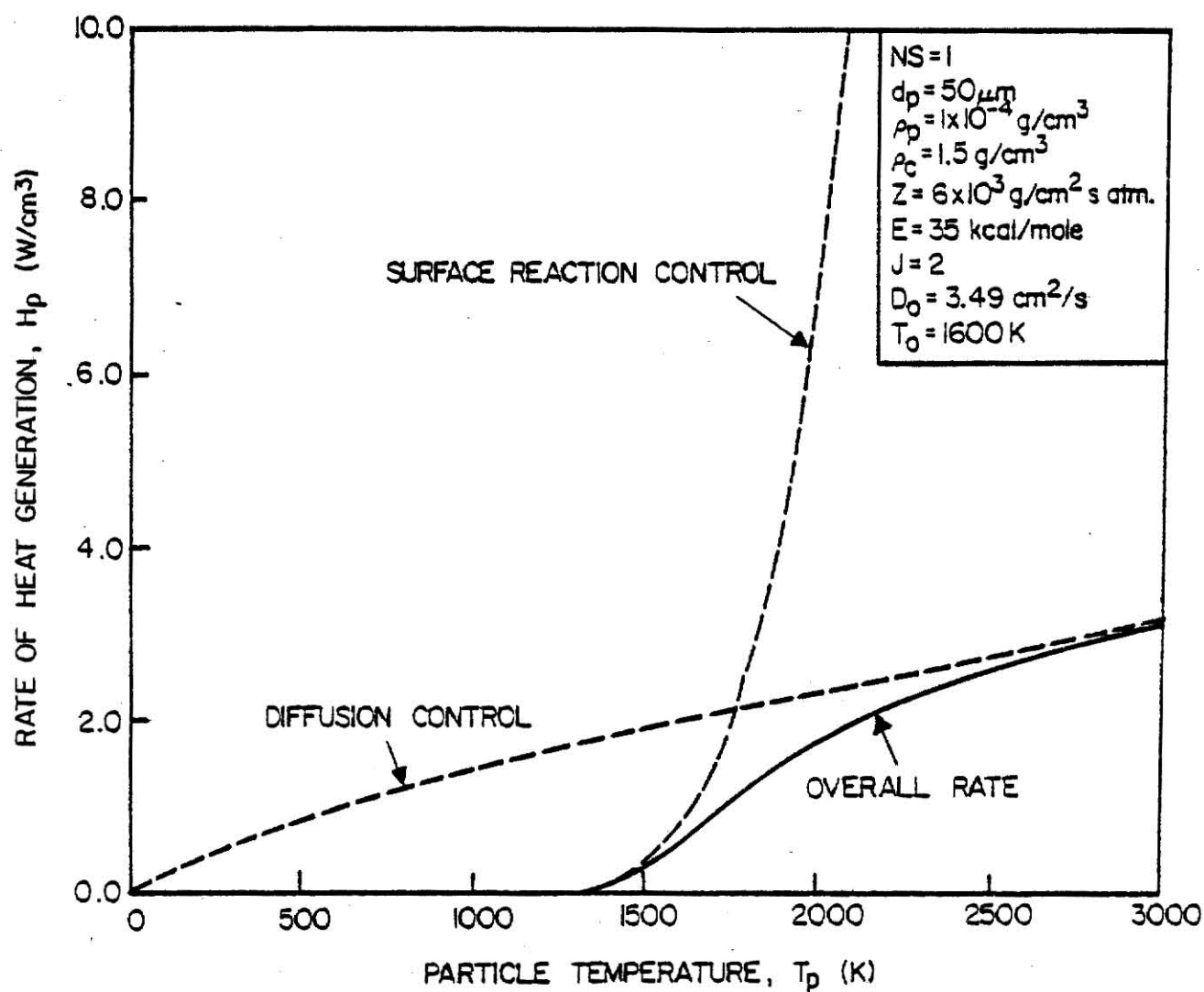


Fig. 5.2. The rate of heat generation by chemical reaction as a function of the particle temperature. Dashed lines give the diffusional control and surface reaction control limits of the heat generation rate.

Limiting forms of H_p under diffusional control ($K_d \ll K_s$) and surface reaction control ($K_s \ll K_d$) are also shown in Fig. 5.2. The overall rate is seen to be controlled almost exclusively by the chemical reaction for $T_p < 1500$ K and by oxygen diffusion for $T_p > 2000$ K.

5.2.2 The Inter-Species Convection Term

The convective term Q_{cp} in the particle energy balance, Eq. (5.5), may be written^{4,5,16}

$$Q_{cp} = \sum_{k=1}^{NS} \left[\frac{Nu}{d_{pk}} \lambda (T_p - T_g) \right] S_{vk}, \quad (5.19)$$

where Nu is the Nusselt number (which takes the value of 2 for a spherical particle at rest relative to the surrounding fluid),^{4,5} and λ is the thermal conductivity of the gas evaluated at the mean temperature in the particle boundary layer. The thermal conductivity varies as $T^{0.75}$,¹⁶ and therefore λ may be expressed

$$\lambda = \lambda_o \left(\frac{(T_p + T_g)/2}{T_o} \right)^{0.75}, \quad (5.20)$$

where λ_o is the gas thermal conductivity at a temperature T_o .

The convective heat loss term Q_{cp} thus becomes

$$Q_{cp} = 2 \lambda_o \left(\frac{T_p + T_g}{2T_o} \right)^{0.75} (T_p - T_g) \sum_{k=1}^{NS} \frac{S_{vk}}{d_{pk}}. \quad (5.21)$$

5.3 Dimensionless Form of the Energy Balance

Substitution for Q_{rp} [from Eq. (5.6)], H_p [from Eq. (5.15)], and Q_{cp} [from Eq. (5.21)] into the particle energy balance, and non-

dimensionalizing the resulting equation by division of each term by $4\sigma_a \hat{\sigma}(E/R)^4$ yields

$$\begin{aligned} \tau_p^4(x) = \psi(x) + \frac{a}{\sum_k F_{ak} S_{vk}} \sum_{k=1}^{NS} \frac{S_{vk}}{b_k [\tau_p(x) + \tau_g(x)]^{-0.75} + \frac{1}{Z} \exp[1/\tau_p(x)]} \\ - \frac{c}{\sum_k F_{ak} S_{vk}} \sum_{k=1}^{NS} \frac{S_{vk}}{d_{pk}} [\tau_p(x) + \tau_g(x)]^{0.75} [\tau_p(x) - \tau_g(x)], \end{aligned} \quad (5.22)$$

where the substitution $\sigma_a = \frac{1}{4} \sum_k F_{ak} S_{vk}$ [from Eq. (3.3)] has been made, and where

$$\tau_p(x) = T_p(x)/T^* \quad (\text{dimensionless particle temperature}) \quad (5.23)$$

$$\tau_g(x) = T_g(x)/T^* \quad (\text{dimensionless gas temperature}) \quad (5.24)$$

$$T^* = E/R \quad (\text{reference temperature}) \quad (5.25)$$

$$\begin{aligned} \psi(x) = \phi(x)/(4\phi^*) = 2\pi \int_{-1}^1 I(x, \mu) d\mu / (4\phi^*) \\ (\text{dimensionless integrated intensity}) \end{aligned} \quad (5.26)$$

$$\phi^* = \hat{\sigma} T^{*4} = \hat{\sigma} (E/R)^4 \quad (\text{reference integrated intensity}). \quad (5.27)$$

The quantities T^* and ϕ^* are constants which have dimensions of temperature and intensity, respectively. The parameters a , b_k , and c in Eq. (5.22) are

$$a = P_{02} \Delta h_r / \phi^* \quad (5.28a)$$

$$b_k = \left[\frac{24 JD_o T_o^{*0.75}}{2^{0.75} T_o^{1.75} R d_{pk}} \right]^{-1} \quad (5.28b)$$

$$c = \frac{2\lambda_o T_o^{*1.75}}{(2T_o)^{0.75} \phi^*} \quad (5.28c)$$

Equation (5.22) is a dimensionless energy balance on the volume element at the point x ; the left hand side represents the dimensionless radiant emission by the coal char particles, while the terms on the right side are dimensionless forms of the radiant energy absorption, the chemical heat generation, and the heat conduction to the gas phase. The equation is simplified by assuming the particle size distribution to be monodisperse (i.e., $NS = 1$). Equation (5.22) becomes

$$\begin{aligned} \tau_p^4(x) = \psi(x) + \frac{A}{[\tau_p(x) + \tau_g(x)]^{-0.75} + B \exp[1/\tau_p(x)]} \\ - C [\tau_p(x) + \tau_g(x)]^{0.75} [\tau_p(x) - \tau_g(x)], \end{aligned} \quad (5.29)$$

where

$$A = a/F_a b \quad (5.30a)$$

$$B = 1/Zb \quad (5.30b)$$

$$C = c/F_a d_p. \quad (5.30c)$$

If the gas and particle temperatures are assumed equal (i.e., $\tau_p = \tau_g$), the convective term vanishes, and Eq. (5.29) becomes

$$\tau_p^4(x) = \psi(x) + \frac{A}{[2\tau_p(x)]^{-0.75} + B \exp[1/\tau_p(x)]} \quad (5.31)$$

5.4 Calculation of the Equilibrium Temperature at a Fixed Point

The first and last terms in Eq. (5.31) are denoted by $E[\tau_p(x)]$ and $H[\tau_p(x)]$, respectively, i.e.,

$$E[\tau_p(x)] = \Psi(x) + H[\tau_p(x)] \quad (5.32)$$

For a fixed value of x , this becomes

$$E(\tau_p) = \Psi + H(\tau_p). \quad (5.33)$$

The equilibrium particle temperature at any x must satisfy the energy balance, Eq. (5.33). The solution of Eq. (5.33) for the dimensionless particle temperature τ_p is illustrated in Fig. 5.3. The dimensionless radiant emission $E(\tau_p)$ and two different heat generation functions, $H_1(\tau_p)$ and $H_2(\tau_p)$, are shown as functions of τ_p . The heat generation functions were obtained using different assumed values of the parameter A , with the parameter B kept constant. The term Ψ , which represents the radiant energy absorption, serves to shift each generation function upward by a constant amount for all values of τ_p . The equilibrium particle temperature is simply the temperature at which the displaced generation function and the emission function intersect. It may be seen from Fig. 5.3 that, for any value of Ψ , the displaced function $H_1 + \Psi$ always intersects the emission function at a unique temperature. On the other hand, the displaced function $H_2 + \Psi$ may intersect the emission function at a unique temperature (as with $H_2 + \Psi_2$) or at three different temperatures (as with $H_2 + \Psi_1$). It is easily verified that multiple intersections are possible only

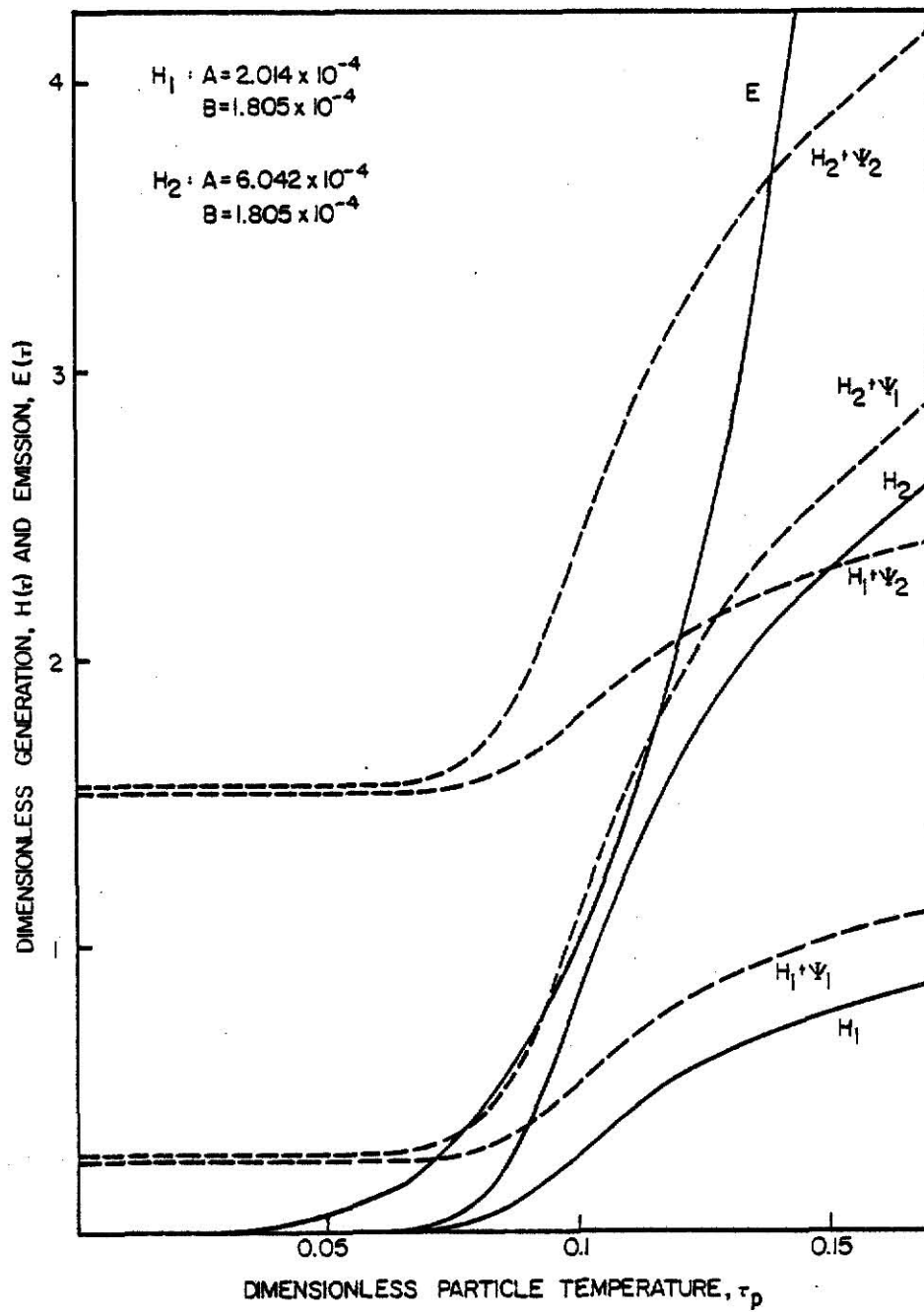


Fig. 5.3. Determination of the equilibrium particle temperature from the intersection of the displaced generation function $H + \Psi$ and the emission function E for two different rates of heat generation (H_1 and H_2) and two different assumed rates of radiant energy absorption (Ψ_1 and Ψ_2).

if at some temperature, the slope of the generation function exceeds the slope of the emission function; i.e., if at some τ_p , the condition

$$\frac{A [1.5 (2\tau_p)^{-1.75} + B \exp(1/\tau_p)/\tau_p^2]}{[(2\tau_p)^{-0.75} + B \exp(1/\tau_p)]^2} > 4\tau_p^3$$

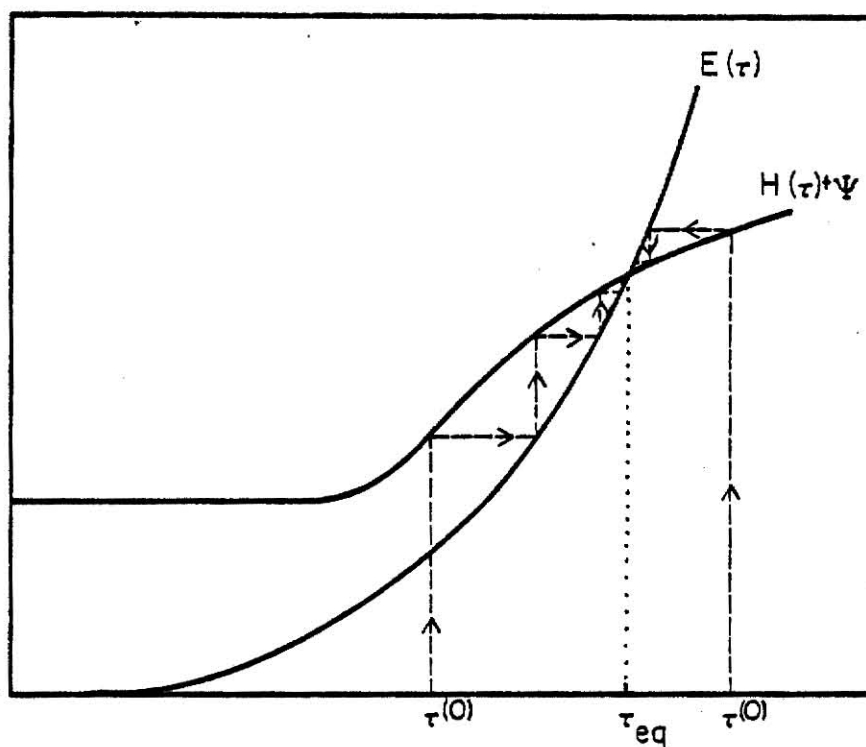
is met.

If more than one intersection exists, it may be shown that the middle one is unstable; whereas the intersection at the lowest or highest temperature represents a possible equilibrium temperature. The particular temperature attained by the particles in this case depends on its previous temperature history.¹⁶ It should be noted that the stable equilibrium temperatures occur when the emission function varies more rapidly with temperature than the displaced generation function (at their point of intersection). The equilibrium particle temperature can thus be computed by a basic iteration method which involves inversion of the more rapidly varying emission function.⁶³ Successive estimates of the temperature $[\tau^{(n+1)}$ and $\tau^{(n)}]$ are thus related by

$$\tau^{(n+1)} = \left[\psi + \frac{A}{[2\tau_p^{(n)}]^{-0.75} + B \exp[1/\tau_p^{(n)}]} \right]^{0.25}, \quad (5.34)$$

with a possible initial guess $\tau^{(0)} = \psi^{0.25}$. This iteration is repeated until convergence of the temperature is obtained. If a unique equilibrium temperature exists, the iterative procedure always converges to that temperature, regardless of the initial guess, as shown in Fig. 5.4(a). If three equilibrium temperatures exist, the iterative

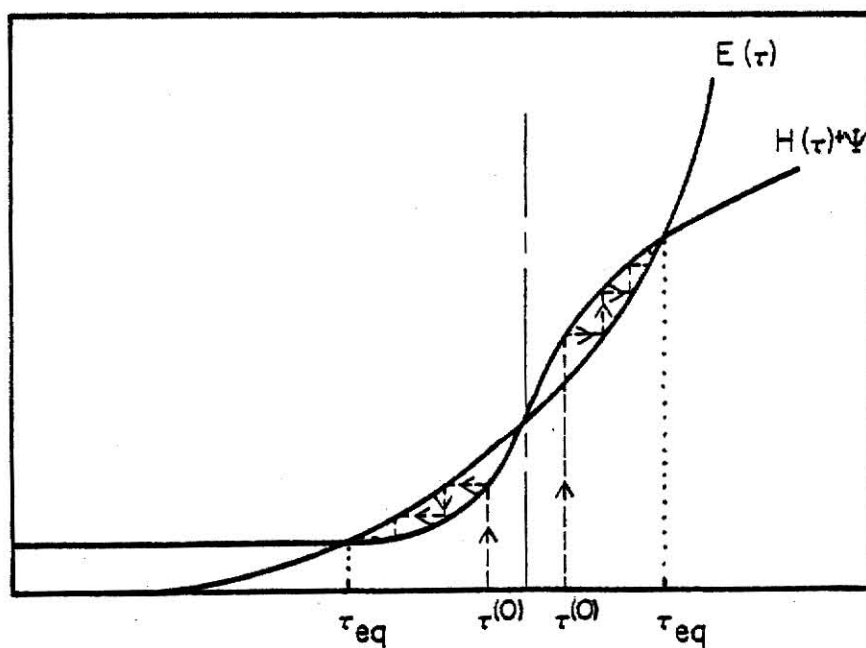
DIMENSIONLESS GENERATION OR EMISSION



DIMENSIONLESS TEMPERATURE

(a)

DIMENSIONLESS GENERATION OR EMISSION



DIMENSIONLESS TEMPERATURE

(b)

Fig. 5.4. Convergence of the iterative calculation of the equilibrium particle temperature for (a) single intersection case and (b) triple intersection case.- The quantity τ_{eq} represents a stable equilibrium temperature.

procedure converges to the higher equilibrium temperature for initial temperature guesses greater than the unstable equilibrium temperature and to the lower equilibrium temperature for guesses less than the unstable temperature. The convergence of the iterative solution in the multiple intersection case is illustrated in Fig. 5.4(b).

The equilibrium particle temperature distribution is obtained by determining the temperature at which the displaced generation function and the emission function intersect at every point in the system. Therefore, the amount of radiant energy absorbed must be computed throughout the medium. In this study,

$$\Psi = 2\pi \int_{-1}^1 I(x, \mu) d\mu / (4\Phi^*) = \Phi(x) / (4\Phi^*)$$

is determined from solution of the radiative transfer equation by both the discrete ordinates method (for the intensity I) and the diffusion approximation (for the directionally integrated intensity Φ).

5.5 Simultaneous Solution of the Energy Balance with the Equation of Transfer

Since the coal dust cloud is assumed homogeneous, and its radiation properties are independent of frequency, the steady-state, plane symmetric equation of transfer can be written

$$\mu \frac{\partial I(\xi, \mu)}{\partial \xi} + I(\xi, \mu) = \frac{\omega}{2} \int_{-1}^1 I(\xi, \mu') p(\mu' \rightarrow \mu) d\mu' + (1-\omega) \frac{\hat{\sigma} T_p^4(\xi)}{\pi}, \quad (5.35)$$

where the substitution $\sigma_a / \sigma_e = 1-\omega$ has been made. This equation can be non-dimensionalized by division of each term by $\Phi^* [= \hat{\sigma}(E/R)^4]$ to obtain

$$\mu \frac{\partial I'(\xi, \mu)}{\partial \xi} + I'(\xi, \mu) = \frac{\omega}{2} \int_{-1}^1 I'(\xi, \mu') p(\mu' \rightarrow \mu) d\mu' + (1-\omega) \frac{\tau_p^4(\xi)}{\pi}, \quad (5.36)$$

where $I'(\xi, \mu) = I(\xi, \mu)/\Phi^*$. The particle energy balance, Eq. (5.29), is rewritten upon substitution for the dimensionless absorption term from Eq. (5.26) as

$$\tau_p^4(\xi) = \frac{\pi}{2} \int_{-1}^1 I'(\xi, \mu) d\mu + \frac{A}{[\tau_p(\xi) + \tau_g(\xi)]^{-0.75} + B \exp[1/\tau_p(\xi)]} - C [\tau_p(\xi) + \tau_g(\xi)]^{0.75} [\tau_p(\xi) - \tau_g(\xi)]. \quad (5.37)$$

For a given gas temperature distribution [i.e., $\tau_g(\xi)$ specified], Eqs. (5.36) and (5.37) are two equations in two unknowns, the dimensionless intensity and particle temperature. Substitution for $\tau_p^4(\xi)$ from Eq. (5.37) in Eq. (5.36) yields

$$\mu \frac{\partial I'(\xi, \mu)}{\partial \xi} + I'(\xi, \mu) = \frac{\omega}{2} \int_{-1}^1 I'(\xi, \mu') p(\mu' \rightarrow \mu) d\mu' + \frac{1-\omega}{2} \int_{-1}^1 I'(\xi, \mu') d\mu' + \tilde{H}[T(\xi)], \quad (5.38)$$

where

$$\tilde{H}[T(\xi)] = \frac{1-\omega}{\pi} \left\{ \frac{A}{[\tau_p(\xi) + \tau_g(\xi)]^{-0.75} + B \exp[1/\tau_p(\xi)]} - C [\tau_p(\xi) + \tau_g(\xi)]^{0.75} [\tau_p(\xi) - \tau_g(\xi)] \right\}. \quad (5.39)$$

The dimensionless particle temperature $\tau_p(\xi)$ is related to the dimensionless intensity $I'(\xi, \mu)$ by Eq. (5.37), and thus the term $\tilde{H}[T(\xi)]$ is, in principle, expressible as $\tilde{H}[I'(\xi, \mu)]$. Hence, Eq. (5.38) can be written as

$$\mu \frac{\partial I'(\xi, \mu)}{\partial \xi} + I'(\xi, \mu) = \frac{\omega}{2} \int_{-1}^1 I'(\xi, \mu') p(\mu' \rightarrow \mu) d\mu' + \frac{1-\omega}{2} \int_{-1}^1 I'(\xi, \mu') d\mu' + \tilde{H}[I'(\xi, \mu)], \quad (5.40)$$

in which \tilde{H} is a highly non-linear function of I' . Equation (5.40) is a nonlinear, first order, integro-differential equation which involves the intensity as the only unknown (if \tilde{H} is a known function of I'). Unfortunately, the explicit dependence of \tilde{H} on the radiation intensity cannot be determined because of the transcendental relation between the temperature and intensity in Eq. (5.37). Consequently, the energy balance and the equation of transfer must be solved simultaneously.

Solution of the two equations requires a boundary condition for the radiation intensity. Assuming the walls to be diffusely-reflecting, gray surfaces, the boundary condition is

$$I(0, \mu) = \epsilon_{w1} \frac{\hat{\sigma} T_{w1}^4}{\pi} + 2\rho_{w1} \int_0^{-1} \mu' I(0, \mu') d\mu', \quad \mu > 0, \quad (5.41a)$$

and

$$I(\xi_t, \mu) = \epsilon_{w2} \frac{\hat{\sigma} T_{w2}^4}{\pi} + 2\rho_{w2} \int_0^1 \mu' I(0, \mu') d\mu', \quad \mu < 0, \quad (5.41b)$$

where T_{w1} , ρ_{w1} , and ϵ_{w1} are, respectively, the temperature, the reflectivity, and the emissivity of the wall at $\xi=0$; and T_{w2} , ρ_{w2} , and ϵ_{w2} are the corresponding quantities for the wall at $\xi=\xi_t$. The incident intensity from each wall is seen to be composed of an emitted component and a diffusely reflected component. The boundary conditions can also be expressed in dimensionless form (by division

of each term by ϕ^*) as

$$I'(0, \mu) = \frac{\epsilon_{w1}}{\pi} \tau_{w1}^4 + 2\rho_{w1} \int_0^{-1} \mu' I'(0, \mu') d\mu', \quad \mu > 0, \quad (5.42a)$$

and

$$I'(\xi_t, \mu) = \frac{\epsilon_{w2}}{\pi} \tau_{w2}^4 + 2\rho_{w2} \int_0^1 \mu' I'(\xi_t, \mu') d\mu', \quad \mu < 0, \quad (5.42b)$$

where τ_{w1} and τ_{w2} are the dimensionless temperatures of the two walls ($\tau_{w1} = T_{w1}/T^*$ and $\tau_{w2} = T_{w2}/T^*$).

It is important to note that solution of the equation of transfer and the energy balance [Eqs. (5.36) and (5.37)] for the dimensionless intensity and particle temperature depends only on the parameters A, B, and C, the single scatter albedo ω , the phase function $p(\mu' \rightarrow \mu)$, the assumed gas temperature distribution $\tau_g(\xi)$, and on the boundary conditions (i.e., the quantities ϵ_w , ρ_w , τ_w , and ξ_t). Of these parameters, only the optical thickness of the medium ξ_t depends on the particle bulk density ρ_p , the density of coal char ρ_c , or the system size x_t . Therefore, for a given system optical thickness, the computed temperature and radiation intensity are independent of the particular choices of ρ_p , ρ_c , and x_t .

A computer code RATREQ has been written which solves the equation of transfer simultaneously with the particle energy balance. The numerical discrete ordinates method discussed in Chapter 4 is used to compute the radiation intensity at a number of discrete spatial mesh points and in a number of discrete directions. Initially, a temperature is assumed at each mesh point, and the radiation intensity distribution is computed based on the assumed temperatures and an assumed

value of the scattering source term. The radiation intensity is then used to calculate the amount of radiant energy which is absorbed at each discrete point in the medium. This quantity is substituted into the particle energy balance, and the resulting equation is solved by the basic iteration method discussed in Section 5.4 for an updated value of the particle temperature at each point. The computed intensity and the updated temperature distributions are used to recompute the scattering source and the thermal emission source, respectively, which are then used to recompute the radiation intensity. This procedure is repeated until convergence of the temperature and the radiation intensity distributions is obtained.

It should be noted that the procedure used by RATREQ updates the temperature distributions each time the radiation intensity is computed. An alternative procedure is to compute the intensity for the assumed temperature and scattering source distributions and to recompute only the scattering source in each iteration until convergence of the intensity for the assumed temperature distribution. The converged intensity is then used to recompute the temperatures, and the entire procedure is repeated until convergence of the temperature distribution. This procedure is not employed because the re-evaluation of the temperature distribution (based on the computed intensity) requires a simple iterative solution of the energy balance which converges rapidly and therefore requires little computational effort. Therefore, the temperature is continuously updated along with the computed intensity.

The solution of the equation of transfer requires the evaluation of the radiation properties of the particles in the medium. The subroutine DBMIE³⁶ is used to compute the extinction and scattering efficiencies of the coal and char particles (given the particle diameter, the wavelength of radiation, and the complex refractive index of the particle). The computed efficiencies can then be used to calculate the scattering, extinction, and absorption coefficients using Eqs. (3.3)-(3.6). Another subroutine, PHASE, has been written in this study to compute the scattering matrix by the azimuthal integration of the scattering phase function. The phase function for large, diffusely reflecting spheres [given by Eq. (3.7)] is used in this work. Substitution of this phase function into Eq. (2.15) and use of Eq. (2.13) yields

$$p(\mu' \rightarrow \mu) = \frac{4}{3\pi^2} \int_0^{2\pi} \{ \sin[\arccos(\mu\mu' + \sqrt{1-\mu^2} \sqrt{1-\mu'^2} \cos\phi)] - (\mu\mu' + \sqrt{1-\mu^2} \sqrt{1-\mu'^2} \cos\phi) \arccos(\mu\mu' + \sqrt{1-\mu^2} \sqrt{1-\mu'^2} \cos\phi) \} d\phi. \quad (5.43)$$

This integration is performed numerically by PHASE for discrete values of μ and μ' to obtain the scattering matrix.

5.6 Simultaneous Solution with the Diffusion Equation

With the assumption that the coal dust cloud is uniform and that its radiative properties are frequency-independent, the quasi-steady, one-dimensional diffusion equation [Eq. (4.51)] becomes

$$D' \frac{d^2 \phi}{d\xi^2} + \sigma_a' \phi(\xi) = -4\sigma_a' \hat{\sigma}_T^4_p(\xi). \quad (5.44)$$

Division of each term by Φ^* gives the dimensionless form of the diffusion equation

$$\frac{d^2 \Phi'}{d\xi^2} + \beta^2 \Phi'(\xi) = -4 \beta^2 \tau_p^4(\xi), \quad (5.45)$$

where

$$\Phi'(\xi) = \frac{\Phi(\xi)}{\Phi^*} \quad (5.46)$$

$$\beta^2 = \frac{\sigma_a'}{D^*} = \frac{\sigma_a}{D \sigma_e^2}. \quad (5.47)$$

The particle energy balance may be written with the dimensionless radiant absorption term expressed in terms of the integrated intensity as

$$\begin{aligned} \tau_p^4(\xi) = & \frac{\Phi'(\xi)}{4} + \frac{A}{[\tau_p(\xi) + \tau_g(\xi)]^{-0.75} + B \exp[1/\tau_p(\xi)]} \\ & - C [\tau_p(\xi) + \tau_g(\xi)]^{0.75} [\tau_p(\xi) - \tau_g(\xi)]. \end{aligned} \quad (5.48)$$

This equation can be solved for the integrated intensity $\Phi'(\xi)$. Substitution of the result into the second term of the diffusion equation yields

$$\frac{d^2 \Phi'(\xi)}{d\xi^2} + 4\beta^2 \hat{H}[\tau_p(\xi)] = 0, \quad (5.49)$$

where the last two terms in Eq. (5.48) have been denoted by $\hat{H}[\tau_p(\xi)]$.

In principle, it is also possible to solve Eq. (5.48) for the particle temperature $\tau_p(\xi)$ as a function of the integrated intensity $\Phi'(\xi)$ and to express $\hat{H}[\tau_p(\xi)]$ as $\hat{H}[\Phi'(\xi)]$. Equation 5.49 would become

$$\frac{d^2 \phi'(\xi)}{d\xi^2} + 4\beta^2 \hat{H}[\phi'(\xi)] = 0 \quad (5.50)$$

where $\hat{H}[\phi'(\xi)]$ is a highly nonlinear function of the integrated intensity. Equation (5.50) is a nonlinear, second order differential equation and contains only one unknown function, the integrated intensity. However, the explicit dependence of $\tau_p(\xi)$ on $\phi'(\xi)$ cannot be determined from Eq. (5.48) and consequently, \hat{H} cannot be written as an explicit function of the integrated intensity. As was the case with the radiative transfer equation, the diffusion equation must be solved simultaneously with the particle energy balance via an iterative procedure.

The boundary conditions on the integrated intensity are obtained by angular integration of the boundary conditions on the intensity [Eqs. (5.41a) and (5.41b)], as explained in Section 4.4. The boundary conditions for diffusely reflecting, gray walls become

$$\frac{d\phi(0)}{d\xi} = a_1 \phi(0) - b_1, \quad (5.51)$$

and

$$\frac{d\phi(\xi_t)}{d\xi} = -a_2 \phi(\xi_t) + b_2, \quad (5.52)$$

where

$$a_1 = \frac{1}{2D'} \frac{1-\rho_{w1}}{1+\rho_{w1}} \quad (5.53a)$$

$$a_2 = \frac{1}{2D'} \frac{1-\rho_{w2}}{1+\rho_{w2}} \quad (5.53b)$$

$$b_1 = \frac{2}{D'} \frac{\epsilon_{w1} \hat{\sigma}_T^4}{1+\rho_{w1}} \quad (5.53c)$$

$$b_2 = \frac{2}{D'} \frac{\epsilon_{w2} \hat{\sigma} T_{w2}^4}{1 + \rho_{w2}}. \quad (5.53d)$$

These boundary conditions are nondimensionalized by division of each term by ϕ^* to obtain

$$\frac{d\phi'(0)}{d\xi} = a_1 \phi'(0) - b_1' \quad (5.54)$$

$$\frac{d\phi'(\xi_t)}{d\xi} = -a_2 \phi'(\xi_t) + b_2', \quad (5.55)$$

where $b_1' = b_1/\phi^*$ and $b_2' = b_2/\phi^*$.

The diffusion equation and the particle energy balance can be solved for the integrated intensity and the particle temperature subject to the boundary conditions, Eqs. (5.54) and (5.55). Again, for a given system optical thickness ξ_t , the solution is independent of the particle bulk density ρ_p , the density of coal char ρ_c , and the system size x_t . This is verified by the independence of the parameters (other than ξ_t) in the diffusion equation, the energy balance, and the boundary conditions of the quantities ρ_p , ρ_c , and x_t .

A computer code DIFFEQ has been written which solves the diffusion equation by the numerical procedure described in Section 4.4. The code solves the diffusion equation simultaneously with the particle energy balance by an iterative procedure. An initial temperature distribution is guessed, and the integrated intensity is computed based on this guess. The integrated intensity is then substituted into the energy balance to recompute the temperature at each point by the basic iteration technique. This procedure is repeated until

convergence of the temperature and the integrated intensity. Since only thermal emission contributes to the source term of the diffusion equation, no re-evaluation of a scattering source term is required to compute the integrated intensity corresponding to a given temperature distribution.

As is the case with RATREQ, the radiation properties needed to solve the diffusion equation using DIFFEQ are calculated using DBMIE³⁶. The scattering phase function does not appear in the diffusion equation, and hence the subroutine PHASE is not used by DIFFEQ. However, the evaluation of the diffusion coefficient $D [= \{3(\sigma_e - \sigma_s \bar{\mu}^*)\}^{-1}]$ requires calculation of the average cosine of the scattering angle, $\bar{\mu}^*$. Substitution of the phase function into the expression for $\bar{\mu}^*$, Eq. (4.46), yields

$$\bar{\mu}^* = \frac{4}{3\pi} \int_{-1}^1 d\mu^* [\mu^* \sqrt{1-\mu^{*2}} - \mu^{*2} \arccos \mu^*]. \quad (5.56)$$

This expression can be evaluated analytically to obtain

$$\bar{\mu}^* = -4/9. \quad (5.57)$$

5.7 Numerical Results

5.7.1 Testing of Computer Codes

The proper operation of the programs RATREQ and DIFFEQ was verified by numerous test problems. First, the convergence of computed temperature and radiation intensity distributions with respect to spatial and angular discretization was verified. The results were found to converge to within 1% of a benchmark value (computed with very fine spatial

and angular grids) if ten mesh points per mean free path (unit optical thickness) and eight angular quadrature ordinates are used. The convergence criterion (i.e., the stopping condition) which was used in the iterative solutions is that the computed temperature and intensity distributions change by less than 0.1% between successive iterations at each spatial and angular mesh point. The independence of computed temperature and radiation intensity distributions of the initial source distribution guesses was verified. The solutions were also checked by performing an energy balance on the entire system and it was verified, upon convergence of the solution, that the coal dust medium satisfied an energy balance in which the radiation leakage from the system equals the heat generated by chemical reaction minus the heat lost by convection to the gas phase (if the gas and particles are not assumed to be in thermal equilibrium).

The computer codes were additionally checked by comparison of results computed for simple test cases with results presented in Field et al.¹⁶ The first problem considered is that of a combustor with cold black walls in which the rate of heat generation by chemical reaction is constant (i.e., temperature-independent), convective losses are absent, and scattering of radiation neglected. The temperature distribution is computed by RATREQ and DIFFEQ and compared in Fig. 5.5 with that computed by the no-scattering solution of Usiskin and Sparrow⁶⁴ (and presented by Field et al.¹⁶). These results show that the discrete ordinates solution (of RATREQ) is in excellent agreement with the solution of Usiskin and Sparrow, with a maximum

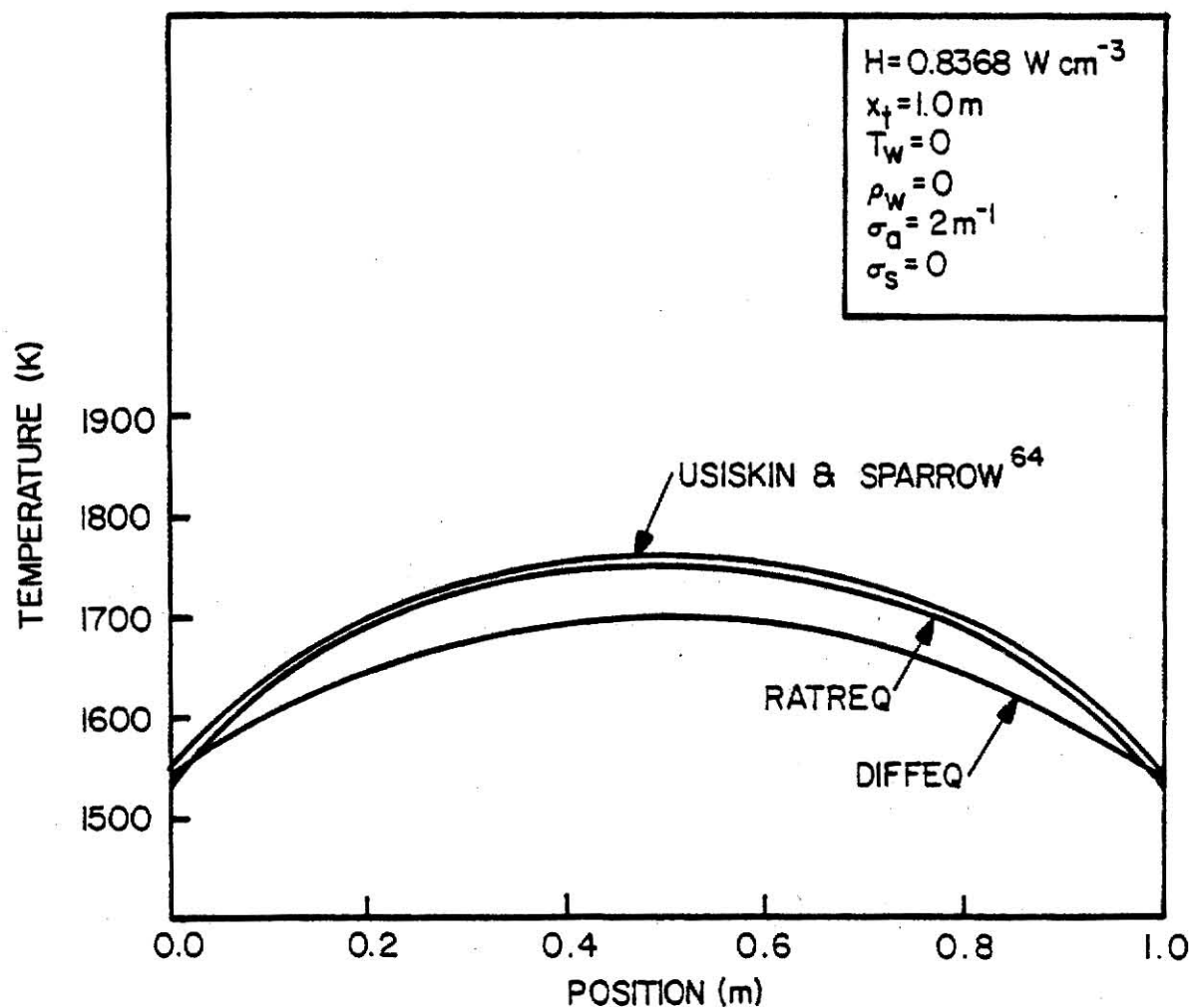


Fig. 5.5. Comparison of the temperature distribution computed by the discrete ordinates method (RATREQ) and the diffusion approximation (DIFFEQ) to result obtained by the solution of Usiskin and Sparrow⁶⁴ for a non-scattering medium bounded by cold, non-reflecting walls. The rate of heat generation H is uniform and independent of temperature.

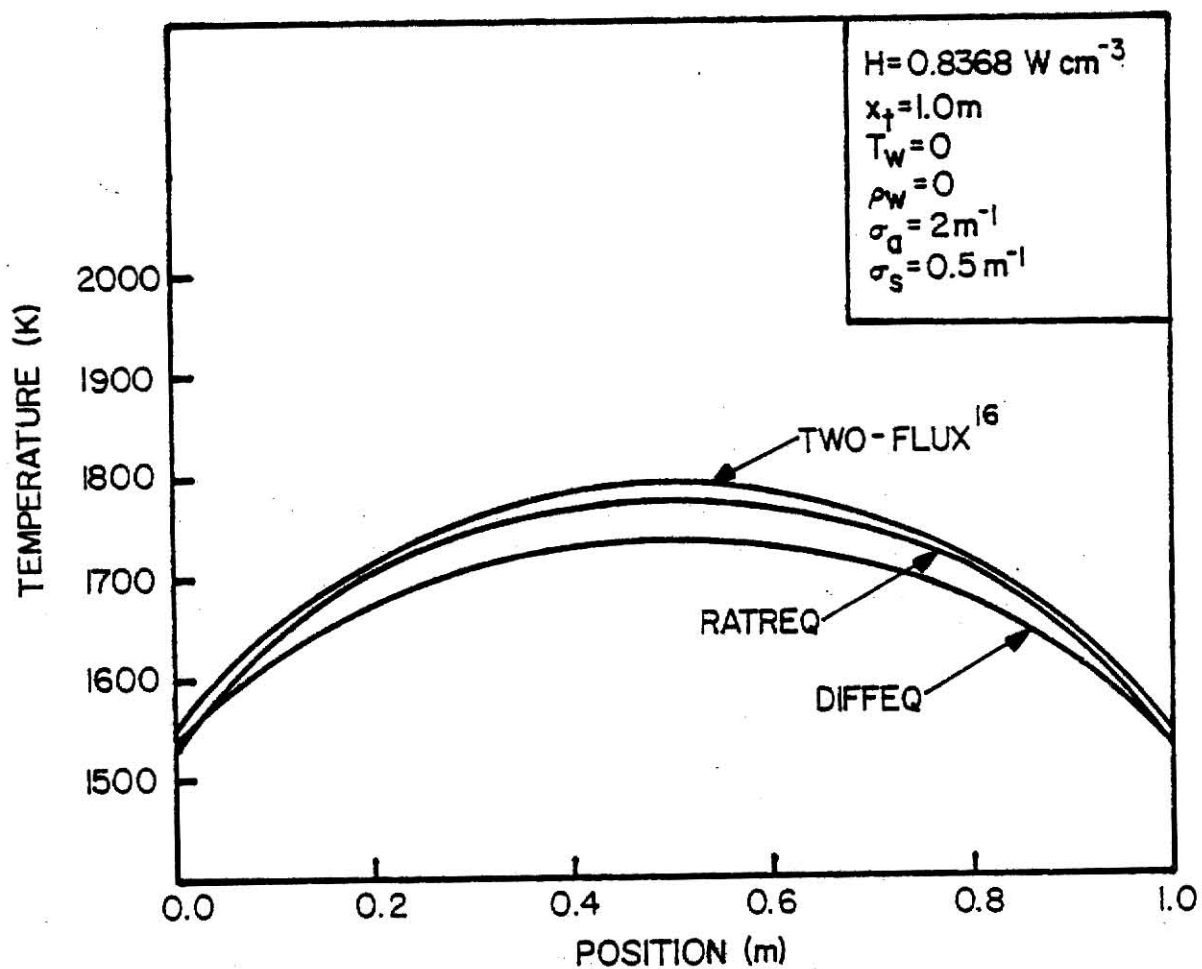


Fig. 5.6. Comparison of temperature distributions computed by the discrete ordinates method and by the diffusion approximation to a two-flux solution¹⁶ for a one-meter thick medium with a constant rate of heat generation. The medium is bounded by cold, non-reflecting walls.

difference in computed temperature of roughly 10 K (i.e., < 1%). The diffusion approximation result (of DIFFEQ) differs by a maximum of 60 K from the other two solutions (i.e., < 4%). A second test problem is considered which is identical to the first problem, except that scattering is present. Here, the solution of Usiskin and Sparrow is not applicable, and the temperature distributions computed by RATREQ and DIFFEQ are compared with the two-flux solution of Schuster and Hamaker²⁶ (presented in Reference 16). This comparison is shown in Fig. 5.6 and indicates a good agreement of the results computed by the various methods.

5.7.2 Comparison of Diffusion and Discrete Ordinates Results

A large number of calculations were performed by RATREQ and DIFFEQ to compare the particle temperature and integrated intensity distributions computed by the discrete ordinates method and the diffusion approximation and to test the effects of various parameters on these results. All calculations were performed with the temperature-dependent heat generation rate H given by Eq. (5.15), and the majority of the calculations are based on the assumption that the particle and gas phases are in thermal equilibrium (i.e., the inter-species convection term Q_{cp} vanishes).

The particle temperature and integrated intensity distributions calculated by the discrete ordinates method and the diffusion approximation for a one-meter thick medium ($\xi_t = 2.234$) bounded by cold, non-reflecting walls are shown in Fig. 5.7. The two methods give nearly the same temperature and integrated intensity at the system boundaries,

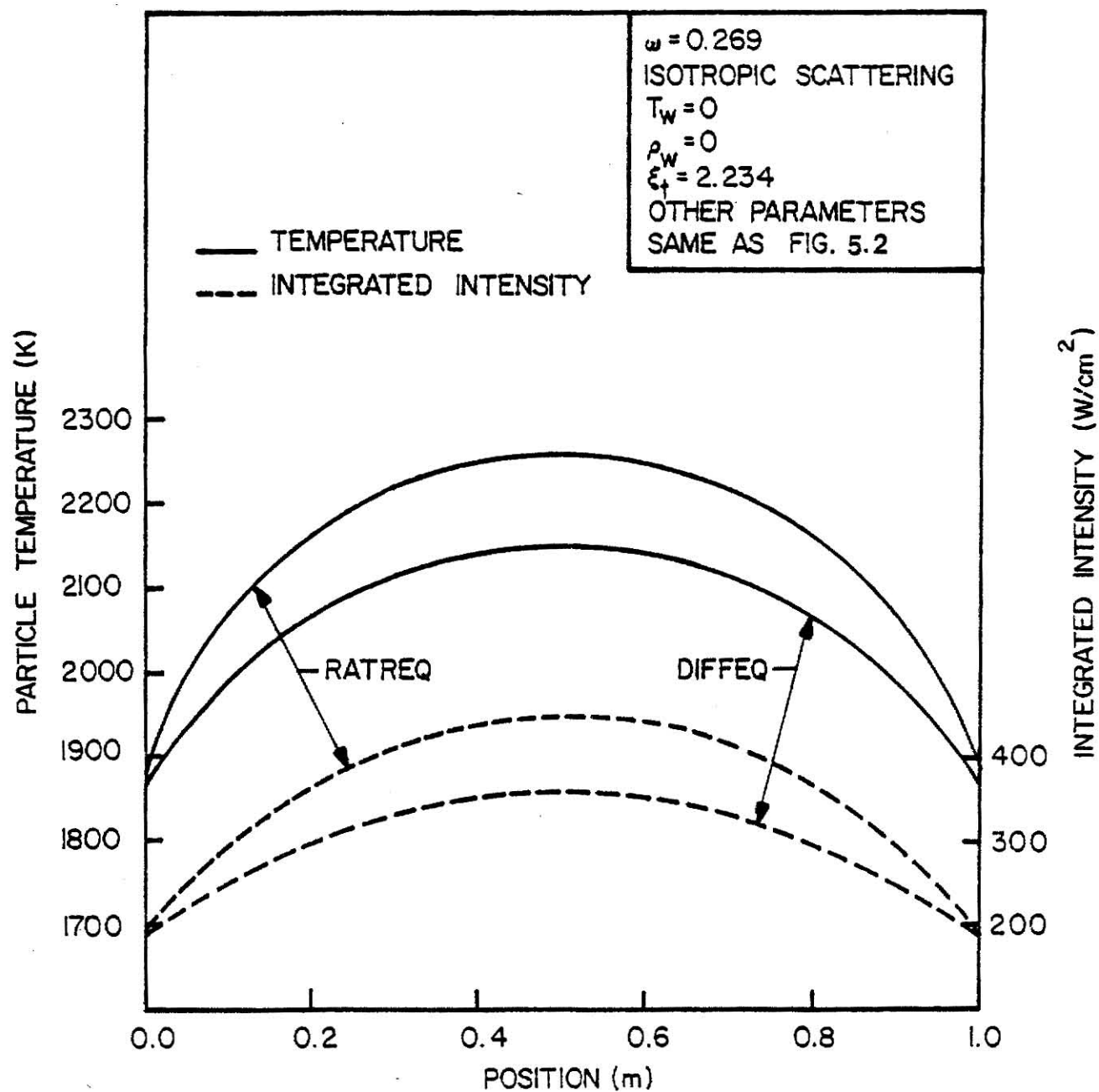


Fig. 5.7. Comparison of the particle temperature and integrated intensity distributions computed by RATREQ and DIFFEQ for a one-meter thick system with the temperature-dependent heat generation rate. The computed radiation leakage at each wall is 102.0 W cm^{-2} (RATREQ) and 94.8 W cm^{-2} (DIFFEQ).

with the error introduced by the diffusion approximation increasing to a maximum at the center of the medium. The maximum difference in temperature is approximately 5%, while the maximum error in the integrated intensity is considerably larger (roughly 20%). The computed radiation leakage at each wall is also shown with Fig. 5.7, and the results agree to within 8%.

The same comparisons are made for a two-meter thick system ($\xi_t = 4.468$) in Fig. 5.8. Again the agreement between the discrete ordinates and diffusion results is best at the system boundaries, with a maximum difference in temperature (at the center) of 3%, a maximum difference in integrated intensity of 6%, and a difference in the radiant leakage from each wall of 4%. The increase in system size improves the agreement between the two solutions because of the decreased anisotropy of the radiation intensity associated with larger systems. This increases the validity of the P_1 approximation which is used to derive the diffusion equation.

It should be noted that the only errors introduced by the discrete ordinates solution of the equation of transfer result from the spatial and angular discretizations. However, if the solution is fully converged with respect to the spatial and angular grid sizes, the discrete ordinates solution is exact. The discrete ordinates results are therefore inherently more accurate than the diffusion approximation results, and the effects of various parameters on the computed temperature distributions are best tested using the discrete ordinates model.

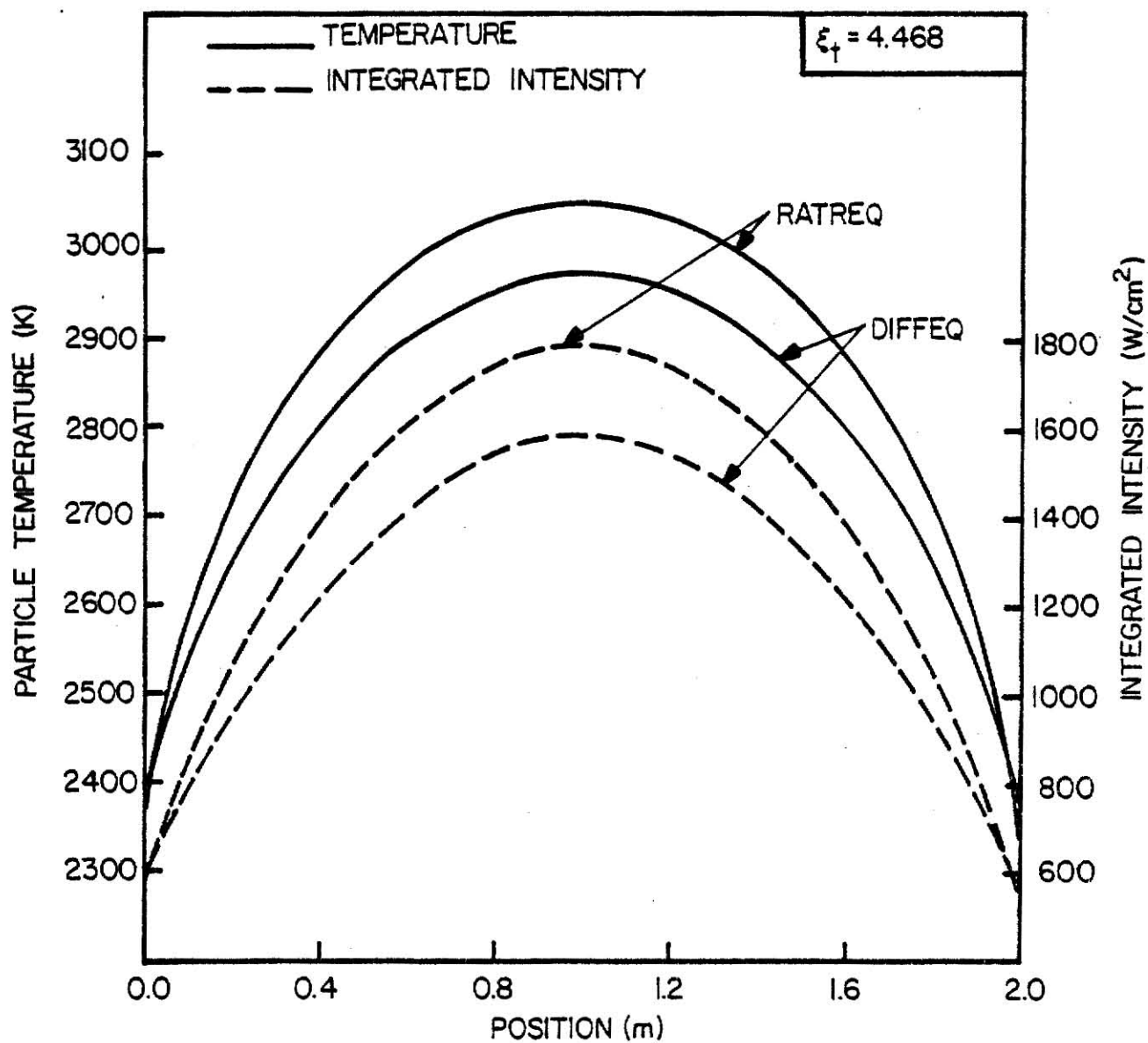


Fig. 5.8. Comparison of the particle temperature and integrated intensity distributions computed by RATREQ and DIFFEQ for a two-meter system. The computed radiation leakage at each wall is 303.2 W cm^{-2} (RATREQ) and 289.8 W cm^{-2} (DIFFEQ).

5.7.3 Effect of Scattering

The effect of scattering on the computed particle temperature distribution is tested using RATREQ. First, scattering is assumed isotropic, and a number of temperature profiles are computed for a one-meter thick suspension based on different assumed values of the refractive index of the char particles (i.e., different scattering efficiencies and single scatter albedos). These results are then compared with a case in which scattering is neglected entirely and a case in which scattering is anisotropic. These results are shown in Fig. 5.9 and indicate that increasing the scattering albedo causes an increase of the particle temperature at every point in the medium, as well as increasing slightly the curvature of the temperature profile. This may be explained by the fact that scattering of radiation contributes to the source term (i.e., the right side) of the equation of transfer. The increase of the source term causes an increase in the radiation intensity, and consequently an increase in particle temperature. The maximum difference in computed temperature between the cases in which scattering is most significant (i.e., the highest refractive index) and scattering is neglected is approximately 120 K, which represents a difference of roughly 5%.

The effect of the anisotropy of scatter is to raise the overall temperature profile. This increase is caused by the predominance of backward scattering from the large, diffusely reflecting coal and char particles. The backward scattering decreases the leakage of radiant energy at the walls, since a larger fraction of the radiation propagating away from the center of the medium is redirected back towards

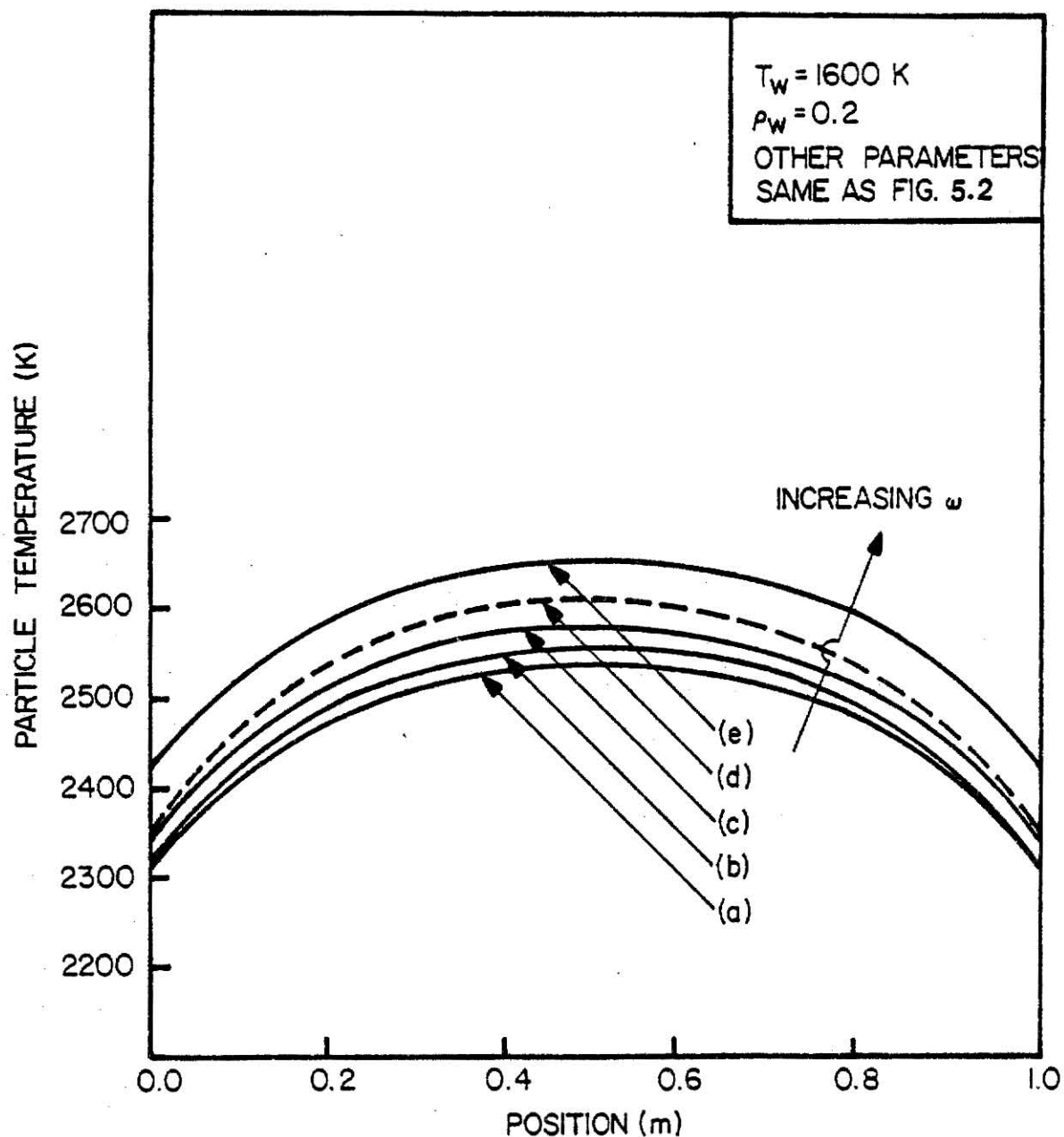


Fig. 5.9. Effect of scattering on the particle temperature distribution - (a) no scattering; (b) $m=1.5(1-i0.1)$, $\omega=0.125$, isotropic scattering; (c) $m=1.93(1-i0.53)$, $\omega=0.269$, isotropic scattering; (d) same as c, anisotropic scattering; (e) $m=3.0(1-i1.0)$, $\omega=0.514$, isotropic scattering.

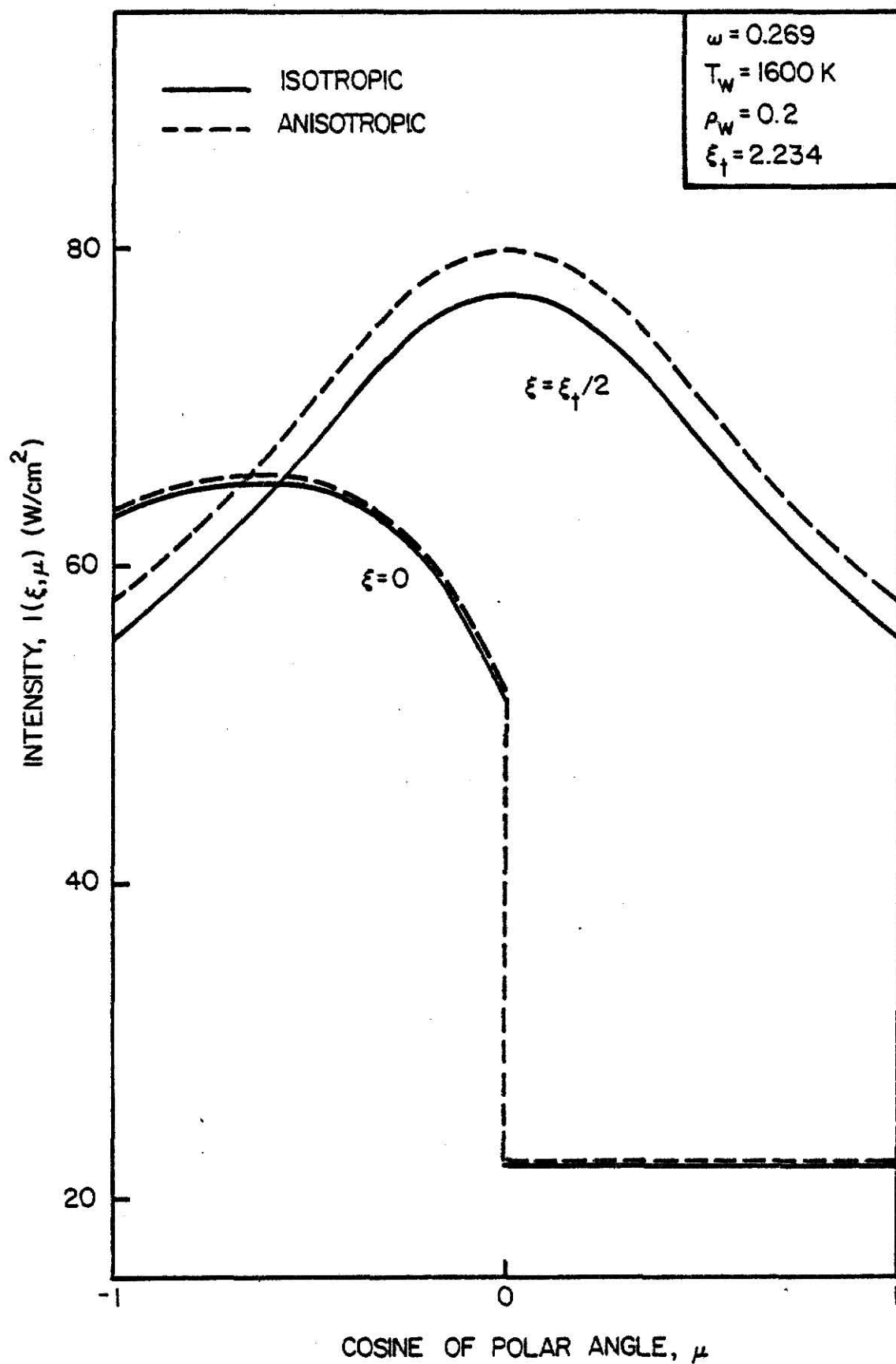


Fig. 5.10. The effect of the backward-peaked phase function on the angular dependence of the radiation intensity in a one-meter thick suspension at two different positions. Thirty-two angular quadrature ordinates were used.

the center than is the case with isotropic scattering. The decreased radiation leakage leads to an increased radiation intensity throughout the system and consequently an increase in temperature.

The effect of the anisotropy of scattering on the angular dependence of the radiation intensity is shown in Fig. 5.10. The intensity is shown as a function of μ at two positions in a one-meter thick suspension (the boundary and the center). The anisotropy is seen to increase the intensity distribution for all values of μ , with the greater shift occurring at the center of the medium.

5.7.4 Effect of Boundary Conditions

The effect of the assumed temperature and reflectivity of the walls bounding a one-meter thick suspension on the temperature distribution computed by RATREQ is illustrated in Fig. 5.11; the wall temperature is increased from 0 K to 1600 K, and the reflectivity is varied from 0 to 0.2. The increase of either the wall temperature or reflectivity causes an increase of the particle temperature at every point in the medium. Since the walls emit radiant energy at a rate proportional to the fourth power of their temperature, an increase in wall temperature increases significantly the intensity incident on the suspension from the walls, which causes the increase in particle temperature. Similarly, an increase of the wall reflectivity causes a larger fraction of the radiant energy incident on the walls to be returned to the medium, again yielding higher temperatures. Interestingly, the increase of the particle temperature produces an increase in the rate of heat generation by chemical reaction, which

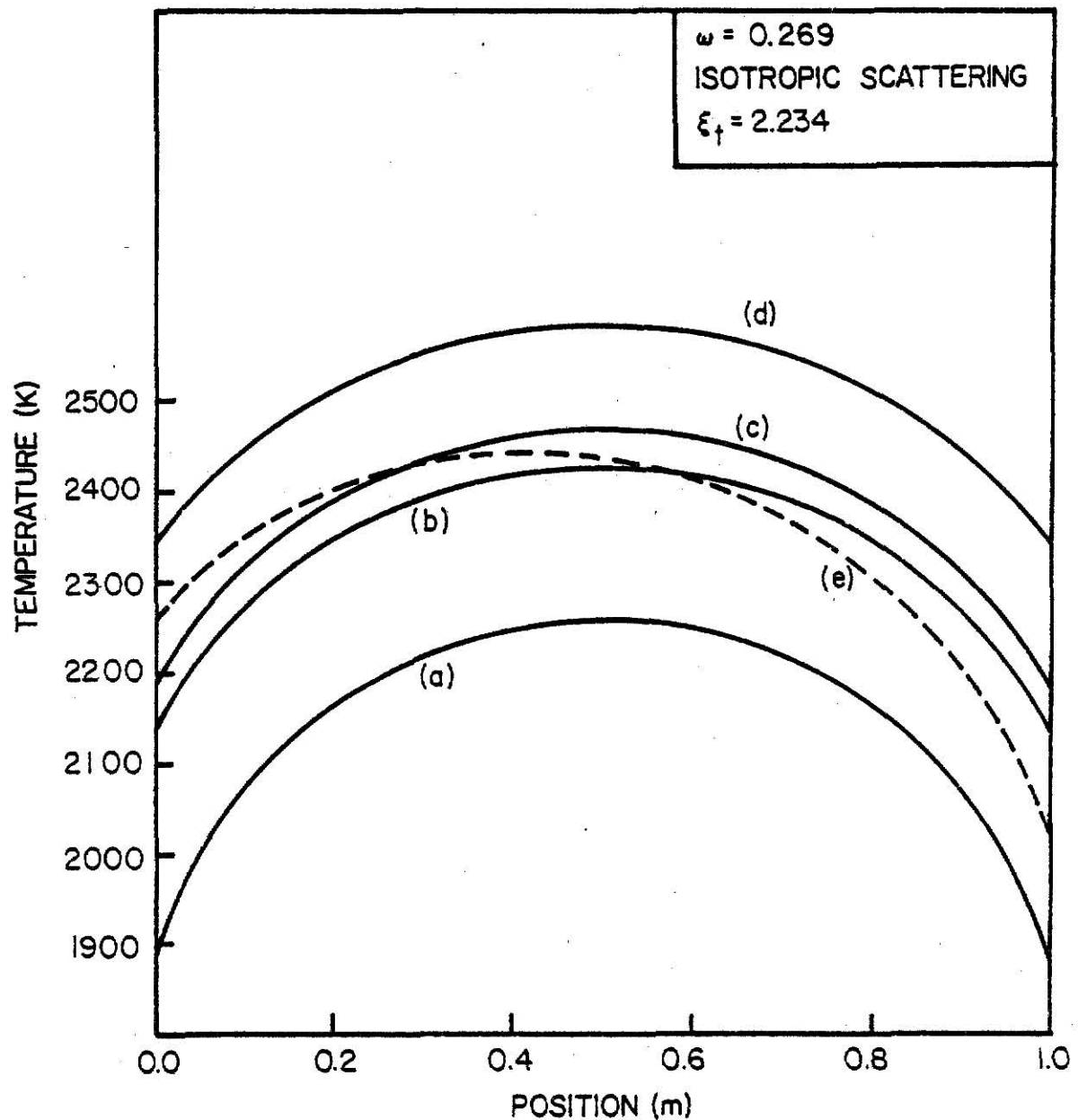


Fig. 5.11. Effect of the wall temperature and reflectivity on the particle temperature distribution - (a) $T_w=0$, $\rho_w=0$, radiant leakage at each wall (RL) = 102.0 W cm^{-2} ; (b) $T_w=0$, $\rho_w=0.2$, RL = 118.7 W cm^{-2} ; (c) $T_w=1600 \text{ K}$, $\rho_w=0$, RL = 122.4 W cm^{-2} ; (d) $T_w=1600 \text{ K}$, $\rho_w=0.2$, RL = 131.8 W cm^{-2} ; (e) $T_{w1}=1600 \text{ K}$, $\rho_{w1}=0.2$, RL₁ = 99.6 W cm^{-2} , $T_{w2}=0$, $\rho_{w2}=0$, RL₂ = 141.1 W cm^{-2} .

necessitates an increase of the radiation leakage rate from the medium (to maintain the energy balance of the entire system). Therefore, the increase of the wall temperature or reflectivity also increases the radiant heat loss from the medium. The computed radiant losses are given with Fig. 5.11 for the various conditions of wall temperature and reflectivity.

The effect of assuming the two walls surrounding the medium to have different temperatures and reflectivities is also shown in Fig. 5.11. As expected, the maximum temperature in this case occurs at a point closer to the hotter and more reflective wall. It should also be noted that the radiation leakage is greater at the cooler wall, since that wall neither emits any radiation towards the medium nor reflects any incident radiation, and thus all the radiant energy incident on the wall is lost by leakage.

5.7.5 Effect of Particle Size

The particle temperature distribution was computed by RATREQ for 50 μm particles and compared with temperature distributions computed for 25 μm particles based on the same particle bulk density ρ_p , the same particle number density N , and the same particle surface area per unit volume S_v . These results are shown in Fig. 5.12.

The temperature distribution for the 25 μm particles is seen to be much higher than that of the 50 μm particles when the comparison is based on equal bulk densities. Even though the same amount of fuel mass is present per unit volume, the surface area per unit volume is much larger for the smaller 25 μm particles. Since the particle

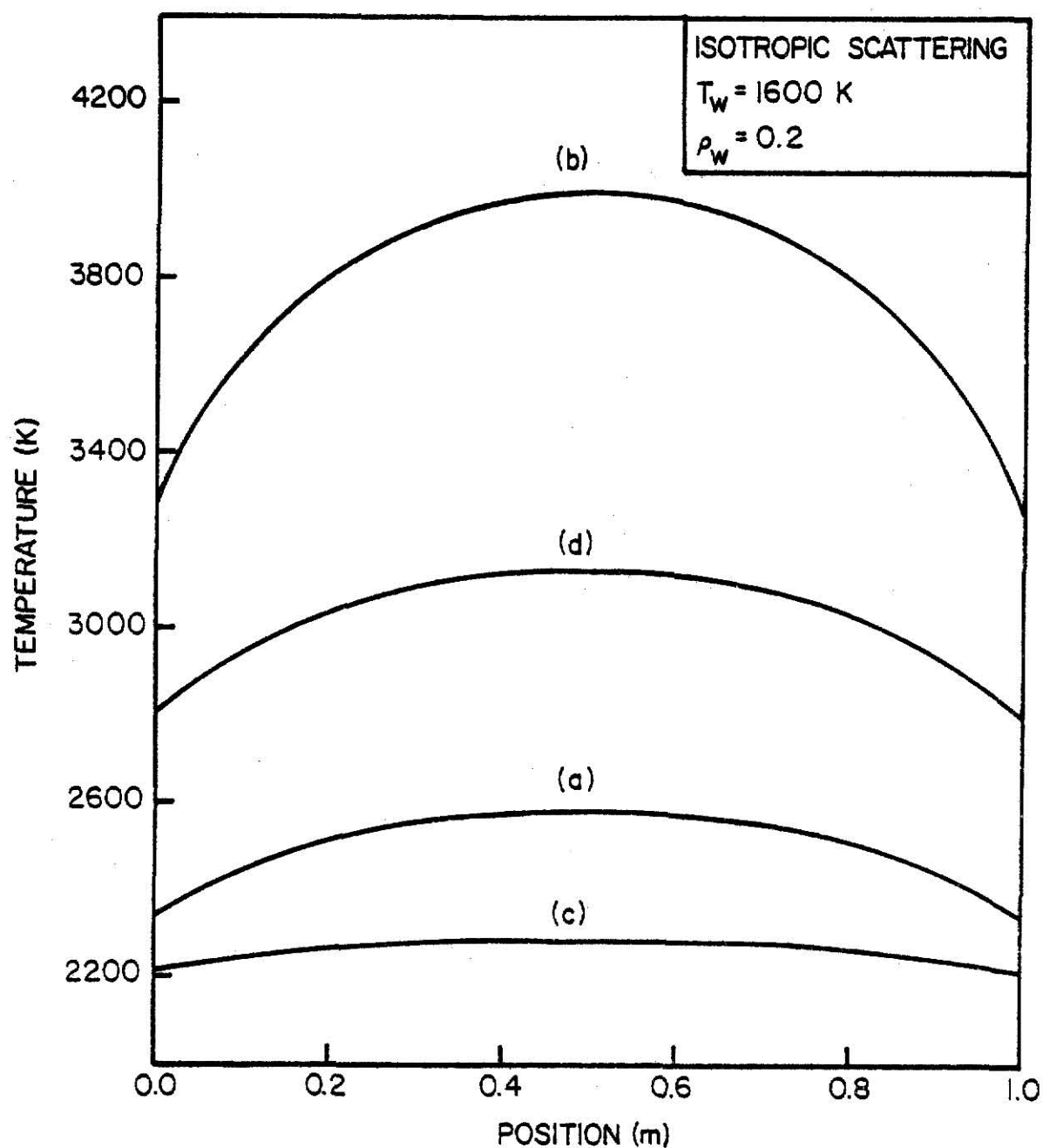


Fig. 5.12. Comparison of temperature distributions computed for suspensions of different sized particles - (a) $d_p = 50 \text{ } \mu\text{m}$, $\rho_p = 10^{-4} \text{ g cm}^{-3}$, $N = 1.019 \times 10^3 \text{ cm}^{-3}$, $S_v = 0.08 \text{ cm}^{-1}$; (b) $d_p = 25 \text{ } \mu\text{m}$, ρ_p same as a); (c) $d_p = 25 \text{ } \mu\text{m}$, N same as a); (d) $d_p = 25 \text{ } \mu\text{m}$, S_v same as a). The suspension thickness is 1 m in each case, and the assumed particle refractive index is $1.93(1-i0.53)$.

surface is the site of the heterogeneous chemical reaction of the particles, the smaller particles possess greater reaction surface area and consequently a larger heat generation rate per unit volume. The increased rate of heat generation leads to the greatly increased temperature of the smaller particles. The opposite is true when the comparison of the temperatures of the two particle sizes is based on the same particle number density. In this case, it is the larger particles which are characterized by a greater surface area per unit volume, a larger volumetric heat generation rate, and a higher temperature. Finally, the comparison based on equal values of the particle surface area per unit volume indicate the smaller particles attain higher temperatures. This is explained by the fact that the diffusional rate coefficient K_d (which appears in the expression for the particle burning rate r_p) is inversely proportional to particle size, and hence the reaction rate of large particles is more limited by the diffusion of oxygen to the particle surface. The decreased particle burning rate causes a decrease of the heat generation rate and the computed temperatures for the larger particles.

5.7.6 Effect of Convection to Gas Phase

The effect of assuming a gas temperature which is not equal to the particle temperature at each point in the system is shown in Fig. 5.13. The computed particle temperature distributions corresponding to two assumed values of a uniform gas temperature distribution [$T_g(\xi) = 1800$ K, and $T_g(\xi) = 2200$ K] are compared to the particle temperature distribution corresponding to thermal equilibrium between the two

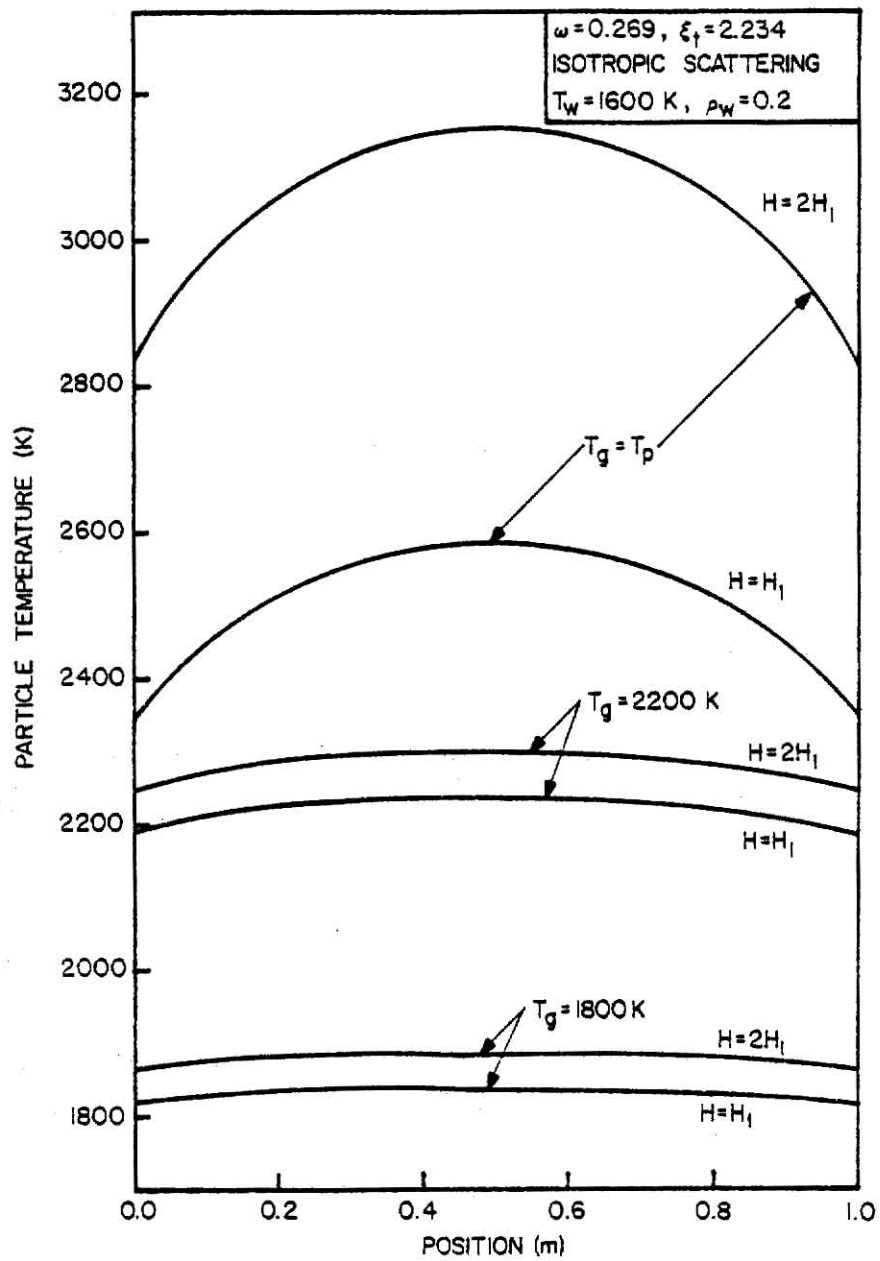


Fig. 5.13. Effect of the assumed gas temperature distribution and the heat generation rate on the computed particle temperature distribution. The heat generation rate H_1 is normalized to 1 W cm^{-3} at $T_p = T_g = 1750 \text{ K}$.

phases [$T_g(\xi) = T_p(\xi)$]. The comparison is performed for a one-meter thick suspension for two different rates of heat generation [$H(T) = H_1(T)$ and $H(T) = 2H_1(T)$]. The heat generation function H_1 is the same as that shown in Fig. 5.2, and the thermal conductivity of the gas was assumed to be $8.368 \times 10^{-4} \text{ W cm}^{-1} \text{ K}^{-1}$ at a temperature of 1600 K.

The assumed gas temperatures of 1800 K and 2200 K are seen to yield a drastically different particle temperature distribution from that computed in the thermal equilibrium case. For an assumed gas temperature of 1800 K, the computed particle temperature at any point in the medium differs by less than 40 K from the assumed gas temperature (for $H = H_1$), and by less than 90 K (for $H = 2H_1$). For a gas temperature of 2200 K, the particle temperature differs by a maximum of 40 K from the gas temperature (for $H = H_1$), and by roughly 100 K (for $H = 2H_1$). Thus the maximum difference in temperature between the two phases increases slightly with an increase in the assumed gas temperature, particularly for large rates of heat generation. However, this temperature difference is limited by the increased thermal conductivity of the gas phase at elevated temperatures, which leads to larger rates of inter-species convection heat transfer, thereby offsetting the thermal disequilibrium between the two phases. Therefore, the gas phase is an effective heat sink which prevents the particle temperature from deviating greatly from its own. Consequently, the assumption of thermal equilibrium between the two phases is largely justified.

Since the gas phase energy balance equation is not considered in this study, no provision is made for transfer of the heat gained (or lost) by the gas phase by convection from the solid phase. This is tantamount to the assumption that the gas phase is characterized by an infinite heat capacity and is thus able to absorb or release any amount of heat without a change in temperature. This assumption has also been made by Essenhig and Csaba¹⁷ in their calculation of the particle temperature in coal suspensions.

5.7.7 Effect of Optical Thickness

It has been shown in Sections 5.4 and 5.5 that for a given optical thickness of the medium, the simultaneous solution of the equation of transfer and the particle energy balance (for the intensity and temperature distributions) is independent of the actual system thickness x_t and the particle bulk density ρ_p . The sole effect of changing either of these parameters is to change the optical thickness of the medium, and therefore their individual effects on the computed temperature distributions are not considered. The effect of varying the optical thickness on the temperature distribution is shown in Fig. 5.14. It can be seen that doubling the optical thickness causes a considerable increase in particle temperature, as well as a somewhat smaller spatial temperature variation. The temperature increase for the larger system is a result of the decrease in the surface area available for radiation leakage relative to the volume of the medium.

An interesting behavior of the particle temperature is observed if the maximum temperature attained by the particles (i.e., the

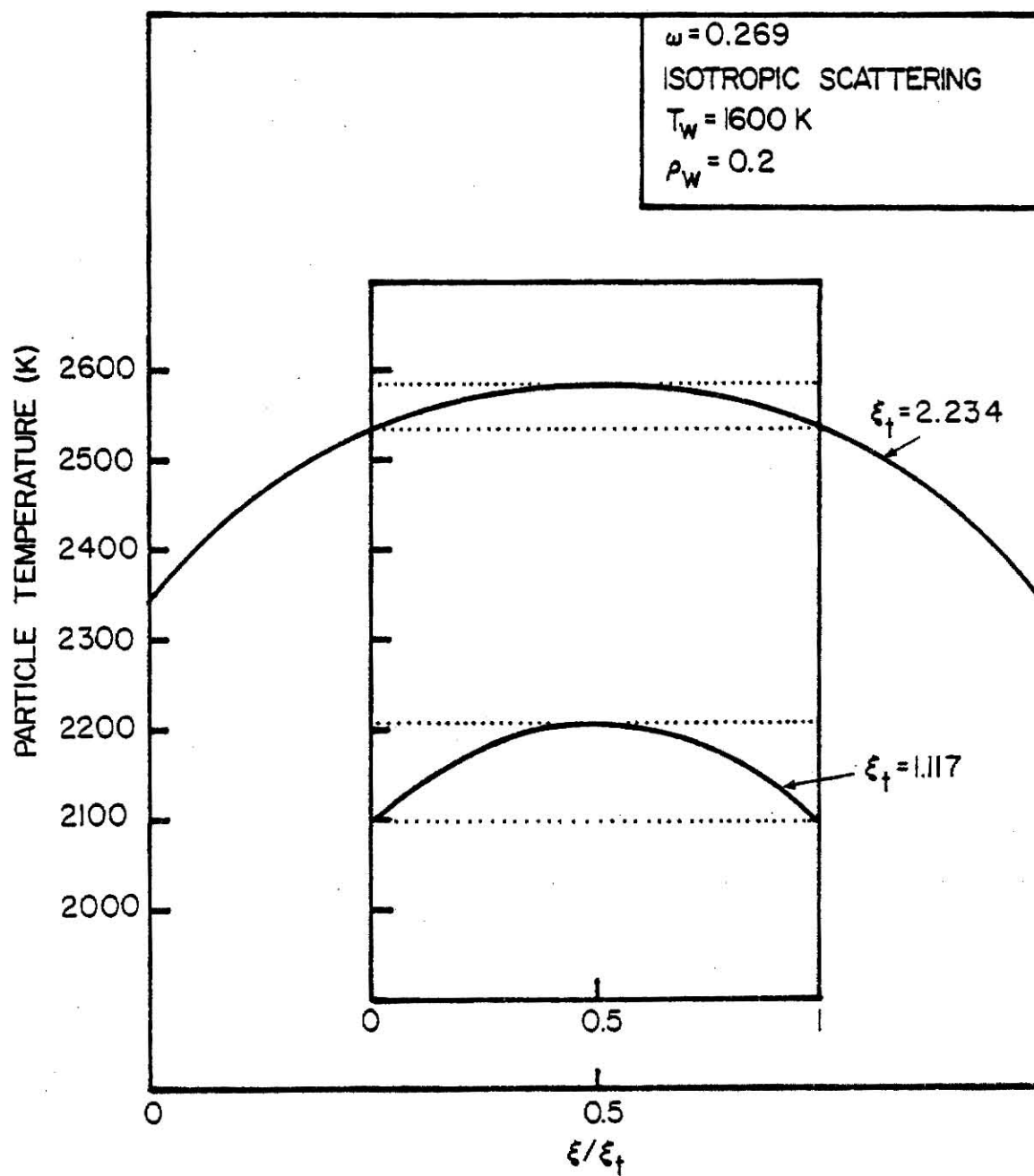


Fig. 5.14. Particle temperature distributions for two different suspension optical thicknesses.

temperature at the center of the suspension) is plotted as a function of the optical thickness of the medium. The behavior is best illustrated by curve (a) in Fig. 5.15, for which the gas and particle temperatures are equal (i.e., particles do not gain or lose energy by convection) and the walls are cold and non-reflecting (i.e., no radiation is incident on the medium at the boundaries). The maximum particle temperature is seen to be zero for values of the system optical thickness below a critical value ξ_{cr} . As the system size passes through the critical value, the maximum temperature changes discontinuously (i.e., exhibits a bifurcation) to a non-zero value. The medium ignites only for system optical thicknesses greater than ξ_{cr} . For thicknesses smaller than ξ_{cr} , non-zero temperature (and intensity) distributions yield radiant heat losses by leakage through the walls that exceed the energy which is generated by chemical reaction. This excess of leakage over the heat production forces the system temperature to an equilibrium value of zero (for which both the leakage and heat generation rates are equal to zero).

The discontinuous change of the maximum temperature with optical thickness is also observed when the heat generation rate is tripled [curve (b) of Fig. 5.15]. This increase in heat production is seen to cause both a decrease in the critical optical thickness and a significant increase of the maximum particle temperature at any given optical thickness.

The curves (c) and (d) of Fig. 5.15 illustrate the effect of assuming a uniform gas temperature distribution different from that

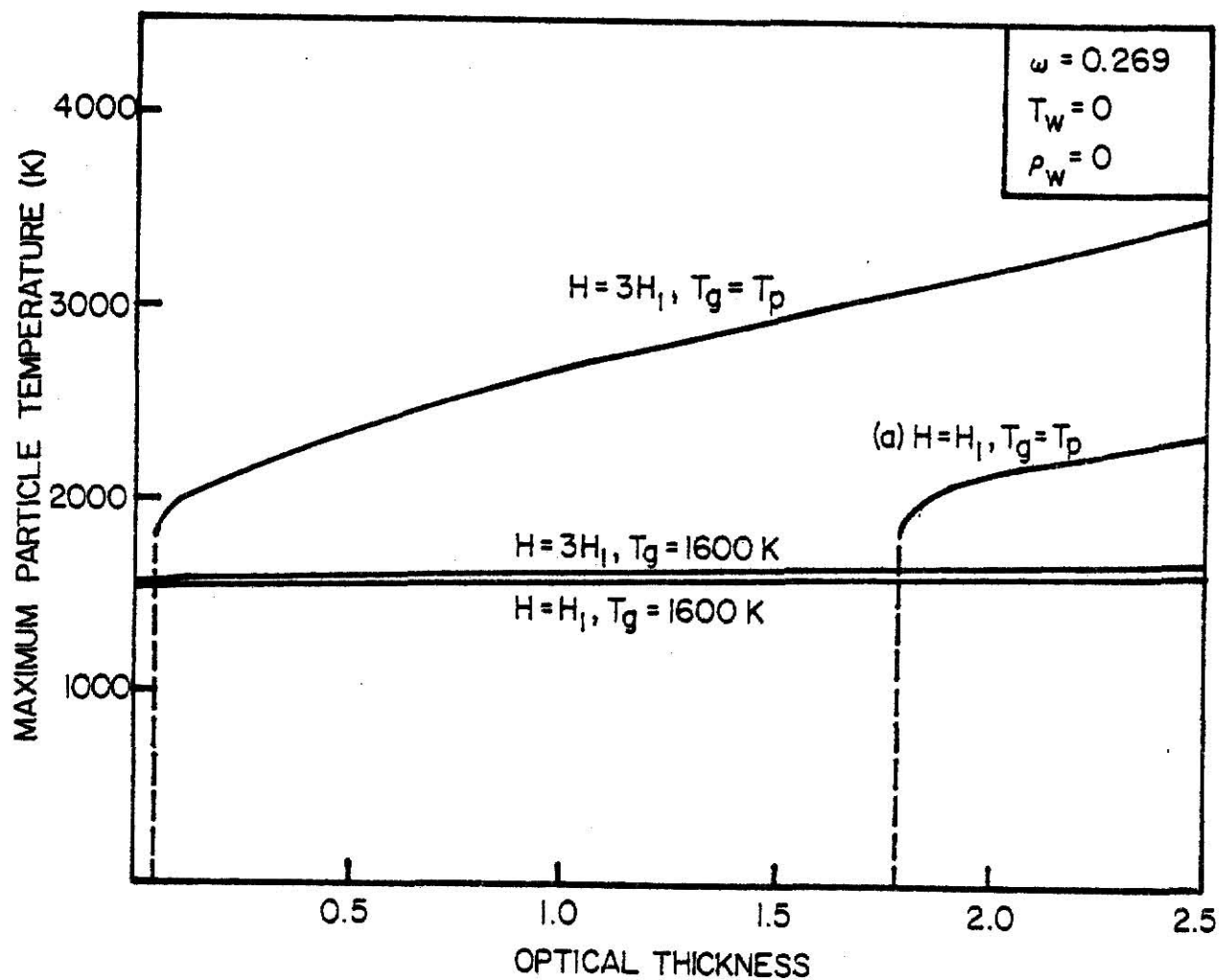


Fig. 5.15. Variation of the maximum particle temperature with optical thickness in a suspension surrounded by cold, non-reflecting walls for two heat generation rates and two different gas temperatures.

of the particle phase. The curves for this unrealistic situation do not exhibit the ignition behavior which characterizes curves (a) and (b). The insensitivity of the maximum temperature to the optical thickness (when the two phases are not in thermal equilibrium) is a result of the heat transferred by convection between the two phases. The particle temperature cannot deviate greatly from the gas temperature because the effectiveness of the gas as a heat source or sink is roughly proportional to the temperature difference between the two phases. Therefore, even for optically thin suspensions in which the leakage exceeds the chemical heat generation, and for which the particle temperature would consequently be expected to decrease, the convective gains from the gas phase prevent the particle temperature from falling to zero. Similarly, for very large systems, in which the particle temperature would tend to increase, a particle temperature is maintained close to the assumed gas temperature by convection of heat to the gas phase.

The effect of the activation energy on the variation of the maximum temperature with optical thickness is shown in Fig. 5.16. A small variation of the activation energy is seen to yield a considerable change in the critical optical thickness, with the critical value decreasing for the smaller activation energy. However, for optical thicknesses greater than the critical values, the effect of the different activation energies on the maximum temperature is seen to be minimal due to the predominance of the diffusional control mechanism at high temperatures. The variation of ξ_{cr} with the acti-

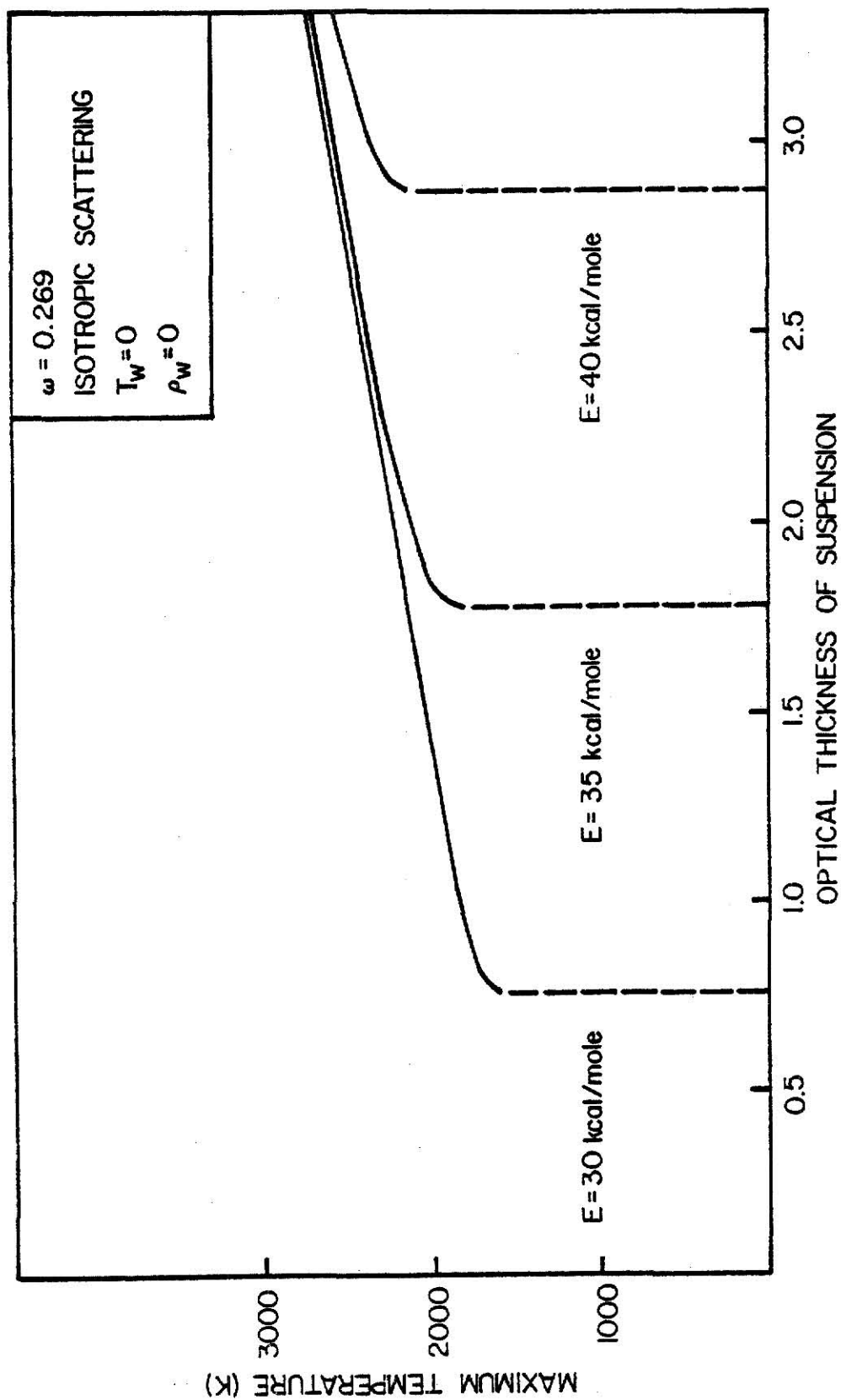


Fig. 5.16. Effect of the activation energy on the variation of the maximum particle temperature with the system optical thickness.

vation energy E is caused by the increased rate of heat generation at any given temperature with decreased values of E . This greater heat production rate (for given temperature and intensity distributions) allows optically thinner systems to ignite.

The effect of the assumed wall temperature on the variation of the maximum temperature with optical thickness is illustrated in Fig. 5.17. Curve (a) in this figure is identical to curve (a) of Fig. 5.15 and represents the observed variation for cold, non-reflecting walls. The wall temperature is progressively increased in curves (a) through (d), while the reflectivity remains zero. An increase in wall temperature to 1000 K [curve (b)] yields particle temperatures equal to the wall temperature for system thicknesses below a critical value which is smaller than the critical value observed with cold walls. Further increases in the wall temperature cause both the critical thickness and the temperature jump at the critical thickness to decrease [curves (c) to (f)]. At a wall temperature of 1600 K, the bifurcation of the maximum temperature is not observed, and the particles are seen to ignite regardless of the system optical thickness. The decrease in the critical thickness with increasing wall temperature is illustrated in Fig. 5.18 for different wall reflectivities. This decrease of ξ_{cr} may be explained by the fact that the emission from the walls is a source of radiation to the reacting system. This incident radiation causes an increase of the particle temperature throughout the medium and, consequently, an increase of the heat generation rate, thereby allowing optically thinner systems to ignite.

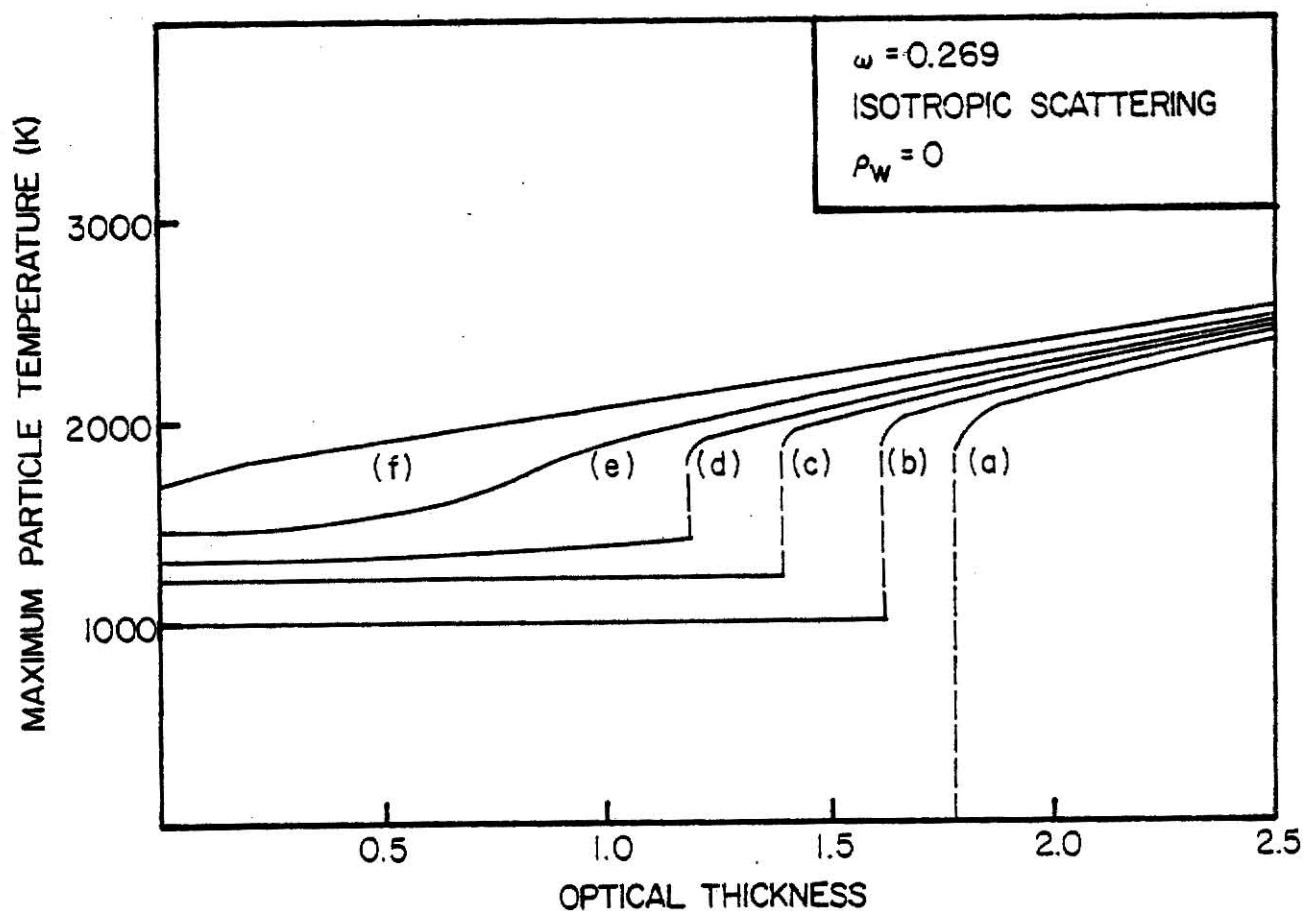


Fig. 5.17. Variation of the maximum particle temperature with the optical thickness of the medium for different temperatures of the bounding walls - (a) $T_w = 0$, (b) $T_w = 1000$ K, (c) $T_w = 1200$ K, (d) $T_w = 1300$ K, (e) $T_w = 1400$ K, (f) $T_w = 1600$ K.

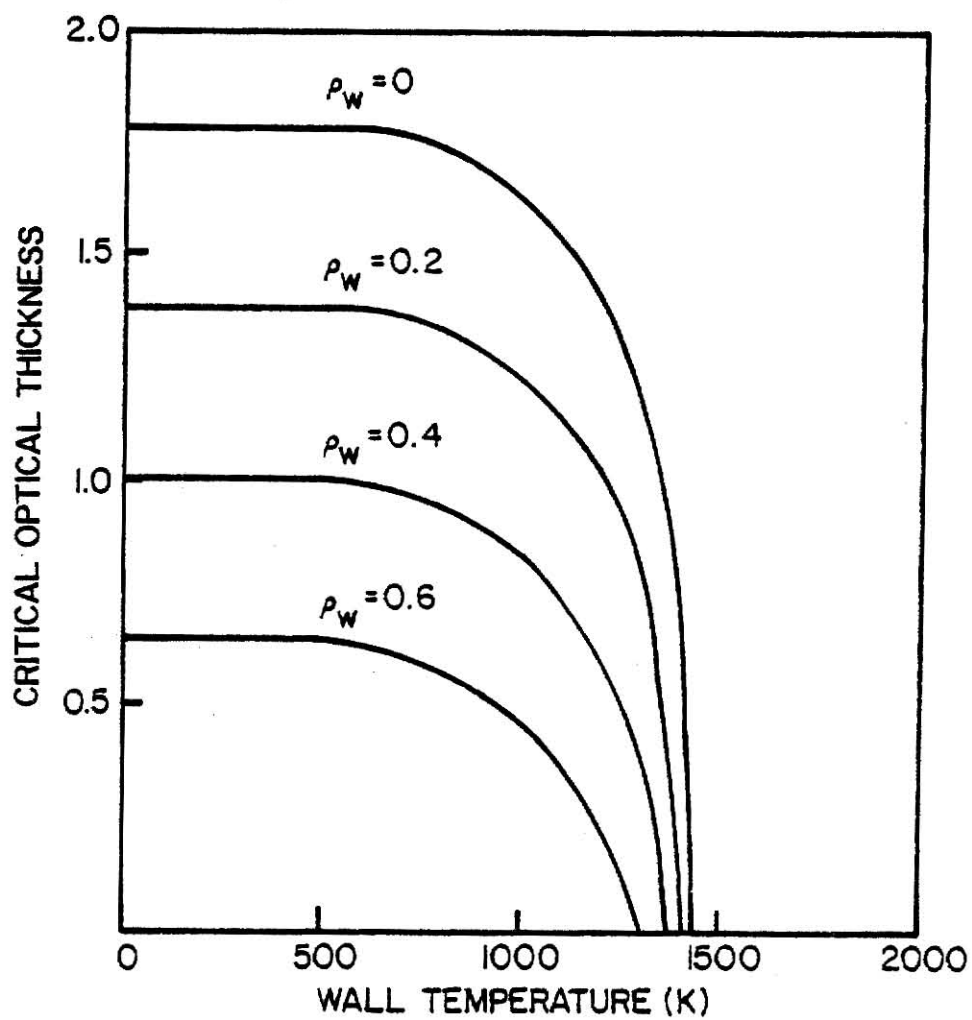


Fig. 5.18. The critical optical thickness as a function of wall temperature for different values of wall reflectivity.

The effect of varying the wall reflectivity on the maximum temperature vs. optical thickness curves is illustrated in Fig. 5.19 for the case of cold walls. The increase of wall reflectivity is seen to have two effects, raising the maximum temperature for a given optical thickness and decreasing the critical optical thickness. The variation of the critical optical thickness with wall reflectivity is shown in Fig. 5.20 and is seen to be nearly linear for several assumed wall temperatures. The decreased critical thickness for increasing reflectivity is caused by the decreased fraction of radiation incident on the walls that is lost by leakage, which allows smaller systems to ignite.

A comparison of the ignition curves obtained from the discrete ordinates solution and the diffusion approximation of the equation of transfer is shown in Fig. 5.21. The maximum particle temperature in a medium bounded by cold, non-reflecting walls is shown in each case as a function of the optical thickness. The critical thickness is seen to be smaller by roughly 10% for the discrete ordinates solution. For any specified optical thickness, the discrete ordinates solution yields a higher maximum temperature than the diffusion approximation (with a difference in maximum temperature of approximately 10% for $\xi_t = 2$, and 1.5% for $\xi_t = 5$). As expected, the error (in maximum temperature) due to the diffusion approximation decreases dramatically with increasing optical thickness of the suspension.

It should be noted that the actual numerical values of the many results presented in this chapter are of limited significance, since

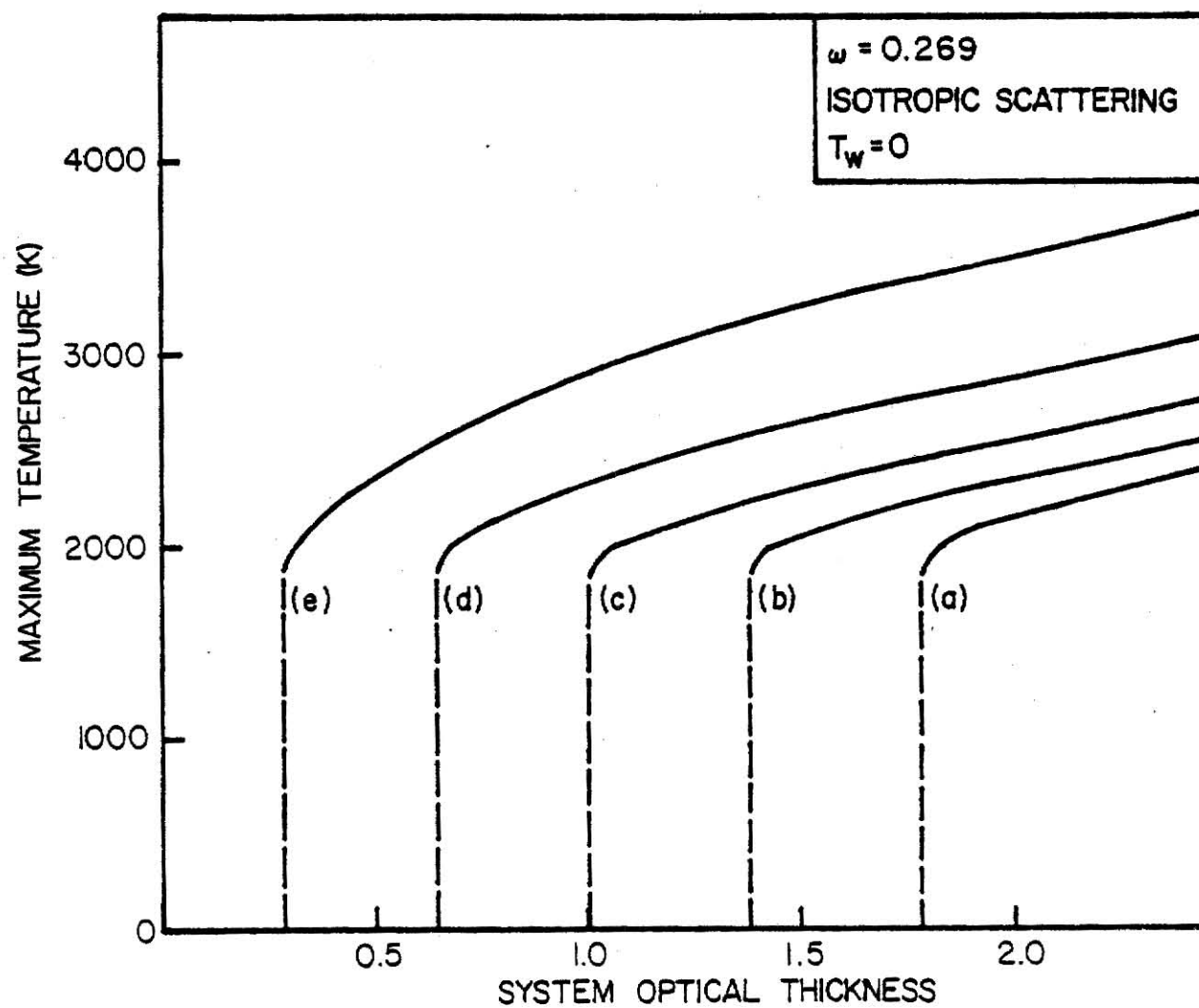


Fig. 5.19. Variation of the maximum particle temperature with the optical thickness of the medium for different values of the wall reflectivity - (a) $\rho_w = 0$, (b) $\rho_w = 0.2$, (c) $\rho_w = 0.4$, (d) $\rho_w = 0.6$, (e) $\rho_w = 0.8$.

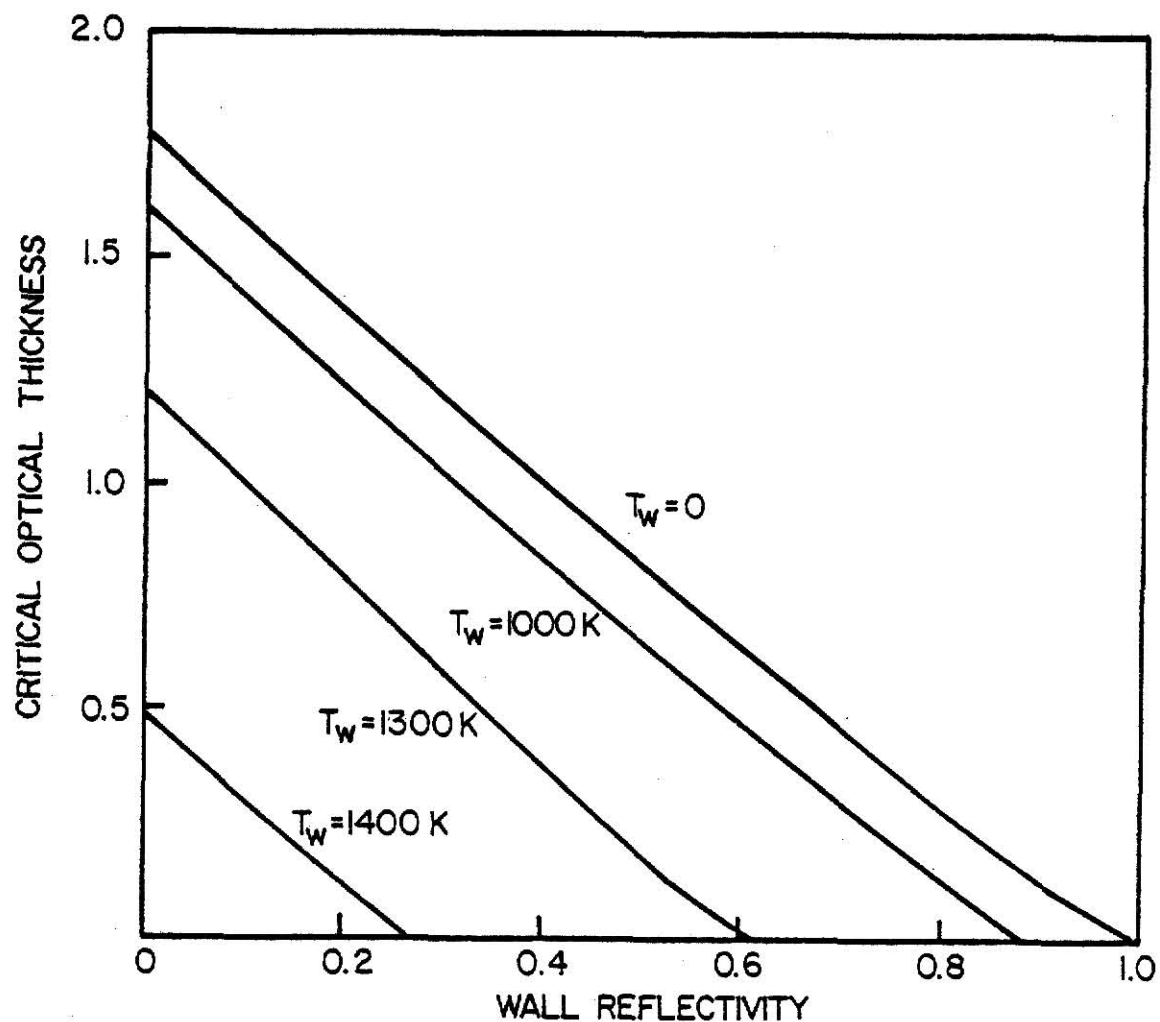


Fig. 5.20. The critical optical thickness as a function of wall reflectivity for several values of the wall temperature.

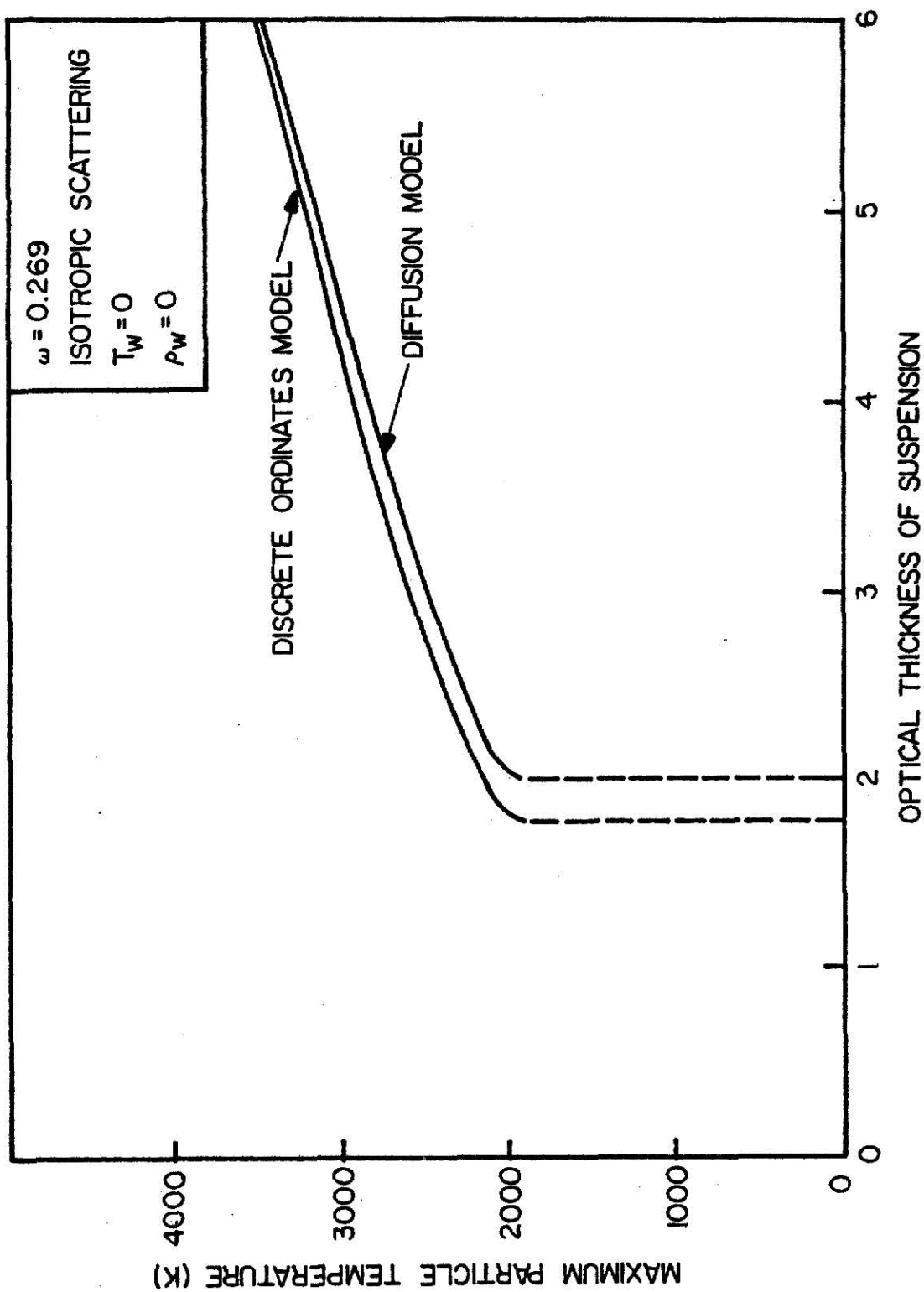


Fig. 5.21. Maximum particle temperature as a function of system optical thickness computed by the discrete ordinates (RATREQ) and the diffusion equation (DIFFEQ) solutions for a medium bounded by cold, non-reflecting walls.

they are specific to the simplified energy balance and heat generation models developed in this chapter. However, valuable insight was gained by examination of the trends exhibited by these results. A number of generalizations of these simplified models are proposed in the following chapter, together with a brief summary of this study and the associated conclusions.

6.0 SUMMARY, CONCLUSIONS, AND RECOMMENDATIONS

6.1 Summary and Conclusions

The purpose of this study was two-fold: to formulate the general theory of the radiative transfer problem in chemically reacting particle-gas mixtures, and to apply the solution of the equation of transfer by techniques developed in neutron transport theory to the calculation of the temperature and radiation intensity distributions in pulverized coal suspensions. A number of numerical solution methods for the radiative transfer equation have been reviewed. In particular, the discrete ordinates method and the diffusion approximation were used to calculate the radiation transport for a model of combustion in particle suspensions. The discrete ordinates method has been applied in this study for the first time to the solution of the radiative transfer equation in a medium containing a temperature-dependent heat source distribution. The combination of a numerical discrete ordinates method with an iterative solution procedure allows the extension of this solution algorithm to the calculation of the radiant energy transfer in media containing energy sources or sinks with an arbitrary temperature dependence.

Simplifications of the energy balance on a pulverized coal suspension and of the geometry of the suspension allowed consideration of a numerical example that exhibited many important features of realistic problems (e.g., non-linear energy production rate, multiple anisotropic scattering of thermal radiation, bounding walls which reflect and emit radiation). This numerical example was used to

study the effects of the numerous problem parameters on the computed temperature and intensity distributions and to compare results obtained from the discrete ordinates and the diffusion approximation solutions of the radiative transfer equation.

The diffusion approximation was shown to yield numerical results in good agreement with the more accurate results obtained by the discrete ordinates method. The error in integrated intensity was found to be somewhat larger than the error in temperature for a given optical thickness of the pulverized coal suspension. As expected, the accuracy of the diffusion approximation improved with increasing optical thickness due to the decreased anisotropy of the radiation intensity in optically thick suspensions, which are characterized by a reduced spatial variation of the intensity. Therefore, if solutions are sought in media whose optical thickness $\xi_t \geq 5$, the diffusion approximation can be used to compute the radiation transport with little error.

In the absence of all heat loss modes other than radiation, coal dust suspensions were found to ignite only if their optical thickness exceeds a critical value. This critical optical thickness depends on the temperature and reflectivity of the walls bounding the suspension and is very sensitive to the parameters of the heat generation model. Steady state solutions for the temperature and intensity distributions were found to exist for any system optical thickness, and the critical optical thickness represented a point at which the steady state solutions increased discontinuously to a large value.

This same behavior has been observed with gaseous combustible mixtures characterized by an Arrhenius heat production rate and energy losses by conductive heat transfer only.⁶⁵ Although the ignition behavior observed in this study was based on a simplified energy production rate, the results are useful because a minimum explosive particle concentration can be inferred given the system thickness and values of the wall temperature and reflectivity.

The effect of the assumed optical properties of the coal particles on the computed temperature distribution was found to be small, although not negligible. The assumption of isotropic scattering was shown to yield little error in either the angular dependence of the radiation intensity at a given point or the computed temperature distribution. All results were obtained for particles in the so-called large particle limit, for which the scattering phase function is backward peaked (since diffracted radiation is treated as being unscattered). For very small coal and char particles (with size parameters ≤ 5), the diffraction angle increases, and diffraction can no longer be treated as purely forward scattering. The scattering phase function becomes forward peaked and must be determined from Mie theory. The effect of Mie scattering by these small particles on the computed temperature and intensity distributions was not investigated in this work.

The effects of particle size and the boundary conditions on the particle temperature distribution and the radiant energy loss from the suspension was found to be significant. Smaller particles and

hotter, more highly reflective walls yielded higher temperatures and greater radiation leakage rates at the boundaries. Finally, most calculations in this study were based on the assumption of thermal equilibrium between the solid and gas phases. If the gas phase temperature distribution was assumed a priori, the particle temperature was found to converge to a value nearly equal to the gas temperature at every point in the suspension.

6.2. Recommendations for Further Study

It is apparent that many generalizations can be made to the simple model of radiant heat transfer in pulverized coal clouds investigated in Chapter 5 of this work. Consideration of polydisperse particle size distributions and a generalized set of coal reactions (i.e., devolatilization, moisture vaporization, and char oxidation) can be incorporated into the present model, and the solution algorithm would remain unchanged. Other generalizations can be included at the expense of many additional coupled equations that must again be solved by iterative, numerical techniques. The most important of these generalizations are the incorporation of a description for the consumption of coal particles and the calculation of the gas phase temperature distribution by consideration of a separate energy balance for the gaseous species.

The additional equations which must be solved simultaneously with the equations of the present model are the gas and particle continuity equations, and the gas energy balance equation. Clearly,

steady state conditions can exist in a reacting coal dust cloud only if the fuel and oxidizer that are consumed are replaced by their continuous introduction into the reacting system at a finite velocity. Since fuel and oxidizer are consumed along the flow direction (and product gases are formed), the particle and gas concentrations, as well as the particle diameter and density vary along this direction. The particle and gas continuity equations are needed to compute this variation of the particle and gas concentrations along the flow direction. The gas phase energy balance would allow for heat transfer by conduction and the energy release resulting from gas phase chemical reactions. Both the gas and solid phase energy balances can be simplified greatly by assuming that the flow is low-speed (laminar), and thus the convective transport of kinetic energy is negligible (as was mentioned in Chapter 1). The momentum equations for the two phases can be eliminated by assuming the phases to be in dynamic equilibrium and by neglecting pressure gradients, body forces, and viscous dissipation.

The variation of the particle concentration and particle diameter along the flow direction causes the rate of heat generation and the radiation properties to be functions of position. Consequently, the temperature and intensity distributions are functions of at least two spatial coordinates (one along the flow direction, the other normal to it). Therefore, the equation of transfer, the continuity equations, and the energy equations must be solved in two-dimensional geometry. Since the discrete ordinates solution of the equation of transfer

requires large computer storage capacity and computational effort in multi-dimensional geometries, it is recommended that the diffusion approximation be used to compute the transport of radiation either in x-y plane geometry or in r-z cylindrical geometry.

The improvement of the calculation of the radiation transport in coal dust suspensions is heavily dependent on advances in the experimental and theoretical evaluation of the radiation properties of the many components present in pulverized coal flames. For example, additional data are needed for the optical properties of ash particles, particularly at infrared wavelengths. Furthermore, more experimental evidence is needed regarding the formation of soot in pulverized coal flames, as the emission of radiation by soot particles is directly proportional to their mass concentration. Finally, data for the absorption coefficient of the various gaseous species as a function of frequency are needed to assess accurately the contribution by combustion gases to radiant absorption and emission. A knowledge of the radiation properties as a function of frequency (and position) in coal suspensions allows calculation of gaseous (banded) radiation, and radiation from non-gray particles by solving the multi-frequency range formulation of the equation of transfer.

7.0 REFERENCES

1. Selcuk, N. and Siddall, R. G., "Two-Flux Spherical Harmonic Modelling of Two-Dimensional Radiative Transfer in Furnaces," Int. J. Heat Mass Transfer 19, 313 (1976).
2. Gray, W. A., Kulham, J. K., and Müller, R., Heat Transfer from Flames, Elek Science, 1976.
3. Essenhigh, R. H., "Combustion and Flame Propagation in Coal Systems: A Review," Sixteenth Symposium (International) on Combustion, p. 353, The Combustion Institute, 1976.
4. Smoot, L. D. and Pratt, D. T., Pulverized Coal Combustion and Gasification, Plenum Press, 1979.
5. Krazinski, J. L., Buckius, R. O., and Krier, H., "A Model for Flame Propagation in Low Volatiles Coal Dust - Air Mixtures," J. Heat Transfer 100, 105 (1978).
6. Kerker, M., The Scattering of Light and Other Electromagnetic Radiation, Academic Press, 1969.
7. Tien, C. L., "Thermal Radiation Properties of Gases," Advances in Heat Transfer 5, 253 (1968).
8. Khalil, E. E. and Truelove, J. S., "Calculation of Radiative Heat Transfer in a Large Gas Fired Furnace," Letters in Heat and Mass Transfer 4, 353 (1977).
9. Grosshandler, W. L. and Sawyer, R. F., "Radiation from a Methanol Furnace," ASME Publication (Aug. 1977).
10. Yuen, W. W. and Tien, C. L., "A Simple Calculation Scheme for the Luminous Flame Emissivity," Sixteenth Symposium (International) on Combustion, p. 1481, The Combustion Institute, 1976.
11. Stull, V. R. and Plass, G. N., "Emissivity of Dispersed Carbon Particles," J. Opt. Soc. America 50, 121 (1960).
12. Hottel, H. C. and Sarofim, A. F., Radiative Transfer, McGraw-Hill, 1967.
13. Palmer, H. B. and Beér, J. M., Combustion Technology, Academic Press, 1974.
14. Laurendeau, M. L., "Heterogeneous Kinetics of Coal Char Gasification and Combustion," Prog. Energy Combust. Sci. 4, 221 (1978).

REFERENCES - continued

15. Smoot, L. D., Horton, M. D., and Williams, G., "Propagation of Laminar Pulverized Coal-Air Flames," Sixteenth Symposium (International) on Combustion, p. 375, The Combustion Institute, 1976.
16. Field, M. A., Gill, D. W., Morgan, D. B., and Hawksley, P. G. W., Combustion of Pulverized Coal (The British Coal Utilization Research Association, Leatherhead, Surrey, England), 1967.
17. Essenhigh, R. H. and Csaba, J., "The Thermal Radiation Theory for Plane Flame Propagation in Coal Dust Clouds," Ninth Symposium (International) on Combustion, p. 111, Academic Press, 1963.
18. Bhaduri, D. and Bandyopadhyay, S., "Combustion in Coal Dust Flames," Combust. Flame 17, 15 (1971).
19. Smoot, L. D., Coates, R. L., and Simonson, J. M., "Mixing and Combustion of Compressible, Particle-Laden Ducted Flows," Paper No. 69-460, AIAA 5th Propulsion Join Specialist Conference, U.S. Air Force Academy, Colorado (June 1969).
20. Soo, S. L., Fluid Dynamics of Multi-Phase Systems, Ginn Blaisdell, 1967.
21. Bird, R. B., Stewart, W. E., and Lightfoot, E. N., Transport Phenomena, Wiley and Sons, 1960.
22. DeGroot, S. R. and Mazur, P., Non-Equilibrium Thermodynamics, North-Holland Publishing Co., 1962.
23. Zucrow, J. M., and Hoffman, J. D., Gas Dynamics, Wiley and Sons, 1976.
24. Taylor, A. E., Advanced Calculus, Ginn and Company, 1955.
25. Siegel, R. and Howell, J. R., Thermal Radiation Heat Transfer, McGraw-Hill, 1972.
26. Chandrasekhar, S., Radiative Transfer, Dover, 1960.
27. Sobolev, V. V., A Treatise on Radiative Transfer, Van Nostrand, 1963.
28. Kourganoff, V., Basic Methods in Transfer Problems, Dover, 1963.
29. Inönü, E. and Zweifel, P. F., Developments in Transport Theory, Academic Press, 1967.

**THE FOLLOWING
PAGES ARE BADLY
SPECKLED DUE TO
BEING POOR
QUALITY
PHOTOCOPIES.**

**THIS IS AS
RECEIVED FROM
CUSTOMER.**

REFERENCES - continued

30. Love, T. J. and Grosh, R. J., "Radiative Heat Transfer in Absorbing, Emitting, and Scattering Media," J. Heat Transfer 87, 161 (1965).
31. Bell, G. I. and Glasstone, S., Nuclear Reactor Theory, Van Nostrand Reinhold, 1970.
32. Odom, J. P., "Neutron Transport with Highly Anisotropic Scattering," Ph.D. Dissertation, Kansas State University, Manhattan, Kansas, 1975.
33. Duderstadt, J. J. and Martin, W. R., Transport Theory, Wiley and Sons, 1979.
34. Foster, P. J. and Howarth, C. R., "Optical Properties of Carbons and Coals in the Infrared," Carbon 6, 719 (1968).
35. Blokh, A. G., Therm. Engng USSR 11, 19 (1964).
36. Dave, J. V., "Subroutines for Computing the Parameters of the Electromagnetic Radiation Scattered by a Sphere," IBM Report 320-3237, Palo Alto Scientific Center, Palo Alto, California (May 1978).
37. Edwards, D. K. and Balakrishnan, A., "Thermal Radiation by Combustion Gases," Int. J. Heat Mass Transfer 16, 25 (1973).
38. Felske, J. D. and Tien, C. L., "A Theoretical Closed Form Expression for the Total Band Absorptance of Infrared-Radiating Gases," Int. J. Heat Mass Transfer 17, 155 (1974).
39. DeRis, J., "Fire Radiation - A Review," Seventeenth Symposium (International) on Combustion, p. 1003, The Combustion Institute, 1978.
40. Case, K. M. and Zweifel, P. F., Linear Transport Theory, Addison-Wesley, 1967.
41. Houf, W. G., "An Assessment of Techniques for Predicting Solar Radiation Transfer in Shallow Water Layers," M.S. Thesis, Purdue University, West Lafayette, Indiana, 1978.
42. Tien, C. L. and Tong, T. W., "Network Representation of Radiative Heat Transfer with Particulate Scattering," Paper 79-42, Western States Section, The Combustion Institute - 1979 Fall Meeting.
43. Howell, J. R. and Perlmutter, M., "Monte Carlo Solution of Thermal Transfer Through Radiant Media Between Gray Walls," J. Heat Transfer 86, 116 (1964).

REFERENCES - continued

44. "Monte Carlo Method," Government Printing Office, National Bureau of Standards Applied Mathematics Series, No. 12, Washington, D. C. (1951).
45. Roux, J. A. and Smith, A. M., "Comparison of Three Techniques for Solving the Radiative Transport Equation," *Thermophysics and Spacecraft Thermal Control* 35, 3 (1974).
46. Hsia, H. M. and Love, T. J., "Radiative Heat Transfer Between Parallel Plates Separated by a Nonisothermal Medium with Anisotropic Scattering," *J. Heat Transfer* 89, 197 (1967).
47. Coddington, E. A. and Levinson, N., Theory of Ordinary Differential Equations, McGraw-Hill, 1955.
48. Miller, K. S., Linear Differential Equations, Norton and Co., Inc., 1963.
49. Davison, B., Neutron Transport Theory, Oxford University Press, 1958.
50. Liou, K. N., "A Numerical Experiment on Chandrasekhar's Discrete Ordinates Method for Radiative Transfer: Application to Cloudy and Hazy Atmospheres," *J. Atmospheric Sciences* 31, 1303 (1973).
51. Cheng, H. S., McDaniel, C. T., and Leonard, A., "A Nodal Integral Transport Method for Calculation of Two-Dimensional Power Distributions in Non-Uniform Lattices," *Proc. Symp. New Developments in Reactor Mathematics and Applications*, CONF-710302, U.S. Atomic Energy Commission 2, 655 (March 1971).
52. Khalil, H., Weiss, Z., and Shultis, J. K., "Coarse-Mesh Equations for the Numerical Solution of the Transport Equation," *Trans. Am. Nucl. Soc.* 33, 324 (1979).
53. Greenspan, H., Kelber, C. N., and Okrent, D., Computing Methods in Reactor Physics, Gordon and Breech, 1968.
54. Hobson, E. W., Theory of Ellipsoidal and Spherical Harmonics, Chelsea Publishing Co., 1955.
55. Chu, C. M. and Churchill, S. W., "Numerical Solution of Problems in Multiple Scattering of Electromagnetic Radiation," *J. Phys. Chem.* 59, 855 (1955).
56. Carlson, B. G., "Solution of the Transport Equation by S_N Approximations," Los Alamos Scientific Laboratory Report LA-1599 (1953).

REFERENCES - continued

57. Hong, K. J., "Anisotropic Transport Techniques and Associated Neutron Transfer Cross Section Evaluation," Ph.D. Dissertation, Kansas State University, Manhattan, Kansas, 1979.
58. Duederstadt, J. J. and Hamilton, L. J., Nuclear Reactor Analysis, Wiley and Sons, 1976.
59. Lamarsh, J. R., Nuclear Reactor Theory, Addison-Wesley, 1972.
60. Ayers, F., Theory and Problems of Matrices, McGraw-Hill, 1962.
61. Seeker, W. R., Samuelson, G. S., Heap, M. P., Hess, C. F., and Trolinger, J. D., "Physical and Chemical Effects Occuring During Thermal Decomposition of Coal Particles," Fifth EPA-FCR Contractor's Workshop, Newport Beach, California (Jan. 1980).
62. Essenhigh, R. H., "Predicted Burning Time of Solid Particles in an Idealized Dust Flame," J. Inst. Fuel 34, 239 (1961).
63. Bajpai, A. C., Mustoe, L. R. and Walker, D., Engineering Mathematics, Wiley and Sons, 1974.
64. Usiskin, C. M. and Sparrow, E. M., "Thermal Radiation Between Parallel Plates Separated by an Absorbing-Emitting Nonisothermal Gas," Int. J. Heat Mass Transfer 1, 28 (1960).
65. Kordylewski, W., "Critical Parameters of Thermal Explosion," Combust. Flame 34, 109 (1979).
66. Carnahan, B., Luther, H. A., and Wilkes, J. O., Applied Numerical Methods, Wiley and Sons, 1969.

8.0 ACKNOWLEDGEMENTS

The author wishes to express his gratitude to his major professors, Dr. J. Kenneth Shultis and Dr. Thomas W. Lester, for their help and guidance throughout the course of this investigation. Thanks are also due to Dr. Zbigniew Weiss, whose advice during the early stages of this study was extremely beneficial, and to Dr. N. Z. Azer for serving on the supervisory committee.

The author also wishes to thank the Kansas State University Department of Nuclear Engineering for providing financial support in the form of a graduate research assistantship. In addition, the friendly attitude of the students and faculty of the department has created an environment very conducive to learning.

Finally, grateful recognition is extended to Ms. Shelly Kemnitz for her skillful typing, and to Mr. Charles O'Brien for his assistance in drafting the figures and graphs.

9.0 APPENDICES

9.1 RATREQ Computer Code

The computer program RATREQ computes the particle temperature, the radiation intensity, and the directionally integrated intensity distributions in a mono-disperse, plane-symmetric suspension of coal and char particles. The numerical discrete ordinates method discussed in Section 4.2.2 of this work is used to solve the gray, LTE form of the radiative transfer equation. This equation is solved simultaneously with the particle energy balance equation, Eq. (5.29), by the iterative procedure described in Section 5.5. Equation (5.34) is used to calculate the particle temperature distribution corresponding to the radiation intensity distribution computed in each iteration. The gas phase temperature profile must be assumed a priori (or may be taken as equal to that of the solid phase). Allowance is made for either isotropic or anisotropic scattering. With isotropic scattering, the scattering matrix $p(\mu_j \rightarrow \mu_i)$ [see Eq. (4.9)] is unity for all pairs of μ_j and μ_i ; while for anisotropic scattering, the scattering matrix is computed by the subroutine PHASE by the numerical integration of the scattering phase function over the azimuthal angle [using Eq. (5.43)]. A detailed description of the input parameters to RATREQ is given with the program listing.

9.2 DIFFEQ Computer Code

The DIFFEQ computer program calculates the particle temperature and the integrated intensity distributions by the simultaneous solution

of the radiation diffusion equation [Eq. (5.45)] and the particle energy balance [Eq. (5.48)]. The iterative solution procedure is discussed in Section 5.6, while the solution of the diffusion equation for a specified thermal emission source term is described in Section 4.4. The subroutine INNER solves the tridiagonal system of equations [Eq. (4.73)] for integrated intensity distribution given the emission source at each mesh point. A direct elimination procedure⁶⁶ is used to solve this system of equations. The recalculation of the particle temperature is performed by the basic iteration technique of Eq. (5.34). Both isotropic and anisotropic scattering can be accommodated by DIFFEQ by varying the average cosine of the scattering angle, $\bar{\mu}^*$. For isotropic scattering, $\bar{\mu}^* = 0$; while for the backward-peaked phase function of Eq. (3.7), $\bar{\mu}^* = -4/9$. Again, the gas temperature distribution may either be specified a priori or may be assumed equal to the solid phase temperature profile. The input parameters to DIFFEQ and further description of the program are given with the program listing.

```

C****
C**** PROGRAM RATREQ
C****
C**** PURPOSE
C****
C**** TO COMPUTE THE RADIATION INTENSITY, THE DIRECTIONALLY INTEGRATED
C**** INTENSITY, AND THE PARTICLE TEMPERATURE DISTRIBUTIONS IN A MONO-
C**** DISPERSE, PLANE-SYMMETRIC PULVERIZED COAL SUSPENSION. THE SUSPEN-
C**** SION GENERATES HEAT BY CHEMICAL REACTION AND IS BOUNDED BY INFINITE,
C**** PARALLEL, FLAT WALLS.
C****
C**** PROCEDURE
C****
C**** THE GRAY, LTE FORM OF THE EQUATION OF TRANSFER IS SOLVED BY A
C**** NUMERICAL DISCRETE ORDINATES METHOD SIMULTANEOUSLY WITH AN ENERGY
C**** BALANCE EQUATION FOR THE PARTICLES. INITIALLY A SOURCE TERM
C**** (SCATTERING+THERMAL EMISSION) IS ASSUMED. THE EQUATION OF TRANSFER
C**** IS SOLVED FOR THE RADIATION INTENSITY BASED ON THIS INITIAL SOURCE
C**** GUESS. THIS INTENSITY IS THEN SUBSTITUTED INTO THE ENERGY BALANCE,
C**** AND THE PARTICLE TEMPERATURE DISTRIBUTION IS COMPUTED BY A BASIC
C**** ITERATION PROCEDURE. THE COMPUTED TEMPERATURE AND INTENSITY
C**** DISTRIBUTIONS CAN BE USED TO UPDATE THE SOURCE TERM, AND THE
C**** ITERATIVE PROCEDURE IS REPEATED UNTIL CONVERGENCE IS ACHIEVED.
C****
C**** INPUT DATA
C****
C**** NSCAT = 1 FOR ISOTROPIC SCATTERING
C****          = 2 FOR ANISOTROPIC SCATTERING
C**** NCOND = 1 IF THE SOLID AND GAS PHASES ARE ASSUMED TO BE IN
C****          THERMAL EQUILIBRIUM
C****          = 2 IF THE GAS PHASE TEMPERATURE DISTRIBUTION IS ASSUMED
C****          A PRIORI
C**** NP = NUMBER OF DISCRETE MESH POINTS
C**** ND = NUMBER OF DIRECTION COSINES (DISCRETE ORDINATES)
C**** U(I) = DIRECTION COSINES, I=1,ND
C**** A(I) = WEIGHTS, I=1,ND
C**** NDZ = QUADRATURE SIZE USED TO PERFORM THE AZIMUTHIAL INTEGRATION
C**** OF THE SCATTERING PHASE FUNCTION (NEEDED ONLY IF NSCAT=2)
C**** UZ(I) = ORDINATES, I=1,NDZ
C**** AZ(I) = WEIGHTS, I=1,NDZ
C**** EPSI = TEMPERATURE CONVERGENCE CRITERION
C**** IIMAX = MAXIMUM NUMBER OF SOURCE TERM ITERATIONS
C**** JIMAX = MAXIMUM NUMBER OF TEMPERATURE ITERATIONS
C**** DP = PARTICLE DIAMETER (CM)
C**** FEXT = EXTINCTION EFFICIENCY
C**** FSCAT = SCATTERING EFFICIENCY
C**** DIM = THICKNESS OF SUSPENSION (CM)
C**** TW1 = WALL TEMPERATURE AT X=0 (K)
C**** TW2 = WALL TEMPERATURE AT X=DIM (K)
C**** RW1 = WALL REFLECTIVITY AT X=0
C**** RW2 = WALL REFLECTIVITY AT X=DIM
C**** RHJD = PARTICLE BULK DENSITY (G/CM**3)
C**** RHJP = DENSITY OF COAL PARTICLES (G/CM**3)
C**** PGAS = OXYGEN (O2) PARTIAL PRESSURE (ATM)
C**** TG(J) = ASSUMED GAS TEMPERATURE PROFILE (NEEDED ONLY IF NCOND=2),
C****          J=1,NP (K)
C**** PHI = 1 FOR C + O2 = CO2
C****          = 2 FOR C + 0.5 O2 = CO

```

```

C**** ENTH1 = SPECIFIC ENERGY RELEASE FOR PHI=1 (CAL/G)
C**** ENTH2 = SPECIFIC ENERGY RELEASE FOR PHI=2 (CAL/G)
C**** EACT = ACTIVATION ENERGY OF HETEROGENEOUS REACTION (CAL/MOL)
C**** EE = PRE-EXPONENTIAL FACTOR (G/(CM**2*S*ATM))
C**** DCO = GAS DIFFUSIVITY AT TG=TSO (CM**2/G)
C**** THCO = GAS THERMAL CONDUCTIVITY AT TG=TSO (W/(CM*K))
C**** FRAC = FACTOR USED TO NORMALIZE THE HEAT GENERATION RATE
C****
C**** OUTPUT QUANTITIES
C****
C**** Q(J,I) = CONVERGED SOURCE DISTRIBUTION, J=1,NP, I=1,ND (W/CM**3)
C**** R(J,I) = INTENSITY DISTRIBUTION, J=1,NP, I=1,ND (W/CM**2)
C**** FLJX(J) = DIRECTIONALLY INTEGRATED INTENSITY DISTRIBUTION, J=1,NP
C**** (W/CM**2)
C**** T(J) = PARTICLE TEMPERATURE DISTRIBUTION, J=1,NP (K)
C**** RLJAD1 = RADIANT ENERGY LEAKAGE AT X=0 (W/CM**2)
C**** RLJAD2 = RADIANT ENERGY LEAKAGE AT X=DIM (W/CM**2)
C**** COND = ENERGY TRANSFERRED BY CONDUCTION TO GAS PHASE (W/CM**2)
C**** GEN = ENERGY GENERATED BY CHEMICAL REACTION (W/CM**2)
C**** DIFF = RLOAD1+RLOAD2+COND-GEN (W/CM**2); THIS QUANTITY EQUALS
C**** ZERO WHEN THE ENERGY BALANCE ON THE ENTIRE PARTICLE
C**** SUSPENSION IS SATISFIED.
C****
C**** SUBROUTINES REQUIRED
C****
C**** PHASE - COMPUTES THE SCATTERING MATRIX IF NSCAT=2
C**** TIC - PERFORMS THE ITERATIVE CALCULATION OF THE PARTICLE TEM-
C**** PERATURE PROFILE IF NCOND=2
C****
IMPLICIT REAL*8 (A-H,O-Z)
DIMENSION Q(51,17),R(51,17)
DIMENSION T(51),TI(51),TS(51),FLUX(51)
DIMENSION X(17),XH(17),XX(17)
COMMON /TC/ XI(51),S(51),TG(51),BND,CND,DND,EPSI2,GEN,COND,JIMAX,
CNP
COMMON /PHA/ P(17,17),U(17),A(17),F(17),UZ(64),AZ(64),ND,NDZ
C****
C**** ASSIGN VALUES OF INPUT VARIABLES
C****
NSCAT=1
NCOND=1
NP=11
ND=8
EPSI=1.00
IIMAX=100
JIMAX=40
DP=50.0-4
DIM=1.02
NACC=1
NI=5
BOL=5.6693D-12
DO 1 K=1,NP
1 TG(K)=2.2D3
READ (5,1000) EE,EACT
READ (5,1000) FEXT,FSCAT
READ (5,1100) TW1,EW1,RW1
READ (5,1100) TW2,EW2,RW2
READ (5,1100) PGAS,RHOD,RHOP

```

```

      READ (5,1100) TSO,DCO,THCO
      READ (5,1200) ENTH1,ENTH2,PHI,FRAC
      READ (5,1000) (U(I),A(I),I=1,ND)
C****
C**** COMPUTE MISCELLANEOUS PARAMETERS
C****
      PI=DARCOS(-1.00)
      NPM=NP-1
      DELX=DIM/NPM
      NOH=ND/2
      NOHP=NOH+1
      SW=6.00/(DP*RHOP)
      SIGA=0.2500*(FEXT-FSCAT)*RHOD*SW
      ALB=FSCAT/FEXT
      TAUD=DIM*SIGA*FEXT/(FEXT-FSCAT)
      DEL=TAUD/NPM
      TREF=EACT/1.98700
      PHIREF=BOL*TREF**4
      EPSI2=EPSI/TREF
      DELH=ENTH1*(2.00/PHI-1.00)+ENTH2*(2.00-2.00/PHI)
      EMIS1=EW1*BOL*TW1**4/PI
      EMIS2=EW2*BOL*TW2**4/PI
C****
C**** PRINT INPUT PARAMETERS
C****
      WRITE (6,6000)
      WRITE (6,3000) DIM,DP
      WRITE (6,3100) FEXT,FSCAT,RHOD,SW,RHOP
      WRITE (6,3200) ALB,TAUD,SIGA
      WRITE (6,3300) TW1,EW1,RW1,TW2,EW2,RW2
      WRITE (6,3350) EE
      WRITE (6,3400) EACT,DELH,PGAS
      WRITE (6,3410) DCO,THCO
      WRITE (6,3500) NP,ND,EPSI,IIMAX,JIMAX
      WRITE (6,3600)
      WRITE (6,3700) (U(I),A(I),I=1,NDH)
      WRITE (6,5000)
      WRITE (6,2000) ENTH1,ENTH2,PHI,DELH,BOL,EPSI2
      WRITE (6,2000) TSO,TREF,PHIREF,EMIS1,EMIS2,FRAC
C****
C**** COMPUTE DIMENSIONLESS CONSTANTS NEEDED FOR TEMPERATURE ITERATION
C****
      BB=2.4001*PHI*DCO*TREF**0.7500/((2.00*TSO)**0.7500*TSO*82.0600*DP)
      CC=6.00*PGAS*DELH**4.18400*RHOD*FRAC/(DP*RHOP)
      DD=1.201*THCO*RHOD*TREF**1.7500/(RHOP*DP**2*(2.00*TSO)**0.7500)
      FF=1.00/(4.00*SIGA*PHIREF)
      WRITE (6,2000) BB,CC,DD,FF
      BND=BB/EE
      CND=FF*CC*BB
      DND=DD*FF
      WRITE (6,2000) BND,CND,DND
      DO 5 K=1,NP
5      TG(K)=TG(K)/TREF
C****
C**** COMPUTE QUANTITIES NEEDED FOR SOURCE ITERATION
C****
      DO 10 I=1,ND
      X(I)=DEL/U(I)

```

```

      XH(I)=0.500*X(I)
10  XX(I)=(1.00-XH(I))/(1.00+XH(I))
C****
C**** COMPUTE EXACT KERNEL FORM OF THE SCATTERING PHASE FUNCTION
C****
      IF (NSCAT.EQ.1) GO TO 15
      NDZ=16
      READ (5,1000) (UZ(I),AZ(I),I=1,NDZ)
      CALL PHASE
      GO TO 30
15  DO 20 I=1,ND
      DO 20 J=1,ND
      20  P(I,J)=1.00
      WRITE (6,2300) ((P(I,J),J=1,ND),I=1,ND)
C****
C**** GUESS AN INITIAL SOURCE DISTRIBUTION AND LEFT BOUNDARY INTENSITY
C****
      30  DO 40 K=2,NP
      DO 40 I=1,ND
      40  Q(K,I)=7.501
      DO 50 I=NDHP,ND
      50  R(1,I)=0.00
      IACC=0
      II=1
C****
C**** FORWARD SWEEP
C****
      60  SUM=0.00
      DO 70 I=NDHP,ND
      70  SUM=SUM+A(I)*U(I)*R(1,I)
      CURR1=DABS(SUM)
      DO 80 I=1,NDH
      80  R(1,I)=EMIS1+2.00*RW1*CURR1
      DO 90 K=2,NP
      DO 90 I=1,NDH
      90  R(K,I)=R(K-1,I)*XX(I)+Q(K,I)*X(I)/(1.00+XH(I))
C****
C**** BACKWARD SWEEP
C****
      SUM=0.00
      DO 100 I=1,NDH
      100 SUM=SUM+A(I)*U(I)*R(NP,I)
      CURR2=DABS(SUM)
      DO 110 I=NDHP,ND
      110 R(NP,I)=EMIS2+2.00*RW2*CURR2
      DO 120 K=1,NPM
      DO 120 I=NDHP,ND
      120 R(NP-K,I)=R(NP-K+1,I)/XX(I)-Q(NP-K+1,I)*X(I)/(1.00-XH(I))
C****
C**** COMPUTE THE TEMPERATURE DISTRIBUTION
C****
      WRITE (6,1000) IACC
      WRITE (6,2200) II
      GEN=0.00
      COND=0.00
      DO 140 K=1,NP
      SUM=0.00
      DO 130 I=1,ND

```

```

130 SUM=SUM+A(I)*R(K,I)
   S(K)=2.00*PI*SUM/(4.00*PHIREF)
   IF (II.EQ.1) XI(K)=S(K)**0.2500
140 CONTINUE
   GEN=0.00
   COND=0.00
   IF (INCOND.EQ.2) GO TO 132
C**** THERMAL EQUILIBRIUM CASE
   DO 131 K=1,NP
   DO 135 JI=1,JIMAX
     AND=XI(K)
     Z1=(XI(K)+AND)**0.7500
     Z2=DEXP(1.00/XI(K))
     FAC1=COND/(1.00/Z1+BND*Z2)
     FAC2=OND*Z1*(XI(K)-AND)
     XXI=(S(K)+FAC1-FAC2)**0.2500
     IF (DABS(XXI-XI(K)).LE.EPSI2) GO TO 138
     XI(K)=XXI
135 CONTINUE
138 T(K)=XXI*TREF
   Z=1.00
   IF ((K.EQ.1).OR.(K.EQ.NP)) Z=0.500
   GEN=GEN+Z*FAC1
   COND=COND+Z*FAC2
131 CONTINUE
   GO TO 134
C**** INTER-SPECIES CONDUCTION CASE
132 CALL TIC
   DO 133 K=1,NP
     T(K)=XI(K)*TREF
133 CONTINUE
134 DO 136 K=1,NP
     TS(K)=T(K)
136 CONTINUE
   WRITE (6,2300) (T(K),K=1,NP)
C****
C**** COMPUTE RADIANT LEAKAGE, CONDUCTION LOSSES, AND TOTAL HEAT GENERATION
C****
   GEN=GEN*DELX/FF
   COND=COND*DELX/FF
   RLOAD1=2.00*PI*(1.00-RW1)*CURR1-PI*EMIS1
   RLOAD2=2.00*PI*(1.00-RW2)*CURR2-PI*EMIS2
   SUM=RLOAD1+RLOAD2
   DIFF=SUM+COND-GEN
   WRITE (6,2000) SUM,COND,GEN,DIFF
   IF (II.EQ.1) GO TO 160
C****
C**** CHECK FOR CONVERGENCE OF THE TEMPERATURE DISTRIBUTION
C****
   DO 150 K=1,NP
     IF (DABS(T(K)-TI(K)).GT.EPSI1) GO TO 155
150 CONTINUE
   GO TO 200
C****
C**** CONVERGENCE ACCELERATION OPTION
C****
155 IF (INACC.EQ.1) GO TO 160
   ACCPAR=DFLGAT(IIMAX)/II

```

```

      DO 167 K=1,NP
      IF (T(K).LE.TI(K)) GO TO 164
167  CONTINUE
      IACC=IACC+1
      IF (IACC.EQ.NI) GO TO 169
      GO TO 160
164  DO 166 K=1,NP
      IF (T(K).GE.TI(K)) GO TO 165
166  CONTINUE
      IACC=IACC-1
      IF (IACC.EQ.-NI) GO TO 169
      GO TO 160
169  DO 168 K=1,NP
      TS(K)=TI(K)+(T(K)-TI(K))*ACCPAR
168  CONTINUE
165  IACC=0
C****
C**** RECOMPUTE THE SOURCE DISTRIBUTION
C****
160  II=II+1
      IF (II.GT.IIMAX) GO TO 200
      DO 180 K=2,NP
      TEMP=0.500*(TS(K)+TS(K-1))
      QBB=(1.00-ALB)*BOL*TEMP**4/PI
      DO 180 I=1,ND
      SUM=0.00
      DO 170 J=1,ND
      RMID=0.500*(R(K,J)+R(K-1,J))
170  SUM=SUM+A(J)*RMID*P(J,I)
      QSCAT=ALB*SUM/2.00
180  Q(K,I)=QSCAT+QBB
      DO 190 K=1,NP
190  TI(K)=T(K)
      GO TO 60
C****
C**** CALCULATE RESULTS FOR THE CONVERGED TEMPERATURE PROFILE
C****
200  WRITE (6,2200) II
      DO 220 K=1,NP
      SUM=0.00
      DO 210 I=1,ND
210  SUM=SUM+A(I)*R(K,I)
220  FLUX(K)=SUM*2.00*PI
C****
C**** PRINT RESULTS
C****
      WRITE (6,2300) (Q(K,I),I=1,ND),K=2,NP)
      WRITE (6,5000)
      WRITE (6,2300) ((R(K,I),I=1,ND),K=1,NP)
      WRITE (6,5000)
      WRITE (6,2400) (T(K),K=1,NP)
      WRITE (6,5000)
      WRITE (6,2400) (FLUX(K),K=1,NP)
      WRITE (6,5000)
      WRITE (6,2000) RLOAD1,KLOAD2,COND,GEN,DIFF
C****
1000 FORMAT (2G20.12)
1100 FORMAT (3G20.12)

```

```

1200 FORMAT (4G20.12)
2000 FORMAT (6(3X,E12.5))
2200 FORMAT (3X,'ITERATION NO.',I3)
2300 FORMAT (8(1X,E14.7))
2400 FORMAT (5(3X,E12.5))
3000 FORMAT (T10,'SYSTEM SIZE =',E12.5,' CM',/,T10,'PARTICLE DIAMETER =
C',E12.5,' CM',////)
3100 FORMAT (T10,'EXTINCTION EFFICIENCY =',E12.5,/,T10,'SCATTERING EFFI
CENCY =',E12.5,/,T10,'PARTICLE MASS LOADING =',E12.5,' G/CM**3',/
C,T10,'SPECIFIC SURFACE OF PARTICLES =',E12.5,' CM**2/G',/,T10,'PAR
TICLE DENSITY =',E12.5,' G/CM**3',////)
3200 FORMAT (T10,'SINGLE SCATTER ALBEDO =',F7.4,/,T10,'OPTICAL THICKNES
S OF SYSTEM (MFP) =',F8.4,/,T10,'ABSORPTION CROSS SECTION (1/CM) =
C',E12.5,////)
3300 FORMAT (T10,'LEFT WALL:',6X,'TEMP. =',F8.2,' K',5X,'EMISSIVITY =',
CF5.2,5X,'REFLECTIVITY =',F5.2,/,T10,'RIGHT WALL:',5X,'TEMP. =',F8.
C2,' K',5X,'EMISSIVITY =',F5.2,5X,'REFLECTIVITY =',F5.2,////)
3350 FORMAT (T10,'PRE-EXPONENTIAL FACTOR =',E12.5,' G/(CM**2*S*ATM)')
3400 FORMAT (T10,'ACTIVATION ENERGY =',E12.5,' CAL/MOL' ,/,T10,'SPECIF
IC ENERGY RELEASE =',E12.5,' CAL/G',/,T10,'GAS PRESSURE =',F5.2,'
C ATM',////)
3410 FORMAT (T10,'GAS PROPERTIES AT 1600 K:',/,T20,'BINARY DIFFUSION C
COEFF. (O2 IN N2) =',F5.2,' CM**2/S',/,T20,'THERMAL COND. =',E12.5,
C' W/CM*K',////)
3500 FORMAT (T10,'NUMERICAL SOLUTION PARAMETERS:',/,T20,'NO. OF MESH P
POINTS =',I3,/,T20,'NO. OF DISCRETE DIRECTION COSINES =',I3,/,T20,'
CTEMP. CONVERGENCE CRITERION (K) =',E12.5,/,T20,'MAXIMUM NO. OF OUT
ER ITERATIONS =',I4,/,T20,'MAXIMUM NO. OF TEMP. ITERATIONS =',I3,/
C////)
3600 FORMAT (T10,'ANGULAR QUADRATURE SET USED:',/,T25,'ORDINATE',T50,'
CWEIGHT',/)
3700 FORMAT (T21,E14.7,T46,E14.7)
5000 FORMAT (////)
6000 FORMAT ('1')
C****
      STOP
      END

```



```

SUBROUTINE TIC
C**** SUBROUTINE TO COMPUTE THE PARTICLE TEMPERATURE DISTRIBUTION IF THE
C**** PARTICLE AND GAS PHASES ARE NOT IN THERMAL EQUILIBRIUM. THE NEWTON
C**** METHOD IS USED TO COMPUTE THE PARTICLE TEMPERATURE AT EACH DISCRETE
C**** MESH POINT
C****
      IMPLICIT REAL*8 (A-H,O-Z)
      COMMON /TC/ XI(51),S(51),TG(51),BND,CND,DND,EPSI2,GEN,COND,JIMAX,
      CNP
      DO 10 K=1,NP
      DO 20 JI=1,JIMAX
      A1=XI(K)**4
      AND=TG(K)
      A2=XI(K)+AND
      A3=XI(K)-AND
      A4=DEXP(1.00/XI(K))
      A5=DND*A2**0.7500*A3
      A6=BND*A4+1.00/A2**0.7500
      A7=CND/A6
      Z1=4.00*XI(K)**3
      Z2=DND*(A2**0.7500+0.7500*A3/A2**0.2500)
      Z3=(0.7500/A2**1.7500+BND*A4/A1**0.500)*A7/A6
      XXI=XI(K)-(A1+A5-A7-S(K))/(Z1+Z2-Z3)
      IF (0ABS(XXI-XI(K)).LE.EPSI2) GO TO 15
      XI(K)=XXI
20 CONTINUE
15 XI(K)=XXI
      Z=1.00
      IF ((K.EQ.1).OR.(K.EQ.NP)) Z=0.500
      GEN=GEN+Z*A7
      COND=COND+Z*A5
10 CONTINUE
      RETURN
      END

```

```

      SUBROUTINE PHASE
C**** SUBROUTINE TO COMPUTE THE EXACT KERNEL FORM, P(U(I)-->U(J)) OF THE SCAT-
C**** TERING PHASE FUNCTION OF A DIFFUSELY-REFLECTING OPAQUE SPHERE,
C****      P(THETA) = (8/(3*PI))*(SIN(THETA)-THETA*COS(THETA))
C**** WHERE THETA IS THE SCATTERING ANGLE.
C****
      IMPLICIT REAL*8 (A-H,O-Z)
      COMMON /PHA/ P(17,17),U(17),A(17),F(17),UZ(64),AZ(64),ND,NOZ
      NDH=ND/2
      NDHP=NDH+1
      PI=DARCOS(-1.00)
      DO 60 I=1,ND
60    F(I)=DSQRT(1.00-U(I)**2)
      DO 90 I=1,NDH
      DO 90 J=1,ND
      UFAC=U(I)*U(J)
      FFAC=F(I)*F(J)
C**** INTEGRATE OVER THE AZIMUTHAL ANGLE
      SUM=0.00
      DO 80 L=1,NOZ
      CON1=UFAC+FFAC*DCOS(PI*(DARCOS(UZ(L))+1.00))
      CON2=DARCOS(CON1)
80    SUM=SUM+(DSIN(CON2)-CON1*CON2)*AZ(L)
      P(I,J)=4.00*SUM/(3.00*PI)
90  CONTINUE
C**** UTILIZE SYMMETRY OF THE SCATTERING FUNCTION
      DO 50 I=NOHP,ND
      DO 50 J=1,ND
50    P(I,J)=P(ND+1-J,ND+1-I)
      DO 70 J=2,ND
      JM=J-1
      DO 70 I=1,JM
70    P(J,I)=P(I,J)
C**** RENORMALIZE THE SCATTERING MATRIX
      DO 40 I=1,ND
      SUM=0.00
      DO 30 J=1,ND
30    SUM=SUM+A(J)*P(I,J)
40    F(I)=SUM
      DO 20 I=1,ND
      DO 20 J=1,ND
20    P(I,J)=P(I,J)*2.00/F(I)
      WRITE (6,300) (F(I),I=1,ND)
      WRITE (6,200) ((P(I,J),J=1,ND),I=1,ND)
200  FORMAT (4(6X,E14.7))
300  FORMAT (6(2X,E12.5))
      RETURN
      END

```

```

C****
C**** PROGRAM DIFFEQ
C****
C**** PURPOSE
C****
C****     TO COMPUTE THE DIRECTIONALLY INTEGRATED INTENSITY AND THE PARTICLE
C****     TEMPERATURE DISTRIBUTIONS IN A MONO-DISPERSE, PLANE-SYMMETRIC
C****     PULVERIZED COAL SUSPENSION. THE SUSPENSION GENERATES HEAT BY
C****     CHEMICAL REACTION AND IS BOUNDED BY INFINITE, PARALLEL, FLAT WALLS.
C****
C**** PROCEDURE
C****
C****     THE GRAY, LTE FORM OF THE DIFFUSION APPROXIMATION OF THE EQUATION
C****     OF TRANSFER IS SOLVED SIMULTANEOUSLY WITH AN ENERGY BALANCE ON THE
C****     PARTICLES. INITIALLY, A THERMAL EMISSION SOURCE TERM IS ASSUMED.
C****     THE DIFFUSION EQUATION IS SOLVED FOR THE INTEGRATED INTENSITY BASED
C****     ON THIS INITIAL SOURCE GUESS. THIS INTEGRATED INTENSITY IS THEN
C****     SUBSTITUTED INTO THE ENERGY BALANCE, AND THE PARTICLE TEMPERATURE
C****     DISTRIBUTION IS COMPUTED BY A BASIC ITERATION PROCEDURE. THE COM-
C****     PUTED TEMPERATURE PROFILE CAN THEN BE USED TO UPDATE THE THERMAL
C****     EMISSION SOURCE DISTRIBUTION, AND THE ITERATIVE PROCEDURE IS REPEATED
C****     UNTIL CONVERGENCE IS OBTAINED.
C****
C**** INPUT DATA
C****
C****     NCOND = 1  IF THE SOLID AND GAS PHASES ARE ASSUMED TO BE IN
C****                THERMAL EQUILIBRIUM
C****     = 2  IF THE GAS PHASE TEMPERATURE DISTRIBUTION IS ASSUMED
C****           A PRIORI
C****     N      =  NUMBER OF DISCRETE MESH POINTS
C****     EPSI   =  TEMPERATURE CONVERGENCE CRITERION
C****     IIMAX  =  MAXIMUM NUMBER OF SOURCE TERM ITERATIONS
C****     JIMAX  =  MAXIMUM NUMBER OF TEMPERATURE ITERATIONS
C****     UBAR   =  AVERAGE COSINE OF SCATTERING ANGLE
C****     DP     =  PARTICLE DIAMETER (CM)
C****     FEXT   =  EXTINCTION EFFICIENCY
C****     FSCAT  =  SCATTERING EFFICIENCY
C****     DIM    =  THICKNESS OF SUSPENSION (CM)
C****     TW1    =  WALL TEMPERATURE AT X=0 (K)
C****     TW2    =  WALL TEMPERATURE AT X=DIM (K)
C****     RW1    =  WALL REFLECTIVITY AT X=0
C****     RW2    =  WALL REFLECTIVITY AT X=DIM
C****     RHOD   =  PARTICLE BULK DENSITY (G/CM**3)
C****     RHDP   =  DENSITY OF COAL PARTICLES (G/CM**3)
C****     PGAS   =  OXYGEN (O2) PARTIAL PRESSURE (ATM)
C****     TG(I)  =  ASSUMED GAS TEMPERATURE PROFILE (NEEDED ONLY IF NCOND=2),
C****                I=1,N (K)
C****     PHI    =  1  FOR C + O2 = CO2
C****                =  2  FOR C + 0.5 O2 = CO
C****     ENTH1  =  SPECIFIC ENERGY RELEASE FOR PHI=1 (CAL/G)
C****     ENTH2  =  SPECIFIC ENERGY RELEASE FOR PHI=2 (CAL/G)
C****     EACT   =  ACTIVATION ENERGY OF HETEROGENECUS REACTION (CAL/MOL)
C****     EE     =  PRE-EXPONENTIAL FACTOR (G/(CM**2*S*ATM))
C****     DCO    =  GAS DIFFUSIVITY AT TG=TSO (CM**2/G)
C****     THLD   =  GAS THERMAL CONDUCTIVITY AT TG=TSO (W/(CM*K))
C****     FRAC   =  FACTOR USED TO NORMALIZE THE HEAT GENERATION RATE
C****
C**** OUTPUT QUANTITIES

```

```

C****
C****      Q(I)      =  CONVERGED SOURCE DISTRIBUTION, I=1,N (W/CM**3)
C****      FLUX(I)   =  INTEGRATED INTENSITY DISTRIBUTION, I=1,N (W/CM**2)
C****      T(I)      =  PARTICLE TEMPERATURE DISTRIBUTION, I=1,N (K)
C****      RLOAD1    =  RADIANT ENERGY LEAKAGE AT X=0 (W/CM**2)
C****      RLOAD2    =  RADIANT ENERGY LEAKAGE AT X=DIM (W/CM**2)
C****      COND      =  ENERGY TRANSFERRED BY CONDUCTION TO GAS PHASE (W/CM**2)
C****      GEN       =  ENERGY GENERATED BY CHEMICAL REACTION (W/CM**2)
C****      DIFF      =  RLOAD1+RLOAD2+COND-GEN (W/CM**2); THIS QUANTITY EQUALS
C****                  ZERO WHEN THE ENERGY BALANCE ON THE ENTIRE PARTICLE
C****                  SUSPENSION IS SATISFIED.
C****
C**** SUBROUTINES REQUIRED
C****
C****      INNER - COMPUTES THE INTEGRATED INTENSITY DISTRIBUTION GIVEN THE
C****              THERMAL EMISSION SOURCE DISTRIBUTION
C****      TIC   - PERFORMS THE ITERATIVE CALCULATION OF THE PARTICLE TEM-
C****              PERATURE PROFILE IF NCOND=2
C****
      IMPLICIT REAL*8 (A-H,O-Z)
      DIMENSION T(51),TI(51),TS(51)
      COMMON /TC/ XI(51),S(51),TG(51),BND,CND,DND,EPSI2,GEN,COND,HMAX,
      CJIMAX
      COMMON /INN/ Q(51),FLUX(51),H(51),ALPHA(51),DE,D1,DN,DD
      COMMON /INNTC/ N
C****
C**** ASSIGN VALUES OF INPUT VARIABLES
C****
      NCOND=1
      EPSI=1.00
      DP=50.0-4
      DIM=1.02
      N=11
      IIMAX=50
      JIMAX=40
      UBAR=0.00
      BOL=5.66930-12
      NACC=2
      NI=4
      DO 1 K=1,N
1  TG(K)=2.203
      READ (5,1000) EE,EACT
      READ (5,1000) FEXT,FSCAT
      READ (5,1100) TW1,EW1,RW1
      READ (5,1100) TW2,EW2,RW2
      READ (5,1100) PGAS,RHOD,RHOP
      READ (5,1100) TSO,DCO,THCO
      READ (5,1200) ENTH1,ENTH2,PHI,FRAC
C****
C**** COMPUTE MISCELLANEOUS PARAMETERS
C****
      PI=DARCOS(-1.00)
      M=N-1
      DELX=DIM/M
      SW=6.00/(DP*RHOP)
      FAB=FEXT-FSCAT
      SIGA=0.2500*FAB*RHOD*SW
      SIGS=SIGA*FSCAT/FAB

```

```

      SIGT=SIGA*FEXT/FAB
      D=1.00/(3.00*(SIGT-SIGS*UBAR))
      TREF=EACT/1.98700
      PHIREF=BOL*TREF**4
      DELH=ENTH1*(2.00/PHI-1.00)+ENTH2*(2.00-2.00/PHI)
      EPSI2=EPSI/TREF
      EMIS1=EW1*BOL*TW1**4/PI
      EMIS2=EW2*BOL*TW2**4/PI
C****
C**** PRINT INPUT PARAMETERS
C****
      WRITE (6,6000)
      WRITE (6,3000) DIM,DP
      WRITE (6,3100) FEXT,FSCAT,RHOD,SW,RHOP
      WRITE (6,3200) SIGA,SIGS,SIGT,D
      WRITE (6,3300) TW1,EW1,RW1,TW2,EW2,RW2
      WRITE (6,3350) EE
      WRITE (6,3400) EACT,DELH,PGAS
      WRITE (6,3410) DCO,THCO
      WRITE (6,3500) N,EPSI,IIMAX,JIMAX
      WRITE (6,2000) ENTH1,ENTH2,PHI,DELH,BOL,EPSI2
      WRITE (6,2000) TSO,TREF,PHIREF,EMIS1,EMIS2,FRAC
      WRITE (6,5000)
C****
C**** COMPUTE DIMENSIONLESS CONSTANTS NEEDED FOR TEMPERATURE ITRATION
C****
      BB=2.4001*PHI*DCO*TREF**0.7500/((2.00*TSO)**0.7500*TSO**82.0600*DP)
      CC=6.00*PGAS*DELH**4.18400*RHOD*FRAC/(DP*RHOP)
      DD=1.201*THCO*RHOD*TREF**1.7500/(RHOP*DP**2*(2.00*TSO)**0.7500)
      FF=1.00/(4.00*SIGA*PHIREF)
      WRITE (6,2000) BB,CC,DD,FF
      BND=BB/EE
      CND=FF*CC*BB
      DND=DD*FF
      WRITE (6,2000) BND,CND,DND
      WRITE (6,5000)
      DO 5 K=1,N
5      TG(K)=TG(K)/TREF
C****
C**** COMPUTE ELEMENTS OF TRIDIAGONAL MATRIX
C****
      A1=SIGA*DELX**2/D
      A2=DELX/(2.00*D)
      A3=(1.00-RW1)/(1.00+RW1)
      A4=(1.00-RW2)/(1.00+RW2)
      WRITE (6,2000) A1,A2,A3,A4
      FAC1=A2*A3
      FAC2=A2*A4
      FAC3=2.00*PI*EMIS1*DELX/(D*(1.00+PW1))
      FAC4=2.00*PI*EMIS2*DELX/(D*(1.00+RW2))
      WRITE (6,2000) FAC1,FAC2,FAC3,FAC4
      OD=-1.00
      DE=2.00+A1
      DI=1.00+FAC1+0.500*A1
      DN=1.00+FAC2+0.500*A1
      WRITE (6,2000) OD,DE,DI,DN
      WRITE (6,5000)
C****

```

```

C**** SPECIFY INITIAL SOURCE GUESS
C****
      DO 10 K=1,N
10  Q(K)=1.00
      IACC=0
      II=1
C****
C**** BEGIN THE ITERATIVE SOLUTION
C****
      30 Q(1)=0.500*DELX**2*Q(1)+FAC3
      Q(N)=0.500*DELX**2*Q(N)+FAC4
      DO 50 K=2,M
      Q(K)=DELX**2*Q(K)
      50 CONTINUE
      CALL INNER
C****
C**** COMPUTE THE TEMPERATURE DISTRIBUTION
C****
      WRITE (6,5000)
      WRITE (6,1000) IACC
      WRITE (6,2200) II
      WRITE (6,2300) (Q(K),K=1,N)
      DO 60 K=1,N
      S(K)=FLUX(K)/(4.00*PHIREF)
      IF (II.EQ.1) XI(K)=S(K)**0.2500
      60 CONTINUE
      GEN=0.00
      COND=0.00
      IF (NCOND.EQ.2) GO TO 101
C**** THERMAL EQUILIBRIUM CASE
      DO 100 K=1,N
      DO 70 J1=1,J1MAX
      AND=XI(K)
      Z1=(XI(K)+AND)**0.7500
      Z2=DEXP(1.00/XI(K))
      FAC=CND/(1.00/Z1+BND*Z2)
      FAC2=DND*Z1*(XI(K)-AND)
      XXI=(S(K)+FAC-FAC2)**0.2500
      IF (DABS(XXI-XI(K)).LE.EPSI2) GO TO 80
      XI(K)=XXI
      70 CONTINUE
      80 T(K)=XXI*TREF
      IF (K.EQ.(N/2+1)) HMAX=FAC-FAC2
      Z=1.00
      IF ((K.EQ.1).OR.(K.EQ.N)) Z=0.500
      GEN=GEN+Z*FAC
      COND=COND+Z*FAC2
      100 CONTINUE
      GO TO 103
C**** INTER-SPECIES CONDUCTION CASE
      101 CALL TIC
      DO 102 K=1,N
      T(K)=XI(K)*TREF
      102 CONTINUE
      103 DO 104 K=1,N
      TS(K)=T(K)
      104 CONTINUE
      WRITE (6,2300) (T(K),K=1,N)

```

```

C****
C**** COMPUTE RADIANT LEAKAGE, CONDUCTION LOSSES, AND TOTAL HEAT GENERATION
C****
      GEN=GEN*DELX/FF
      COND=CJND*DELX/FF
      RLOAD1=(0.25D0*FLUX(1)*(1.00+A3)-0.50D0*FAC3/DELX)*(1.00-RW1)
      C-EMIS1*PI
      RLOAD2=(0.2500*FLUX(N)*(1.00+A4)-0.50D0*FAC4/DELX)*(1.00-RW2)
      C-EMIS2*PI
      SUM=RLOAD1+RLOAD2
      DIFF=SUM+COND-GEN
      WRITE (6,2000) SUM,COND,GEN,DIFF

C****
C**** CHECK FOR CONVERGENCE OF THE TEMPERATURE DISTRIBUTION
C****
      IF (II.EQ.1) GO TO 110
      DO 150 K=1,N
      IF (DABS(T(K)-TI(K)).GT.EPS1) GO TO 115
150  CONTINUE
      GO TO 200

C****
C**** CONVERGENCE ACCELERATION OPTION
C****
115  IF (INACC.EQ.1) GO TO 110
      ACCPAR=DFLOAT(IIMAX)/II
      DO 120 K=1,N
      IF (T(K).LE.TI(K)) GO TO 135
120  CCNTINUE
      IACC=IACC+1
      IF (IACC.EQ.NI) GO TO 125
      GO TO 110
135  DO 140 K=1,N
      IF (T(K).GE.TI(K)) GO TO 145
140  CCNTINUE
      IACC=IACC-1
      IF (IACC.EQ.-NI) GO TO 125
      GO TO 110
125  DO 130 K=1,N
      TS(K)=TI(K)+(T(K)-TI(K))*ACCPAR
130  CONTINUE
145  IACL=0

C****
C**** RECOMPUTE THE SOURCE DISTRIBUTION
C****
110  II=II+1
      IF (II.GT.IIMAX) GO TO 200
      DO 170 K=1,N
      Q(K)=4.00*SIGA*BOL*TS(K)**4/D
      TI(K)=T(K)
170  CONTINUE
      GO TO 30

C****
C**** CALCULATE AND PRINT RESULTS
C****
200  WRITE (6,2200) II
      WRITE (6,2300) (Q(K),K=1,N)
      WRITE (6,5000)
      WRITE (6,2300) (FLUX(K),K=1,N)

```

```

      WRITE (6,5000)
      WRITE (6,2300) (T(K),K=1,N)
      HMAX=HMAX*UP*RHOP/(6.00*RHOD*FF)
      WRITE (6,2000) HMAX
      WRITE (6,2000) RLOAD1,RLOAD2,CUND,GEN,DIFF
C****
1000 FORMAT (2G20.12)
1100 FORMAT (3G20.12)
1200 FORMAT (4G20.12)
2000 FORMAT (6(3X,E12.5))
2200 FORMAT (3X,'ITERATION NO.',I3)
2300 FORMAT (8(1X,E14.7))
3000 FORMAT (T10,'SYSTEM SIZE =',E12.5,' CM',/,T10,'PARTICLE DIAMETER =
      C',E12.5,' CM',////)
3100 FORMAT (T10,'EXTINCTION EFFICIENCY =',E12.5,/,T10,'SCATTERING EFFI
      CIENCY =',F12.5,/,T10,'PARTICLE MASS LOADING =',E12.5,' G/CM**3',/
      C,T10,'SPECIFIC SURFACE OF PARTICLES =',E12.5,' CM**2/G',/,T10,'PAR
      TICLE DENSITY =',E12.5,' G/CM**3',////)
3200 FORMAT (T10,'CROSS SECTIONS (1/CM):',/,T16,'ABSORPTION =',E12.5,/,
      CT16,'SCATTERING =',E12.5,/,T16,'EXTINCTION =',E12.5,/,T10,'DIFFUS
      CION COEFFICIENT =',E12.5,' CM',////)
3300 FORMAT (T10,'LEFT WALL:',6X,'TEMP. =',F8.2,' K',5X,'EMISSIVITY =',
      CF5.2,5X,'REFLECTIVITY =',F5.2,/,T10,'RIGHT WALL:',5X,'TEMP. =',F8.
      C2,' K',5X,'EMISSIVITY =',F5.2,5X,'REFLECTIVITY =',F5.2,////)
3350 FORMAT (T10,'PRE-EXPONENTIAL FACTOR =',E12.5,' G/(CM**2*S*ATM)')
3400 FORMAT (T10,'ACTIVATION ENERGY =',E12.5,' CAL/MOL' ,/,T10,'SPECIF
      IC ENERGY RELEASE =',E12.5,' CAL/G',/,T10,'GAS PRESSURE =',F5.2,'
      C ATM',////)
3410 FORMAT (T10,'GAS PROPERTIES AT 1600 K:',/,T20,'BINARY DIFFUSION C
      COEFF. (O2 IN N2) =',F5.2,' CM**2/S',/,T20,'THERMAL CUND. =',E12.5,
      C' W/CM*K',////)
3500 FORMAT (T10,'NUMERICAL SOLUTION PARAMETERS:',/,T20,'NUMBER OF MES
      CH POINTS =',I3,/,T20,'TEMP. CONVERGENCE CRITERION (K) =',E12.5,/,T
      C20,'MAXIMUM NUMBER OF OUTER ITERATIONS =',I4,/,T20,'MAXIMUM NUMBER
      C OF TEMP. ITERATIONS =',I3,////)
5000 FORMAT (////)
6000 FORMAT ('1')
C****
      STOP
      END

```



```

SUBROUTINE INNER
C**** SUBROUTINE TO COMPUTE THE INTEGRATED INTENSITY DISTRIBUTION GIVEN THE
C**** THERMAL EMISSION SOURCE. A DIRECT ELIMINATION PROCEEDURE IS USED TO SOLVE
C**** THE SET OF TRIDIAGONAL EQUATIONS
C****
      IMPLICIT REAL*8 (A-H,O-Z)
      COMMON /INN/ Q(51),FLUX(51),H(51),ALPHA(51),DE,D1,DN,OD
      COMMON /INNTC/ N
      H(1)=OD/D1
      M=N-1
      DO 60 I=2,M
60  H(I)=OD/(DE-OD*H(I-1))
      ALPHA(1)=Q(1)/D1
      DO 55 I=2,M
55  ALPHA(I)=(Q(I)-OD*ALPHA(I-1))/(DE-OD*H(I-1))
      FLUX(N)=(Q(N)-OD*ALPHA(M))/(DN-OD*H(M))
      DO 50 I=1,M
50  FLUX(N-I)=-FLUX(N-I+1)*H(N-I)+ALPHA(N-I)
      RETURN
      END

```

```

SUBROUTINE TIC
C**** SUBROUTINE TO COMPUTE THE PARTICLE TEMPERATURE DISTRIBUTION IF THE
C**** PARTICLE AND GAS PHASES ARE NOT IN THERMAL EQUILIBRIUM. THE NEWTON
C**** METHOD IS USED TO COMPUTE THE PARTICLE TEMPERATURE AT EACH DISCRETE
C**** MESH POINT
C****
      IMPLICIT REAL*8 (A-H,O-Z)
      COMMON /TC/ XI(51),S(51),TG(51),BND,CND,DND,EPSI2,GEN,COND,HMAX,
CJIMAX
      COMMON /INNTC/ N
      DO 10 K=1,N
      DO 20 JI=1,JIMAX
      AND=TG(K)
      A1=XI(K)**4
      A2=XI(K)+AND
      A3=XI(K)-AND
      A4=DEXP(1.00/XI(K))
      A5=DND*A2**0.7500*A3
      A6=BND*A4+1.00/A2**0.7500
      A7=CND/A6
      Z1=4.00*XI(K)**3
      Z2=DND*(A2**0.7500+0.7500*A3/A2**0.2500)
      Z3=(0.7500/A2**1.7500+BND*A4/A1**0.500)*A7/A6
      XXI=XI(K)-(A1+A5-A7-S(K))/(Z1+Z2-Z3)
      IF (DABS(XXI-XI(K)).LE.EPSI2) GO TO 15
      XI(K)=XXI
20 CONTINUE
15 XI(K)=XXI
      IF (K.EQ.(N/2+1)) HMAX=A7-A5
      Z=1.00
      IF ((K.EQ.1).OR.(K.EQ.N)) Z=0.500
      GEN=GEN+Z*A7
      COND=COND+Z*A5
10 CONTINUE
      RETURN
      END

```

RADIATIVE TRANSFER IN PULVERIZED COAL SUSPENSIONS

by

HUSSEIN KHALIL

B.S., Kansas State University, 1978

AN ABSTRACT OF A MASTER'S THESIS

submitted in partial fulfillment of the
requirements for the degree

MASTER OF SCIENCE

Department of Nuclear Engineering

KANSAS STATE UNIVERSITY
Manhattan, Kansas

1980

ABSTRACT

A detailed description of the radiative transfer problem in pulverized coal combustion is presented, with emphasis on the modeling of coal dust-gas mixtures, the solution of the radiative transfer equation, and discussion of the available radiation properties of the materials in pulverized coal systems. In addition, a simple coal suspension model is developed to compute the temperature and radiation intensity distributions in reacting coal dust clouds. A diffusion limited, Arrhenius expression is used to describe the rate of heat generation due to the heterogeneous reaction of the coal particles with the gases in which they are dispersed. The particle suspension is bounded by infinite, parallel, flat walls and is assumed to be optically gray and in local thermodynamic equilibrium. This model is then used to examine the effects of radiation scattering, particle size, particle bulk density, and boundary conditions on the computed temperature profile and on the radiant heat loss at the walls.

The radiation intensity and particle temperature distributions are computed accurately by the simultaneous solution of the radiative transfer equation and an energy balance equation for the particles. Both the discrete ordinates method and the diffusion approximation are used to solve the equation of transfer, and a comparison of the two solution techniques is performed. This discrete ordinates method is applied for the first time to the calculation of the radiation intensity in a medium containing a temperature-dependent, nonlinear heat source. The agreement between the diffusion approximation and the

discrete ordinates solution is shown to improve with increasing optical thickness of the suspension.

Finally, in the absence of all non-radiative heat loss modes, coal dust suspensions are shown to ignite only if their optical thickness exceeds a critical value. This critical optical thickness depends on the temperature and reflectivity of the bounding walls and is very sensitive to the parameters of the heat generation model.